cigre Turkey

EISSN 2791-6049

TEPES

TURKISH JOURNAL OF ELECTRICAL POWER AND ENERGY SYSTEMS

VOLUME 1 • ISSUE 2 • OCTOBER 2021

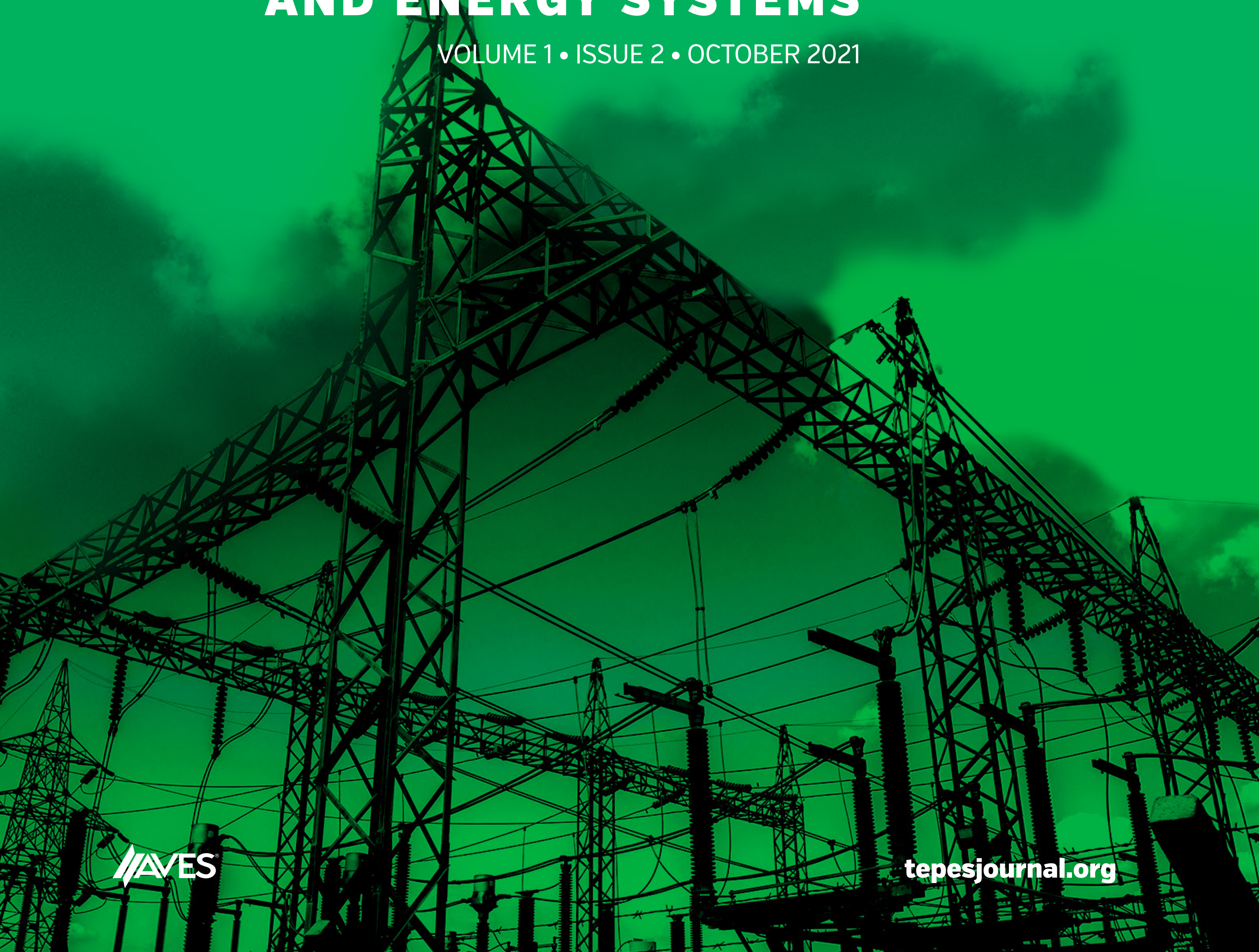

AVES

tepesjournal.org

cigre Turkey

TEPES
TURKISH JOURNAL OF
ELECTRICAL POWER
AND ENERGY SYSTEMS

AVES

Publisher
İbrahim KARA

Director of Operations
Ali ŞAHİN

Editorial Development
Gizem KAYAN TEKAÜT

Deputy Publication Director
Gökhan ÇİMEN

Publication Coordinators
İrem SOYSAL
Arzu YILDIRIM
Deniz KAYA
Bahar ALBAYRAK
Gamze BİLGEN
Irmak BERBEROĞLU
Elif Bahar BAKIRCI
Ebru BOZ

Finance and Administration
Zeynep YAKIŞIRER ÜREN

Project Coordinators
Sinem Fehime KOZ
Doğan ORUÇ
Emre KARA

Graphics Department
Ünal ÖZER

Contact
Address : Büyükdere Cad. No: 105/9 Şişli, İstanbul, Turkey
Phone : +90 212 217 17 00
E-mail : info@avesyayincilik.com

cigre Turkey

TEPES
TURKISH JOURNAL OF
ELECTRICAL POWER
AND ENERGY SYSTEMS

cigre Turkey

TEPES
TURKISH JOURNAL OF
ELECTRICAL POWER
AND ENERGY SYSTEMS

AIMS AND SCOPE

Turkish Journal of Electrical Power and Energy Systems (TEPES) is an international, scientific, open access periodical published in accordance with independent, unbiased, and double-blinded peer-review principles. The journal is the official online-only publication with the support of Association of Turkish Electricity Industry (TESAB) and led by CIGRE Turkish National Committee. and it is published biannually in April and October. The publication language of the journal is English.

TEPES aims to contribute to the literature by publishing manuscripts at the highest scientific level on all fields of electrical power and energy systems. The journal publishes original research and review articles that are prepared in accordance with ethical guidelines.

The scope of the journals includes but not limited to:

1. Power Generation, Transmission and Distribution

- Conventional and renewable power generation
- Transmission systems
- Distribution Systems, automation and control
- Energy efficiency
- Electromagnetic analysis and compatibility in power systems
- HVDC and flexible AC transmission system (FACTS)
- Renewable energy technologies and system
- Transmission and distribution equipment
- Insulated cables
- Overhead lines
- Substations
- Electrical Power System Protection
- Smart-Grid
- Plasma physics and the pulsed power technology
- Information systems and telecommunication
- Electric vehicles and charging networks
- Measurement
- Power System control
- Demand Response

2. Power System Management

- Power system development and economics
- Power system operation, planning and control
- Power system environmental performance
- Power system technical performance
- Electricity markets and regulation
- Load modeling, estimation and forecast

3. High-Voltage Techniques

- Measurement systems
- Electrical materials
- Emerging test techniques
- Insulation condition and coordination in power systems
- Over-voltage, lightning protection and grounding
- Ultra-High Voltage (UHV) technologies
- Electrical installations

4. Electrical Machines

- Power electronics
- Electrical Machines and Drives
- Power transformers and reactors
- Design of Electrical Machines for Sustainable Energy Applications

The target audience of the journal includes academicians, specialists, researchers and professionals who are working and interested in the field of electrical power and energy systems.

The editorial and publication processes of the journal are shaped in accordance with the guidelines of the Institute of Electrical and Electronics Engineers (IEEE), the World Commission on the Ethics of Scientific Knowledge and Technology (COMEST), Council of Science Editors (CSE), Committee on Publication Ethics (COPE), European Association of Science Editors (EASE), and National Information Standards Organization (NISO). The journal is in conformity with the Principles of Transparency and Best Practice in Scholarly Publishing (doaj.org/bestpractice).

Processing and publication are free of charge with the journal. No fees are requested from the authors at any point throughout the evaluation and publication process. All manuscripts must be submitted via the online submission system, which is available at www.tepesjournal.org. The journal guidelines, technical information, and the required forms are available on the journal's web page.

All expenses of the journal are covered by the CIGRE Turkish National Committee. Potential advertisers should contact the Editorial Office. Advertisement images are published only upon the Editor-in-Chief's approval.

Statements or opinions expressed in the manuscripts published in the journal reflect the views of the author(s) and not the opinions of the CIGRE Turkish National Committee, editors, editorial board, and/or publisher; the editors, editorial board, and publisher disclaim any responsibility or liability for such materials.

Editor in Chief: Belgin EMRE TÜRKAY
Address: Department of Electrical Engineering, İstanbul Technical University (ITU) Faculty of Electrical and Electronics Engineering, İstanbul, Turkey
E-mail: info@tepesjournal.org

Publisher: AVES
Address: Büyükdere Cad., 105/9 34394 Mecidiyeköy, Şişli, İstanbul, Turkey
Phone: +90 212 217 17 00
Fax: +90 212 217 22 92
E-mail: info@avesyayincilik.com

cigre Turkey

TEPES
TURKISH JOURNAL OF
ELECTRICAL POWER
AND ENERGY SYSTEMS

INSTRUCTIONS TO AUTHORS

Turkish Journal of Electrical Power and Energy Systems (TEPES) is an international, scientific, open access periodical published in accordance with independent, unbiased, and double-blinded peer-review principles. The journal is the official online-only publication with the support of Association of Turkish Electricity Industry (TESAB) and led by CIGRE Turkish National Committee, and it is published biannually in April and October. The publication language of the journal is English.

TEPES aims to contribute to the literature by publishing manuscripts at the highest scientific level on all fields of electrical power and energy systems. The journal publishes original research and review articles that are prepared in accordance with ethical guidelines.

The scope of the journals includes but not limited to:

1. Power Generation, Transmission and Distribution
- Conventional and renewable power generation
- Transmission systems
- Distribution Systems, automation and control
- Energy efficiency
- Electromagnetic analysis and compatibility in power systems
- HVDC and flexible AC transmission system (FACTS)
- Renewable energy technologies and system
- Transmission and distribution equipment
- Insulated cables
- Overhead lines
- Substations
- Electrical Power System Protection
- Smart-Grid
- Plasma physics and the pulsed power technology
- Information systems and telecommunication
- Electric vehicles and charging networks
- Measurement
- Power System control
- Demand Response

2. Power System Management
- Power system development and economics
- Power system operation, planning and control
- Power system environmental performance
- Power system technical performance
- Electricity markets and regulation
- Load modeling, estimation and forecast

3. High-Voltage Techniques
- Measurement systems
- Electrical materials
- Emerging test techniques
- Insulation condition and coordination in power systems
- Over-voltage, lightning protection and grounding
- Ultra-High Voltage (UHV) technologies
- Electrical installations

4. Electrical Machines
- Power electronics
- Electrical Machines and Drives
- Power transformers and reactors
- Design of Electrical Machines for Sustainable Energy Applications

The target audience of the journal includes academicians, specialists, researchers and professionals who are working and interested in the field of electrical power and energy systems.

EDITORIAL AND PUBLICATION PROCESS

The editorial and publication processes of the journal are shaped in accordance with the guidelines of the Institute of Electrical and Electronics Engineers (IEEE), the World Commission on the Ethics of Scientific Knowledge and Technology (COMEST), Council of Science Editors (CSE), Committee on Publication Ethics (COPE), European Association of Science Editors (EASE), and National Information Standards Organization (NISO). The journal is in conformity with the Principles of Transparency and Best Practice in Scholarly Publishing (doaj.org/bestpractice).

Originality, high scientific quality, and citation potential are the most important criteria for a manuscript to be accepted for publication. Manuscripts submitted for evaluation should not have been previously presented or already published in an electronic or printed medium. The journal should be informed of manuscripts that have been submitted to another journal for evaluation and rejected for publication. The submission of previous reviewer reports will expedite the evaluation process. Manuscripts that have been presented in a meeting should be submitted with detailed information on the organization, including the name, date, and location of the organization.

PEER REVIEW PROCESS

Manuscripts submitted to TEPES will go through a double-blind peer-review process. Each submission will be reviewed by at least two external, independent peer reviewers who are experts in their fields in order to ensure an unbiased evaluation process. The editorial board will invite an external and independent editor to manage the evaluation processes of manuscripts submitted by editors or by the editorial board members of the journal. The Editor in Chief is the final authority in the decision-making process for all submissions.

ETHICAL CONSIDERATIONS

The authors are expected to submit researches that comply with the general ethical principles which include; scientific integrity, collegiality, data integrity, institutional integrity and social responsibility.

Plagiarism and Ethical Misconduct

Turkish Journal of Electrical Power and Energy Systems is extremely sensitive about plagiarism. All submissions are screened by a similarity detection software (iThenticate by CrossCheck) at any point during the peer-review and/or production process.

When you are discussing others' (or your own) previous work, please make sure that you cite the material correctly in every instance.

Authors are strongly recommended to avoid any form plagiarism and ethical misconduct that are exemplified below.

Self- plagiarism (text-recycling): Overlapping sections or sentences with the author's previous publications without citing them. Even if you are the author of the phrases or sentences, the text should not have unacceptable similarity with the previously published data.

Salami slicing: Using the same data of a research into several different articles. Reporting the same hypotheses, population, and methods of a study is into different papers is not acceptable.

Data Fabrication: It is the addition of data that never occurred during the gathering of data or the experiments. Results and their interpretation must be based on the complete data sets and reported accordingly.

Data Manipulation/Falsification: It means manipulating research data with the intention of giving a false impression. This includes manipulating images (e.g. micrographs, gels, radiological images), removing outliers or 'inconvenient' results, changing data points, etc...

In the event of alleged or suspected research misconduct, e.g., plagiarism, citation manipulation, and data falsification/fabrication, the Editorial Board will follow and act according to COPE flowcharts.

AUTHORSHIP

Being an author of a scientific article mainly indicates a person who has a significant contribution to the article and shares the responsibility and accountability of that article. To be defined as an author of a scientific article, researchers should fulfil below criteria:

- Making a significant contribution to the work in all or some of the following phases: Research conception or design, acquisition of data, analysis and interpretation.
- Drafting, writing or revising the manuscript
- Agreeing on the final version of the manuscript and the journal that it will be submitted
- Taking responsibility and accountability of the content of the article

Outside the above-mentioned authorship criteria, any other form of specific contribution should be stated in the Acknowledgement section.

In addition to being accountable for the parts of the work he/she has done, an author should be able to identify which co-authors are responsible for specific other parts of the work. In addition, authors should have confidence in the integrity of the contributions of their co-authors.

If an article is written by more than one person, one of the co-authors should be chosen as the corresponding author for handling all the correspondences regarding the article. Before submission, all authors should agree on the order of the authors and provide their current affiliations and contact details. Corresponding author is responsible for ensuring the correctness of these information.

TEPES requires corresponding authors to submit a signed and scanned version of the Copyright Agreement and Acknowledgement of Authorship form (available for download www.tepesjournal.org) during the initial submission process to act appropriately on authorship rights and to prevent ghost or honorary authorship. If the editorial board suspects a case of "gift authorship," the submission will be rejected without further review. As part of the submission of the manuscript, the corresponding author should also send a short statement declaring that he/she accepts to undertake all the responsibility for authorship during the submission and review stages of the manuscript.

CHANGE OF AUTHORSHIP

TEPES reviews the authorship according to the author's declaration in the Title Page, thus it is the authors responsibility to send the final order of the complete author names. Requests in the change of authorship (e.g. removal/addition of the authors, change in the order etc) after submission are subject to editorial approval. Editorial Board will investigate this kind of cases and act following COPE flowcharts.

Change of authorship requests should be submitted to the Editorial Office with an official letter stating the reasons of the change. The letter must be signed by all authors and include their approval on the change in authorship. If the request is approved by the Editorial Board, authors need to submit a new Copyright Agreement Form according to the final author list.

DECLARATION OF INTEREST

TEPES requires and encourages the authors and the individuals involved in the evaluation process of submitted manuscripts to disclose any existing or potential conflicts of interests, including financial, consultant, and institutional, that might lead to potential bias or a conflict of interest. Any financial grants or other support received for a submitted study from individuals or institutions should be disclosed to the Editorial Board. Cases of a potential conflict of interest of the editors, authors, or reviewers are resolved by the journal's Editorial Board within the scope of COPE guidelines.

APPEAL AND COMPLAINT

The Editorial Board of the journal handles all appeal and complaint cases within the scope of COPE guidelines. In such cases, authors should get in direct contact with the editorial office regarding their appeals and complaints. When needed, an ombudsperson may be assigned to resolve claims that cannot be resolved internally. The Editor in Chief is the final authority in the decision-making process for all appeals and complaints.

COPYRIGHT AND LICENSE

TEPES requires each submission to be accompanied by a Copyright Agreement and Acknowledgement of Authorship form (available for download www.tepesjournal.org). By signing this form, authors retain the copyright of their work and agree that the article, if accepted for publication by the Turkish Journal of Electrical Power and Energy Systems will be licensed under a Creative Commons Attribution-NonCommercial 4.0 International License. This license permits third parties to share and adapt the content by giving the appropriate credit to the original work. Using the content for commercial purposes is not allowed and subject to editorial approval.

When using previously published content, including figures, tables, or any other material in both print and electronic formats, authors must obtain permission from the copyright holder. Legal, financial and criminal liabilities in this regard belong to the author(s).

DISCLAIMER

Statements or opinions expressed in the manuscripts published in TEPES reflect the views of the author(s) and not the opinions of the editors, the editorial board, or the publisher; the editors, the editorial board, and the publisher disclaim any responsibility or liability for such materials. The final responsibility regarding the published content rests with the authors.

MANUSCRIPT PREPARATION

Manuscripts can only be submitted through the journal's online manuscript submission and evaluation system, available at www.tepesjournal.org. Manuscripts submitted via any other medium and submissions by anyone other than one of the authors will not be evaluated.

Manuscripts submitted to the journal will first go through a technical evaluation process where the editorial office staff will ensure that the manuscript has been prepared and submitted in accordance with the journal's guidelines. Submissions that do not conform to the journal's guidelines will be returned to the submitting author with technical correction requests.

Authors are required to submit the Copyright Agreement and Acknowledgement of Authorship Form during initial submission. The form is available for download at www.tepesjournal.org.

Preparation of the Manuscript

Title page: A separate title page should be submitted with all submissions and this page should include:

- The full title of the manuscript as well as a short title (running head) of no more than 50 characters,
- Name(s), affiliations, highest academic degree(s), and ORCID IDs of the author(s),
- Grant information and detailed information on the other sources of support,
- Name, address, telephone (including the mobile phone number), and email address of the corresponding author,
- Acknowledgment of the individuals who contributed to the preparation of the manuscript but who do not fulfill the authorship criteria.

Abstract: An abstract should be submitted with all submissions except for Letters to the Editor. The abstract of articles should be structured without subheadings. Please check Table 1 below for word count specifications.

Keywords: Each submission must be accompanied by a minimum of three to a maximum of five keywords for subject indexing at the end of the abstract. The keywords should be listed in full without abbreviations.

Manuscript Types

Research Articles: This is the most important type of article since it provides new information based on original research. Acceptance of original papers will be based upon the originality and importance of the investigation. The main text of original articles should be structured with Introduction, Methods, Results, and Discussion subheadings. Please check Table 1 for the limitations for Original Articles.

Statistical analysis to support conclusions is usually necessary. Statistical analyses must be conducted in accordance with international statistical reporting standards. Information on statistical analyses should be provided with a separate subheading under the Materials and Methods section and the statistical software that was used during the process must be specified.

Units should be prepared in accordance with the International System of Units (SI).

Editorial Comments: Invited brief editorial comments on selected articles are published in TEPES. Editorials should not be longer than 1000 words excluding references. Editorial comments aim to provide a brief critical commentary by reviewers with expertise or with high reputation in the topic of the research article published in the journal. Authors are selected and invited by the journal to provide such comments. Abstract, Keywords, and Tables, Figures, Images, and other media are not included.

Review Articles: Reviews prepared by authors who have extensive knowledge on a particular field and whose scientific background has been translated into a high volume of publications with a high citation potential are welcomed. These authors may even be invited by the journal. Reviews should describe, discuss, and evaluate the current level of knowledge of a topic in clinical practice and should guide future studies. The subheadings of the review articles should be planned by the authors. However, each review article should include an "Introduction" and a "Conclusion" section. Please check Table 1 for the limitations for Review Articles.

Letters to the Editor: This type of manuscript discusses important parts, overlooked aspects, or lacking parts of a previously published article. Articles on subjects within the scope of the journal that might attract the readers' attention, particularly educative cases, may also be submitted in the form of a "Letter to the Editor." Readers can also present their comments on the published manuscripts in the form of a "Letter to the Editor." Abstract, Keywords, and Tables, Figures, Images, and other media should not be included. The text should be unstructured. The manuscript that is being commented on must be properly cited within this manuscript.

Table 1. Limitations for each manuscript type

Type of manuscript	Word limit	Abstract word limit	Reference limit	Table limit	Figure limit
Research Article	4000	250	35	6	5 or total of 10 images
Review Article	5000	250	50	6	10 or total of 15 images
Letter to the Editor	500	No abstract	5	No tables	No media

Tables

Tables should be included in the main document, presented after the reference list, and they should be numbered consecutively in the order they are referred to within the main text. A descriptive title must be placed above the tables. Abbreviations used in the tables should be defined below the tables by footnotes (even if they are defined within the main text). Tables should be created using the "insert table" command of the word processing software and they should be arranged clearly to provide easy reading. Data presented in the tables should not be a repetition of the data presented within the main text but should be supporting the main text.

Figures and Figure Legends

Figures, graphics, and photographs should be submitted as separate files (in TIFF or JPEG format) through the submission system. The files should not be embedded in a Word document or the main document. When there are figure subunits, the subunits should not be merged to form a single image. Each subunit should be submitted separately through the submission system. Images should not be labeled (a, b, c, etc.) to indicate figure subunits. Thick and thin arrows, arrowheads, stars, asterisks, and similar marks can be used on the images to support figure legends. Like the rest of the submission, the figures too should be blind. Any information within the images that may indicate an individual or institution should be blinded. The minimum resolution of each submitted figure should be 300 DPI. To prevent delays in the evaluation process, all submitted figures should be clear in resolution and large in size (minimum dimensions: 100 × 100 mm). Figure legends should be listed at the end of the main document.

Equations

The equations must be stated separated from the text by a blank line. They should be numbered consecutively in parenthesis at the right side of the equation. Symbols and variables as well as in the main text should be written in italics while vectors and matrices should be written in bold type.

All references, tables, and figures should be referred to within the main text, and they should be numbered consecutively in the order they are referred to within the main text.

Limitations, drawbacks, and the shortcomings of original articles should be mentioned in the Discussion section before the conclusion paragraph.

References

While citing publications, preference should be given to the latest, most up-to-date publications. Authors are responsible for the accuracy of references. Both in-text citations and the references must be prepared according to IEEE Citation Style. In the main text of the manuscript, references should be cited using Arabic numbers in square brackets. The reference styles for different types of publications are presented in the following examples.

Journal Article: H. Ayasso and A. Mohammad-Djafari, "Joint NDT Image Restoration and Segmentation Using Gauss–Markov–Potts Prior Models and Variational Bayesian Computation," IEEE Transactions on Image Processing, vol. 19, no. 9, pp. 2265-77, 2010.

Book Chapter: A. Rezi and M. Allam, "Techniques in array processing by means of transformations" in Control and Dynamic Systems, Vol. 69, Multidemsional Systems, C. T. Leondes, Ed. San Diego: Academic Press, 1995, pp. 133-180.

Book with a Single Author: W.-K. Chen, Linear Networks and Systems. Belmont, CA: Wadsworth, 1993, pp. 123-135.

Conference Proceedings: L. Liu and H. Miao, "A specification based approach to testing polymorphic attributes," in Formal Methods and Software Engineering: Proc. of the 6th Int. Conf. on Formal Engineering Methods, ICFEM 2004, Seattle, WA, USA, November 8-12, 2004, J. Davies, W. Schulte, M. Barnett, Eds. Berlin: Springer, 2004. pp. 306-19.

Report: K. E. Elliott and C.M. Greene, "A local adaptive protocol," Argonne National Laboratory, Argonne, France, Tech. Rep. 916-1010-BB, 1997.

Thesis: M. W. Dixon, "Application of neural networks to solve the routing problem in communication networks," Ph.D. dissertation, Murdoch Univ., Murdoch, WA, Australia, 1999.

Manuscripts Published in Electronic Format: P. H. C. Eilers and J. J. Goeman, "Enhancing scatterplots with smoothed densities," Bioinformatics, vol. 20, no. 5, pp. 623-628, March 2004. [Online]. Available: www.oxfordjournals.org. [Accessed Sept. 18, 2004].

Standard: IEC 60060-2 "High-voltage test techniques, Part 2: Measuring systems", 2010.

Online Document Published in a Web-Site: BIPM, Evaluation of Measurement Data–An Introduction to the "Guide to the Expression of Uncertainty in Measurement" and Related Documents, JCGM 104:2009. [Online]. Available: http://www.bipm.org/utils/common/documents/jcgm/ JCGM_104_ 2009_E.pdf

REVISIONS

When submitting a revised version of a paper, the author must submit a detailed "Response to the reviewers" that states point by point how each issue raised by the reviewers has been covered and where it can be found (each reviewer's comment, followed by the author's reply and line numbers where the changes have been made) as well as an annotated copy of the main document. Revised manuscripts must be submitted within 30 days from the date of the decision letter. If the revised version of the manuscript is not submitted within the allocated time, the revision option may be canceled. If the submitting author(s) believe that additional time is required, they should request this extension before the initial 30-day period is over.

Accepted manuscripts are copy-edited for grammar, punctuation, and format. Once the publication process of a manuscript is completed, it is published online on the journal's webpage as an ahead-of-print publication before it is included in its scheduled issue. A PDF proof of the accepted manuscript is sent to the corresponding author and their publication approval is requested within 2 days of their receipt of the proof.

Editor in Chief: Belgin EMRE TÜRKAY
Address: Department of Electrical Engineering, İstanbul Technical University (ITU) Faculty of Electrical and Electronics Engineering, İstanbul, Turkey
E-mail: info@tepesjournal.org

Publisher: AVES
Address: Büyükdere Cad., 105/9 34394 Mecidiyeköy, Şişli, İstanbul, Turkey
Phone: +90 212 217 17 00
Fax: +90 212 217 22 92
E-mail: info@avesyayincilik.com

TEPES
TURKISH JOURNAL OF
ELECTRICAL POWER
AND ENERGY SYSTEMS

CONTENTS

RESEARCH ARTICLES

REVIEW

TEPES
TURKISH JOURNAL OF
ELECTRICAL POWER
AND ENERGY SYSTEMS

TEPES Vol 1., Issue. 2, 60-68, 2021 **DOI:** 10.5152/tepes.2021.21020

RESEARCH ARTICLE

Feasibility of PV-Based Islanded Microgrids for Affordable Electricity in Sub-Saharan Africa

Ömer Kaan Merev

Department of Electrical Engineering, İstanbul Technical University, Institute of Science Eng. & Tech, İstanbul, Turkey

Cite this article as: Merev Ö. Feasibility of PV-based islanded microgrids for affordable electricity in sub-saharan Africa. *Turk J Electr Power Energy Syst*. 1(2), 60-68, 2021.

ABSTRACT

Many countries in Sub-Saharan Africa (SSA) suffer from the lack of access to electricity due to poverty and a dispersed population. Due to the solar power potential in this region, solar-powered microgrids were examined in this study as a way to supply affordable electricity to the rural population in SSA. Using HOMER Pro as the microgrid optimization tool, a microgrid designed to supply electricity in Burkina Faso was simulated. With one of the cheapest electricity tariffs in SSA ($0.240/kWh), Burkina Faso was selected to ensure that the simulation results can serve as a proof-of-concept for all of the Sub-Saharan countries. Factors like solar panel output degradation and dusting, unexpected component failure, and linearity of the load profile were assessed to determine the lowest-cost and highest-cost results for the simulated microgrid. The performed simulations showed that even without a connection to the main grid, a solar-powered microgrid can be easily profitable while supplying electricity at below the average national tariff, with almost no expected power outages. This paper proves that microgrids with only solar panels as a power source remain a viable option to provide cheap electricity to the impoverished rural regions in SSA, even with almost no component maintenance.

Index Terms—Cost of electricity, electricity access, HOMER pro, microgrid, solar power, Sub-Saharan Africa.

I. INTRODUCTION

A microgrid is an autonomous energy system that supplies electricity to a region by using several power generation methods. Microgrids can function independently; if they are connected to the main grid, they can isolate themselves in case of an emergency. A microgrid that maintains no connection to the main grid is called an islanded microgrid. Islanded microgrids are principally used for providing electricity to isolated villages or outlying regions. Generally, connecting faraway places to the main grid is extremely costly; therefore, a microgrid remains a preferable option. In an islanded configuration, the power generation must be adequate at all times to constantly supply the microgrid's sensitive loads, in accordance with IEEE Std 1547.4-2011 [1]. For this reason, batteries are used to continuously provide electricity when power generation becomes insufficient [2].

For African countries that have large rural regions suffering from poverty, and have no working national grids to supply them with electricity, islanded microgrids become the sole option. The World Bank SE4ALL database's rural population density data are critically valuable in this regard. The data suggest that there are more isolated rural populations in Africa than in the rest of the world [3]. Furthermore, most of the countries in Africa are poverty-stricken. According to the World Bank's World Development Indicator report in 2017, the share of the population that lives in extreme poverty (income of <$1.9 per day) is slightly below 50% in Sub-Saharan Africa (SSA) [3]. The statistics show that SSA, in particular, has exhibited signs of extreme poverty, which explains the region's lack of electricity access. Electricity access in SSA is only 30.5% overall. Rural access is worse: 14.2% [4]. The result is higher electricity tariffs in SSA, which ranges between $0.200/kWh and $0.500/kWh, depending on the country [5]. The worldwide electricity tariff average is $0.134/kWh in comparison [6].

This paper aims to prove that providing cheaper electricity in SSA is possible with photovoltaic (PV)-based islanded microgrids. For this reason, a PV-based microgrid was planned in Burkina Faso, owing to the cheaper overall electricity tariff than other Sub-Saharan countries [7]. Being able to provide cheaper electricity in Burkina Faso ensures that this study can be applicable to most, if not all, of the Sub-Saharan countries in terms of providing cheaper electricity to

Corresponding author: Ömer Kaan Merev, merev15@itu.edu.tr

Received: April 2, 2021
Accepted: April 23, 2021
Published online: August 27, 2021

the population. The simulation was performed using HOMER Pro, a microgrid design and optimization tool.

The rest of the paper includes the following:

- Location selection for the microgrid project with detailed justification for the selection.
- Explanation of the statistical analysis used by HOMER Pro to simulate the microgrid.
- Comprehensive analysis for component selection.
- Presentation of the results.
- Information about the limitations that affected the results.
- Comments about the findings in this paper and their implications.

II. METHODS

A. Location Selection

Burkina Faso's low electrification rates demonstrate the need for a microgrid project. With a combined population of 19.2 million [3], Burkina Faso's urban population makes up 29% of the total population, and only 58% of that urban population has electricity access. Moreover, only 3% of the rural population has electricity access. Note that 70% of Burkina Faso's population lives in rural areas [8]. In addition, Burkina Faso's inability to seamlessly supply electricity to regions under the national grid reinforces the need for the project [9].

Province selection was influenced by several factors. The solar irradiation map of Burkina Faso in [7] was used to determine candidate regions where a solar-powered microgrid could provide maximum power. The referenced map revealed that the country's Northeast region is a suitable region for the microgrid. The next step was to take the population distribution for the suitable regions into account, to identify the most suitable location for the microgrid.

Main Points

- HOMER Pro is used as the microgrid optimization tool to determine the most affordable solutions for the simulated microgrid in Burkina Faso. The pros and cons of HOMER Pro are discussed.
- The effects of maintenance and external factors such as solar panel dusting are evaluated by simulating different lifetime expectations for each component in the microgrid and different derating factor possibilities for the solar panels.
- The importance of load profile linearization is discussed by proving that a more linearized load profile results in a lower cost of electricity (COE).
- It is shown that even with almost no component maintenance, the PV-based microgrid solution offers a COE that can be profitable while setting an electricity tariff that is lower than Burkina Faso's average tariff.
- A future connection to the main grid can lower the microgrid's COE further by selling the excess energy that is wasted while the microgrid is in islanded configuration.

The grid also needs to be relatively close to the main grid to enable a possible future main grid connection. After comparing the population centers and grid distribution with the solar irradiation map, the Namentenga province was selected [7]. With a population of 476 262, this province is relatively populous. Notably, 95.3% of the Namentenga province's population lives in rural areas, where only 1% of the population on average has access to electricity [10]. The exact location of the microgrid project is 13°35.9'N, 0°16.5'W, which lies inside the Department of Yalgo.

B. Statistical Analysis Using HOMER Pro

For the designed microgrid, multiple simulations for multiple scenarios are performed to establish the most economical solution. The project location is used to get the monthly average solar irradiance and clearness index data from HOMER Pro. Clearness index (K_T) is defined as the ratio of the solar radiation that reaches the Earth's surface. This value is between 0 and 1. The clearness index is closer to 1 on a sunny and clear day, whereas it gets closer to 0 in cloudy conditions. The calculation of the clearness index is performed with (1), where H_{ave} is the monthly average radiation on the horizontal surface of the Earth and $H_{o,ave}$ is the extraterrestrial horizontal radiation. In other words, $H_{o,ave}$ is the radiation on a horizontal surface at the top of the Earth's atmosphere [11];

$$K_T = \frac{H_{ave}}{H_{o,ave}} \tag{1}$$

With a given H_{ave}, HOMER Pro can find K_T after calculating $H_{o,ave}$, which involves several steps. The initial step is to calculate the intensity of solar radiation at the top of the Earth's atmosphere (G_{on}) (2);

$$G_{on} = G_{sc} \cdot \left(1 + 0.033 \cdot \cos\left(\frac{360 \cdot n}{365}\right)\right) \tag{2}$$

G_{sc} is the solar constant (1.367 kW/m^2), whereas n is the day of the year. The next step is to obtain the extraterrestrial radiation on the horizontal surface (G_o) which changes with the zenith angle (θ_z). The zenith angle represents the angle between the sun's rays and the vertical. G_o can be calculated using (3) and (4):

$$G_o = G_{on} \cdot \cos\theta_z \tag{3}$$

$$\cos\theta_z = \cos\phi \cdot \cos\delta \cdot \cos\omega + \sin\phi \cdot \sin\delta \tag{4}$$

For (4), ϕ is the latitude, δ is the solar declination, and ω is the hour angle. The solar declination itself is calculated using (5):

$$\delta = 23.45° \cdot \sin\left(360° \cdot \left(\frac{284 + n}{365}\right)\right) \tag{5}$$

A further step involves finding H_o, the average daily extraterrestrial radiation per square meter. Integrating (3) from sunrise to sunset will give H_o. The result of the integration is given in (6):

$$H_o = \frac{24}{\pi} \cdot G_{on} \cdot \left(\cos\phi \cdot \cos\delta \cdot \sin\omega_s + \frac{\pi \cdot \omega_s}{180°} \cdot \sin\phi \cdot \sin\delta\right) \tag{6}$$

ω_s is the sunset hour angle, which can be calculated using (7):

$$\cos\omega_s = -\tan\phi \cdot \tan\delta \tag{7}$$

Finally, $H_{o,ave}$ can be calculated (8). N is the number of days in the month:

$$H_{o,ave} = \frac{\sum_{n=1}^{N} H_o}{N} \tag{8}$$

Using the provided equations, the monthly average solar global horizontal irradiance (GHI) data for Namentenga are presented in Table I.

One of HOMER Pro's most important features is its ability to conduct accurate economic analysis. Attaining accurate results requires data about several economic properties of the region. These properties include the country's inflation rate and nominal discount rate. The nominal discount rate is the interest rate without the effects of inflation. Both inflation and nominal discount rates are used to calculate the cost increase, caused by inflation, of any materials that need to be replaced. Maintenance costs are equally affected by inflation: calculating the maintenance costs of a project with a lifetime of multiple years cannot be done correctly without considering the effects of inflation in the region. Over the last 18 years, Burkina Faso's average inflation rate (*f*) has been 2.3%, whereas the nominal discount rate (*i'*) is 5.14% [12, 13]. These rates are used to determine the real discount rate (real interest rate). The real discount rate (*i*) is the interest rate used to remove the effect of inflation, which is:

$$i = \frac{i' - f}{1 + f} \tag{9}$$

Using (9), the real discount rate is calculated to be 2.78%.

HOMER Pro can also calculate the COE and total net present cost (NPC). The COE is the average cost of producing 1 kWh of electrical energy by the system. NPC represents the entire project's cost for the full length of its determined lifetime. For COE and NPC, the goal is to keep those costs as low as possible. Using (10), COE can be calculated:

$$COE = \frac{Cyear}{E(AC) + E(DC)} \tag{10}$$

C_{year} is the total annualized cost of the microgrid, whereas *E(AC)* and *E(DC)* are the yearly spent AC and DC loads, respectively.

Determining the NPC requires calculating the capital recovery factor (CRF), which is a ratio used to calculate the present value of the cash flow. The present value of a payment changes in time. This change is dependent on the real discount rate and the amount of time, as is apparent with the CRF's following formula (11):

$$CRF(i, N) = i \cdot \frac{(1+i)^N}{(1+i)^N - 1} \tag{11}$$

Note that *N* is the project lifetime, which is 25 years for the project in this paper. Using CRF, NPC can be calculated as (12):

$$NPC = \frac{Cyear}{CRF} \tag{12}$$

After the project lifetime is reached, every component is sold as salvage to recuperate some of the installation costs. The salvage value is calculated using (13):

$$S = C_{rep} \cdot \frac{R_{rem}}{R_{comp}} \tag{13}$$

C_{rep} is the replacement cost, R_{rem} is the remaining lifetime at the end of the project lifetime, and R_{comp} is the component lifetime, which is:

$$R_{rem} = R_{comp} - (N - R_{rep}) \tag{14}$$

R_{rep} is the replacement cost duration, calculated by (15):

$$R_{rep} = R_{comp} \cdot INT\left(\frac{R_{proj}}{R_{comp}}\right) \tag{15}$$

TABLE I
SOLAR GLOBAL HORIZONTAL IRRADIANCE (GHI) DATA FOR NAMENTENGA REGION

Month	K_T	H_{ave} (kWh/m²/day)	Month	K_T	H_{ave} (kWh/m²/day)
January	0.638	5.360	July	0.573	6.050
February	0.680	6.260	August	0.539	5.670
March	0.666	6.690	September	0.573	5.830
April	0.650	6.860	October	0.625	5.880
May	0.638	6.780	November	0.648	5.530
June	0.613	6.470	December	0.632	5.130

K_T, clearness index; H_{ave}, monthly average radiation.

Note that *INT ()* gives the integer value of the equation inside the parentheses.

One can also limit the annual capacity shortage to make sure that the project sufficiently provides consistent electricity to its users. HOMER Pro assumes an annual capacity shortage of 0% by default. However, this can result in situations where a specific load may require excessive energy production to ensure no capacity shortage during peak loads. The result is wasted energy and an increase in the COE and NPC if the microgrid is islanded. After several preliminary simulations, an annual capacity shortage of 2% was allowed in the system.

Furthermore, the project's load profile needs to be determined. The software has certain artificial load profiles and multiple load profiles for several locations within the United States. These load profiles can aid a project even if it is outside the United States by only listing load profiles that match the climate of the project's location. Because electrification of a rural region is desired for the microgrid design, a residential load profile can be assumed. However, the load profile cannot be expected to remain the same throughout the project's 25-year lifespan. Once the electrification is achieved and businesses start to establish in the area, the load profile will turn into a more distributed one. The reason is that the electricity usage will be more varied instead of electricity used primarily for illumination at night and refrigeration. Investigating this factor requires one simulation each for two different load profiles (residential and community, Fig. 1 and Fig. 2). From the results, a two-step microgrid installation was planned. The first step was assumed for a complete residential load profile, serving a small fraction of the planned amount, owing to the less linear nature of the load profile increasing the COE. The second step was assumed for a community load profile. To find the best annual average load for each step, the scale of the project for each load profile needs to be examined. For this reason, a load that satisfies the needs of between 500 and 5000 people was considered, with an increment of 500 people. Yearly average energy consumption per capita in Burkina Faso is 76 kWh [14], which is equal to 208.22 Wh/day. Thus, the average annual load in the simulation is in the range of 104.11–1041.1 kWh/day. Note that with a community load profile, average energy consumption per capita in the region might increase owing to increased economic activity.

C. Component Selection

The required components for the microgrid are solar panels for power generation, maximum power-point (MPP) tracking (MPPT) charge controllers to always output maximum power at a stable DC bus voltage [15], batteries for energy storage, and inverters for DC–AC conversion. There are several considerations to be made for component selection:

- DC bus voltage needs to be at the DC voltage range of the inverter. In addition, most MPPT charge controllers depend upon solar panel output voltage to be above the battery voltage to function. Thus, DC bus voltage needs to be selected in accordance with this fact.
- Battery nominal voltage needs to be at the required DC bus voltage. The string size can be altered to accommodate this specification.
- The selected MPPT charge controller needs to be able to charge the batteries at the specified DC bus voltage. It also needs to

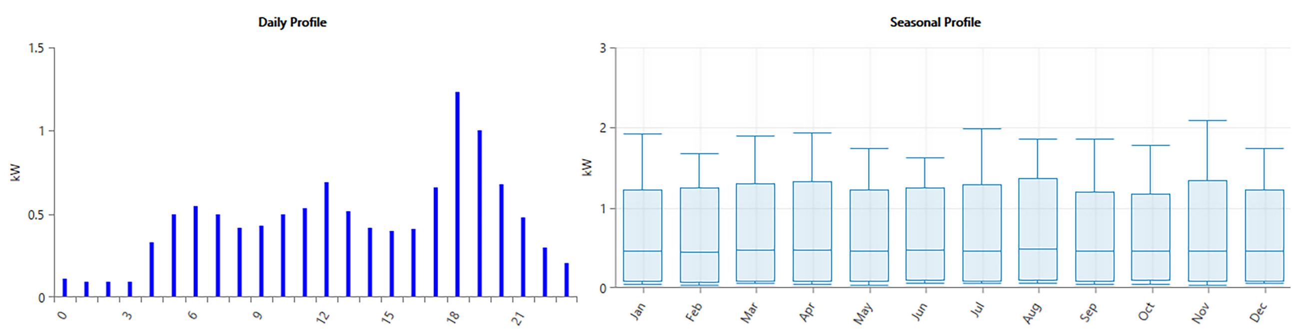

Fig. 1. Residential daily and seasonal load profile.

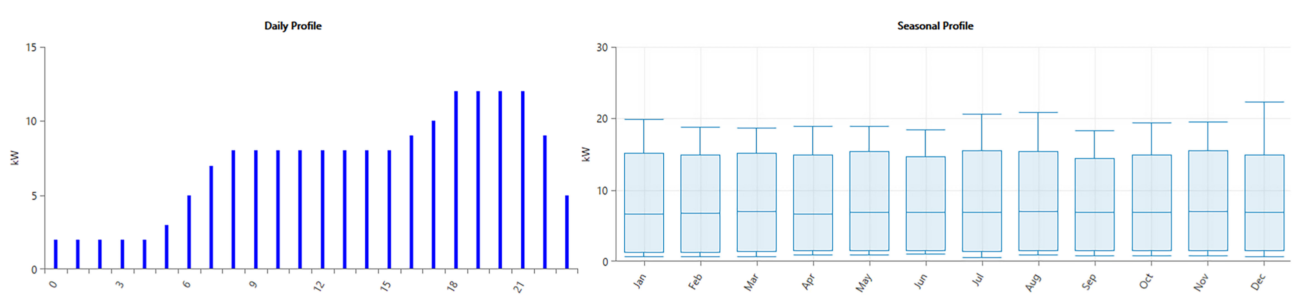

Fig. 2. Community daily and seasonal load profile.

be rated at appropriate maximum PV short circuit current (I_{sc}) and open circuit voltage (V_{oc}) values. A solar panel with a higher short circuit current can damage the controller. The datasheet for the MPPT controller needs to be examined for more potential restrictions.

For solar panels, LG Electronics 365Q1C-A5 was selected for its high efficiency (21%). According to the panel's datasheet, its maximum power (P_{max}) is 365 W, V_{oc} is 42.8 V, and I_{sc} is 10.8 A. Moreover, the output of the solar panel is expected to decline by 2% during the first year. Afterward, an annual output decline of 0.4% is expected [16]. Based on this information, the average solar panel output after 25 years is 93.46% of its initial performance. This factor is included in the simulation as the derating factor (f_{PV}) of the solar panels.

The MPP voltage of the solar panels is 36.7 V [16]. This necessitates a DC bus voltage lower than this value to make sure that the MPPT charge controller is functional. Because most MPPT charge controllers support battery voltages of 12–24–36–48 V, a 12 V DC bus voltage is selected for this project to ensure the continuous operation of MPPT charge controllers.

For energy storage, EnerSys PowerSafe SBS 900 batteries were used. They have a nominal voltage of 12 V and a nominal capacity of 12.1 kWh. The string size does not need to be altered because both the DC bus voltage and the battery nominal voltage are the same. These batteries also need to undergo maintenance every six months. This requirement was factored into the simulation.

The selected MPPT charge controller is Victron BlueSolar MPPT 100/50. Its rated charge current is 50 A; therefore, it is capable of providing 700 W of nominal power at 12 V battery voltage. Its specified maximum V_{oc} and I_{sc} values are 100 V and 60 A, respectively, which satisfy the solar panels' specifications. For this system, each MPPT charge controller can handle two solar panels connected in series. Even though the combined P_{max} is 730 W, the simulation assumes 93.46% of maximum solar panel output, because of the output power degradation mentioned earlier. For this reason, the actual P_{max} is slightly above 682 W, which the MPPT charge controller can provide [17].

Studer Xtender XTH 3000-12 was selected for DC–AC conversion. Its nominal battery voltage is 12 V and it has an input voltage range between 9.5 and 17 V. It can supply continuous power of 2500 VA [18].

Each selected component needs to be replaced after several years, owing to aging. Each component has a certain lifetime specified both in the respective datasheets and in the HOMER Pro software. However, the need for replacement can occur earlier than expected because of suboptimal storage conditions and lack of maintenance. For this reason, several lifetime possibilities were specified for each component. A lack of maintenance can also lower solar panel power output owing to dusting, especially in Africa [19]. This reduction varies between 4% and 32%, according to results in [20–29]. To study the most undesirable possible outcome, the power output reduction of 32% was examined with another derating factor: 63.55% (32% less than the average output of the solar panels throughout their 25-year lifespan). The considered lifetimes, alongside the capital, and operation-and-maintenance (O&M) costs are presented in Table II. Multiple technical reports and papers were used to decide the capital and O&M costs [30–34].

III. RESULTS

Owing to the many sensitivity issues due to the components' lifetime considerations and a change in the f_{PV} of the solar panels, results are provided in steps. These steps are as follows:

- The best case scenario for each average annual load is presented. The load with best results is selected.
- For the selected load, the effect of components' lifetime is provided. f_{PV} is 93.46% for the given results.
- The effect of dusting on solar panels owing to lack of maintenance is then examined using f_{PV} as another sensitivity issue.

A. Simulation Results for the Residential Load Profile

The results for the residential load profile with the best replacement requirements for each component are presented in Table III. Load #3 has the lowest COE of $0.146/kWh. Considering the fact that the average COE in Burkina Faso is $0.194/kWh, this result is definitely acceptable as it allows setting a tariff much lower than Burkina Faso's average ($0.240/kWh) [7]. Lowering electricity tariffs in Burkina Faso is essential, considering the prevalent poverty [3]. In addition, load #3 also provides the best autonomy among all other options. Note that autonomy refers to the amount of time that the microgrid can be sustained by the power accumulated in the batteries, in case of a blackout or during maintenance operations.

TABLE II
COMPONENTS SELECTED FOR THE MICROGRID AND THEIR ASSOCIATED COSTS

Component Type	Component Name	Cost ($/unit)	Simulated Lifetime (years)	O&M Costs ($/unit-year)
Solar Panel	LG 365Q1C-A5	380.00	25, 20	10.95
MPPT Charge Controller	Victron BlueSolar MPPT 100/50	343.00	20, 15	Included in solar panel O&M costs
Battery	EnerSys PowerSafe SBS 900	1440.00	15, 10	25.00
Inverter	Studer Xtender XTH 3000-12	901.00	10, 5	100.00

TABLE III
BEST RESULTS FOR EACH ANNUAL AVERAGE LOAD (RESIDENTIAL LOAD PROFILE)

#	Annual Average Load (kWh/day)	NPC ($)	COE ($/kWh)	Operating Cost ($/year)	Initial Capital ($)	Autonomy (hours)	Excess Electricity (%)
1	104.11	99 240	0.148	2 497	54 650	43.0	10.40
2	208.22	196 958	0.147	4 889	109 667	44.0	10.80
3	312.33	295 067	0.146	7 040	169 363	49.5	11.80
4	416.44	396 499	0.148	9 863	220 390	42.5	12.50
5	520.55	494 683	0.147	12 158	277 597	45.4	11.70
6	624.66	595 689	0.148	15 021	327 479	39.4	13.40
7	728.77	701 454	0.150	17 921	381 473	39.9	11.90
8	832.88	793 141	0.148	19 624	442 739	41.8	14.00
9	936.99	891 060	0.147	21 977	498 642	41.1	14.90
10	1041.1	995 415	0.148	25 197	545 503	39.5	13.10

NPC, net present cost; COE, cost of electricity.

TABLE IV
EFFECT OF COMPONENTS' LIFETIME FOR LOAD #3 (F_{PV} = 93.46%)

#	Component Lifetime (years)				COE ($/kWh)	NPC ($)	Autonomy (hours)	Excess Electricity (%)
	N_{Inv}	N_{Bat}	N_{PV}	N_{MPPT}				
3.1	10	10	20	10	0.176	354 746	40.4	12.10
3.2	10	15	20	10	0.169	341 742	48.9	11.80
3.3	10	10	25	10	0.169	339 684	40.4	12.10
3.4	10	15	25	10	0.162	325 889	45.0	11.70
3.5	5	10	20	10	0.190	383 676	41.7	12.40
3.6	5	15	20	10	0.183	368 215	44.3	12.90
3.7	5	10	25	10	0.184	370 756	43.0	12.00
3.8	5	15	25	10	0.175	352 123	50.2	11.90
3.9	10	10	20	20	0.160	322 700	37.8	14.10
3.10	10	15	20	20	0.154	310 102	49.5	11.80
3.11	10	10	25	20	0.153	307 133	37.2	15.00
3.12	10	15	25	20	0.146	295 067	49.5	11.80
3.13	5	10	20	20	0.176	354 418	43.0	12.00
3.14	5	15	20	20	0.167	336 082	47.6	12.30
3.15	5	10	25	20	0.167	336 463	37.8	15.20
3.16	5	15	25	20	0.159	320 511	46.9	11.70

NPC, net present cost; COE, cost of electricity.

TABLE V
BEST RESULTS FOR EACH ANNUAL AVERAGE LOAD (COMMUNITY LOAD PROFILE)

#	Annual Average Load (kWh/day)	NPC ($)	COE ($/kWh)	Operating Cost ($/year)	Initial Capital ($)	Autonomy (hours)	Excess Electricity (%)
11	104.11	97 975	0.146	2 494	53 445	39.1	10.20
12	208.22	183 292	0.136	4 394	104 828	39.1	11.90
13	312.33	276 256	0.137	6 448	161 129	44.3	11.60
14	416.44	367 460	0.137	8 762	211 003	40.6	11.70
15	520.55	467 017	0.140	11 146	267 990	44.6	9.93
16	624.66	556 652	0.138	13 127	322 253	39.4	15.10
17	728.77	644 890	0.137	15 466	368 738	40.5	11.30
18	832.88	747 539	0.139	18 298	420 818	35.7	14.30
19	936.99	823 816	0.136	19 596	473 910	41.1	11.20
20	1041.1	918 480	0.137	21 679	531 397	41.5	12.20

NPC, net present cost; COE, cost of electricity.

The effect of nonideal replacement requirements for load #3 is examined in Table IV. Even the worst scenario (load #3.5) has a COE ($0.190/kWh) lower than Burkina Faso's average COE. The worst possible dusting further increases the COE to $0.239/kWh, which leaves almost no room for profit without going above the electricity tariff average in Burkina Faso. Note that this is the absolute worst possible result for load #3, owing to the lack of maintenance. Moreover, the solar panels' lifetime typically ranges between 25 and 40 years [35], which makes a COE of $0.239/kWh unlikely for this project.

B. Simulation Results for the Community Load Profile

After an increased economic activity during the day is achieved in the area, a more linearized load profile is expected. Owing to load profile linearization, the relative peak load is reduced, therefore costs are reduced as well, as shown in Table V. The results are achieved with the advertised lifetime of each component. The highest average annual load with the lowest COE of $0.136/kWh is load #19. A comparison between Tables III and V emphasizes the importance of load profile linearization: with a community load profile, a decrease in the COE, NPC, initial capital, and yearly operating costs are achieved in every considered annual average load. In addition, tariffs can be set even lower than what was possible with a residential load profile. Compared with load #3, though, the autonomy decreased from 49.5 hours to 41.1 hours, which can be alleviated by further battery acquisition, but with the caveat of increased COE. As a side note, it must be emphasized that even the COE for load #19 is higher than the worldwide average tariff ($0.134/kWh). This is because of the excess electricity. Thus, the proximity of the main grid to the selected location was crucial owing to this problem: with a future integration to the main grid, excess electricity can be sold to the main grid, thereby reducing the overall COE for the microgrid itself.

Table VI shows the effect of different component lifetimes for load #19. The worst scenario is given in load #19.6. Even though load #19.5 is identical with load #19.6, with the exception of a worse battery lifetime (10 years), it has a lower COE. Owing to the fact that batteries can last longer in load #19.6, it is more sensible to invest more in them, increasing autonomy. However, the subsequent need for more inverters actually increased the COE of load #19.6, which is $0.179/kWh with no PV dusting and $0.221/kWh with PV dusting. The results in Table VI reinforce the fact that a PV-based microgrid project is feasible in Burkina Faso.

IV. DISCUSSION

Several limitations were present owing to the available information about Burkina Faso and the HOMER Pro software. These limitations are as follows:

- No credible information is available about land costs in Burkina Faso. This information is required for more accurate NPC calculation.
- Implementation of the derating factor (f_{PV}) as a way for simulating real-world operating conditions in HOMER Pro is limited because there is no way to input annual power output degradation for solar panels by setting different values for f_{PV} for each year. Entering an f_{PV} for the solar panels' average 25-year output was the best available, albeit still flawed, solution for this limitation. The flaw of this approach is apparent when $N_{PV} = 20$ years, where the solar panels' average output would be higher than 93.46%, especially for the replacements. The simulation of solar panel dusting for this project was also simplistic, owing to the aforementioned limitation of the software.
- No credible information is available about load profiles in the rural regions of Burkina Faso, owing to the lack of electricity access in the country. More accurate results can be achieved

TABLE VI
EFFECT OF COMPONENTS' LIFETIME FOR LOAD #19 (F_{PV}=93.46%)

	Component Lifetime (years)							
#	N_{Inv}	N_{Bat}	N_{PV}	N_{MPPT}	COE ($/kWh)	NPC ($)	Autonomy (hours)	Excess Electricity (%)
19.1	10	10	20	10	0.166	1 002 603	37.2	14.00
19.2	10	15	20	10	0.171	1 031 436	39.1	10.60
19.3	10	10	25	10	0.158	956 404	36.9	14.30
19.4	10	15	25	10	0.158	950 075	32.6	16.40
19.5	5	10	20	10	0.176	1 063 931	36.9	14.30
19.6	5	15	20	10	0.179	1 079 750	39.4	10.40
19.7	5	10	25	10	0.168	1 017 562	36.9	14.30
19.8	5	15	25	10	0.172	1 035 580	39.8	10.40
19.9	10	10	20	20	0.150	903 103	35.6	14.30
19.10	10	15	20	20	0.155	934 489	34.8	13.10
19.11	10	10	25	20	0.142	856 817	35.6	14.30
19.12	10	15	25	20	0.136	823 816	41.1	11.20
19.13	5	10	20	20	0.160	967 227	36.9	14.30
19.14	5	15	20	20	0.155	936 235	38.2	12.60
19.15	5	10	25	20	0.153	922 850	37.4	14.30
19.16	5	15	25	20	0.146	885 176	45.6	11.80

NPC, net present cost; COE, cost of electricity.

with a more location-specific load profile; however, the load profiles used for the project in this paper are accurate enough to base conclusions on.

- Lack of power flow analysis in HOMER Pro makes the optimization fairly simplistic: stability issues that typically arise with intermittent power generation cannot be simulated, although sudden increase in load can be taken into account by setting a day-to-day random variability of the load profile. Furthermore, line losses are also disregarded.

In conclusion, it was found that even without a grid connection, a PV-based microgrid remains a robust option for providing more affordable electricity to Burkina Faso, a country with a lower average electricity tariff than other SSA countries. Component maintenance was proven to be a crucial factor in making sure that the COE remains low throughout the microgrid's operational lifetime. The linearity of the load profile was also shown to affect the results. However, a future main grid connection is required to use the more than 10% excess electricity generated in almost all of the loads in Tables III, IV, V, and VI. This would also decrease the COE, to a level lower than the worldwide average electricity tariff.

Peer-review: Externally peer reviewed.

Conflict of Interest: The author has no conflicts of interest to declare.

Financial Disclosure: The author declares that this study has received no financial support.

REFERENCES

1. IEEE, "IEEE guide for design, operation, and integration of distributed resource island systems with electric power systems, " vol. 1547, pp. 4, 2011. [CrossRef]
2. M. S. Mahmoud, "Microgrid control problems and related issues, ", in *Microgrid: Advanced Control Methods and Renewable Energy System Integration*, Vol. 1. Boston, United States of America: Butterworth-Heinemann, 2017, pp.2–4.
3. The World Bank, *World Development Indicators*. Washington,DC., U.S.A., 2017.
4. R.Golumbeanu and D.Barnes, *Connection Charges and Electricity Access in Sub-Saharan Africa*. The World Bank, 2013. [CrossRef]
5. World Bank, "Getting electricity. " [Online], 2013. Available: https://www.doingbusiness.org/en/data/exploretopics/getting-electricity. [Accessed: Mar. 20, 2021], *Doing Business*, pp. 82–85.
6. International Energy Agency, "(IAE),", *Energy Prices 2020"*. [Online]. Available: https://www.iea.org/reports/energy-prices-2020. [Accessed: Mar. 20, 2021].
7. M. Moner-Girona, K. Bódis, T. Huld, I. Kougias and S. Szabó, "Universal access to electricity in Burkina Faso: Scaling-up renewable energy technologies," *Environmental Research Letters*, vol. 11, no. 8, 2016. [CrossRef]

8. The World Bank, "Rural population (% of total population) - Burkina Faso." [Online]. Available: https://data.worldbank.org/indicator/SP.RUR.TOTL.ZS?locations=BF. [Accessed: Mar. 20, 2021].
9. I. M. Ouedraogo, "Electricity consumption and economic growth in Burkina Faso: a cointegration analysis, " *Energy Economics*, vol. 32, no. 3, pp.524–531, 2010. [CrossRef]
10. Institut National de la Statistique et de la Démohgraphie, "(INSD),", *Annuaire statistique 2019 de la région du Centre-Nord*, INSD, 2020.
11. H. Energy, "How Homer calculates clearness index. " [Online]. Available: https://www.homerenergy.com/products/pro/docs/latest/how_homer_calculates_clearness_index.html. [Accessed: Mar. 16, 2021].
12. Institut National de la Statistique et de la Démohgraphie, "(INSD)," *Indicateurs Economiques*, INSD. [Online]. Available: http://www.insd.bf. [Accessed: Mar. 22, 2021].
13. The World Bank, "Lending interest rate (%) - Burkina Faso. " [Online]. Available: https://data.worldbank.org/indicator/FR.INR.LEND?locations=BF&start=2005&view=chart. [Accessed: Mar. 22, 2021].
14. WorldData, "Energy consumption in Burkina Faso. " [Online]. Available: https://www.worlddata.info/africa/burkina-faso/energy-consumption.php#:~:text=of%20electric%20energy%20per%20year,itself%20with%20self-produced%20energy [Accessed Mar. 16, 2021].
15. O. Ezinwanne, F. Zhongwen and L. Zhijun, "Energy performance and cost comparison of MPPT techniques for photovoltaics and other applications, " *Energy Procedia*, vol. 107, pp.297–303, 2017. [CrossRef]
16. LG Electronics, *"LG Neon R", LG 365Q1C-A5 Datasheet*, 2018.
17. V. Energy, "SmartSolar charge controllers MPPT 100/30 & 100/50, " *Victron Smartsolar MPPT 100/50 Datasheet*, 2017.
18. S. A. Studer Innotec, "Xtender series, " *Studer Xtender XTH*, pp. 3000–3012 datasheet, Apr. 2019.
19. P. Wang, Z. Sun, M. C. Vuran, M. A. Al-Rodhaan, A. M. Al-Dhelaan and I. F. Akyıldız, "Topology analysis of wireless sensor networks for sandstorm monitoring, " IEEE International Conference on Communications (ICC), Vol. 2011, 2011, p.1. [CrossRef]
20. M. Mani and R. Pillai, "Impact of dust on solar photovoltaic (PV) performance: research status, challenges and recommendations, " *Renewable and Sustainable Energy Reviews*, vol.14, no. 9, p.3124–3131, 2010. [CrossRef]
21. M. R. Maghami, H. Hizam, C. Gomes, M. A. Radzi, M. I. Rezadad and S. Hajighorbani, "Power loss due to soiling on solar panel: a review, " *Renewable and Sustainable Energy Reviews*, vol. 59, pp.1307–1316, 2016. [CrossRef]
22. J. Tanesab, D. Parlevliet, J. Whale and T. Urmee, "Energy and economic losses caused by dust on residential photovoltaic (PV) systems deployed in different climate areas, " *Renewable Energy*, vol. 120, pp.401–412, 2018. [CrossRef]
23. M. A. M. Ramli, E. Prasetyono, R. W. Wicaksana, N. A. Windarko, K. Sedraoui and Y. A. Al-Turki, "On the investigation of photovoltaic output power reduction due to dust accumulation and weather conditions, " *Renewable Energy*, vol. 99, pp.836–844, 2016. [CrossRef]
24. Y. Guan, H. Zhang, B. Xiao, Z. Zhou and X. Yan, "In-situ investigation of the effect of dust deposition on the performance of polycrystalline silicon photovoltaic modules, " *Renewable Energy*, vol. 101, pp.1273–1284, 2017. [CrossRef]
25. A. Rao, R. Pillai, M. Mani and P. Ramamurthy, "Influence of dust deposition on photovoltaic panel performance, " *Energy Procedia*, vol.54, pp.690–700, 2014. [CrossRef]
26. J. Wang, H. Gong and Z. Zou, "Modeling of dust deposition affecting transmittance of PV modules, " *Journal of Clean Energy Technologies*, vol.5, no. 3, pp.217–221, 2017. [CrossRef]
27. E. Klugmann-Radziemska, "Degradation of electrical performance of a crystalline photovoltaic module due to dust deposition in northern poland, " *Renewable Energy*, vol.78, pp.418–426, 2015. [CrossRef]
28. H. A. Kazem and M. T. Chaichan, "Experimental analysis of the effect of dust's physical propertieson photovoltaic modules in Northern Oman, " *Solar Energy*, vol. 139, pp.68–80, 2016. [CrossRef]
29. S. Ghazi, K. Ip and A. Sayigh, "Preliminary study of environmental solid particles on solar flat surfaces in the UK, " *Energy Procedia*, vol. 42, pp.765–774, 2013. [CrossRef]
30. National Renewable Energy Laboratory, "Distributed generation energy technology operations and maintenance costs." [Online]. Available: https://www.nrel.gov/analysis/tech-cost-om-dg.html. [Accessed: Mar. 15, 2021].
31. A. Walker, et al., "Model of operation-and-maintenance costs for photovoltaic systems, " NREL/TP-5C00-74840. Golden, CO: National Renewable Energy Laboratory, 2020. [CrossRef]
32. A. Nagarajan, R. Thiagarajan, I. Repins and P. Hacke, "Photovoltaic inverter reliability assessment, " NREL/TP-5D00-74462. Golden, CO: National Renewable Energy Laboratory, 2019. [CrossRef]
33. A. Sangwongwanich, Y. Yang, D. Sera and F. Blaabjerg, "Lifetime evaluation of grid-connected PV inverters considering panel degradation rates and installation sites, " *IEEE Transactions on Power Electronics*, vol. 99, pp. 1–10, 2017. [CrossRef]
34. International Renewable Energy Agency (IRENA), "Electricity storage and renewables: Costs and markets to 2030. " [Online]. Available: https://www.irena.org/-/media/Files/IRENA/Agency/Publication/2017/Oct/IRENA_Electricity_Storage_Costs_2017_Summary.pdf?la=en&hash=2FDC44939920F8D2BA29CB762C607BC9E882D4E9. [Accessed: Mar. 16, 2021].
35. National Renewable Energy Laboratory, "Useful life. " [Online]. Available: https://www.nrel.gov/analysis/tech-footprint.html. [Accessed: Mar. 16, 2021].

TEPES
TURKISH JOURNAL OF
ELECTRICAL POWER
AND ENERGY SYSTEMS

TEPES Vol 1., Issue. 2, 69-74, 2021 **DOI:** 10.5152/tepes.2021.21002

RESEARCH ARTICLE

The Effects of Mobile Battery Energy Storage Systems on the Distribution Network

Oğuzhan Karahan, Ali Özan, Mustafa Bağriyanik

Department of Electrical Engineering, Istanbul Technical University, İstanbul, Turkey

Cite this article as: Karahan O, Özan A, Bağriyanik M. The effects of mobile battery energy storage systems on the distribution network. *Turk J Electr Power Energy Syst.* 1(2), 69-74, 2021.

ABSTRACT

Due to the increased penetration of renewable energy sources in the Electricity Distribution Systems, the idea of connecting a storage system to the distribution systems to provide stable electrical energy is becoming widespread. At this point, Battery Energy Storage Systems (BESS) have emerged as an important option. In this study, Mobile Battery Energy Storage System (MBESS), which have features such as providing island operation of the distribution system, responding to faults in a short time, and can be moved to desired areas and temporarily function as a buffer, have been introduced, and their effect on the distribution system has been investigated. Various scenarios with different battery locations and different short circuit types are produced in the study, using the IEEE 13-bus test system. Simulation studies were carried out on the test system for different scenario types, and the effect of the MBESSs operating mode was examined.

Index Terms—Mobile battery energy storage systems, distribution systems, power loss, short circuit fault, voltage drop.

I. INTRODUCTION

The increasing demand for energy day by day reveals that electricity generation facilities should be diversified. The intermittent energy problem in electricity networks, which arises due to the structure of Renewable Energy Systems (RES), is the subject of many new studies. Short-term and long-term analyses are being carried out for RES, which reveal the problem with energy stability. The areas of application of Battery Energy Storage System (BESS), which have been become widespread recently are increasing, with the solutions they offer [1].

The smart grid concept was developed especially in the early years of the twenty-first century. Although countries differ in their smart grid systems, their goals for the grid are common. In the smart grid model, the RES and battery systems can be integrated into the network, and an island operation feature is provided in the network. Thus, it provides higher reliability. In case of a fault that may occur at any point of the network, the BESSs provide island mode operation, so that the effect of the fault can be reliably and quickly eliminated. It is important to determine the appropriate locations for the BESSs to be used to improve the operating conditions of the electricity distribution network. In addition to the objectives such as ensuring continuity in system operation, reducing losses, and regulating the voltage profile, it is necessary to consider the many limitations such as the limits of current-carrying capacity, voltage limits, etc. There are many studies in the literature to solve these problems and optimize the systems, and to determine the location of BESSs and distributed generation units in the network [2].

Various Energy Management Systems (EMS) have been developed in studies considering the intermittent energy problem caused by RES, while designing distribution systems. The BESSs, which are of two types—fixed and mobile—play an important role at this point, because they have features such as improving the voltage quality in the network, providing reactive power support, reducing demand costs according to the density of the loads, and ensuring power balance. In addition to the fixed BESSs, Mobile Battery Energy Storage System (MBESS) have emerged as an option [3].

The aim of integrating MBESSs into an electricity distribution network is to store excess energy, to contribute to a constant power output, and to provide voltage support with reactive power compensation. To evaluate in terms of cost, the use of MBESSs is beneficial because the energy is provided from the battery when electricity is sold at high prices. In addition, MBESSs can be used for consumers who have a high power demand for a short time [4].

Corresponding author: Oğuzhan Karahan, karahanogu@itu.edu.tr

Received: February 5, 2021
Accepted: May 2, 2021
Published online: August 27, 2021

It is becoming increasingly common for electricity generation units to be located close to loads. The RES, especially, provide a more efficient and reliable network structure. This network structure is called a micro-grid. The network structure, which has the feature of self-isolation in case of errors that may occur on the feeder side, stands out with its lower cost. The presence of intermittent energy in micro grids, high production–consumption imbalance between loads, and the difficulty of controlling this situation increase the use of MBESSs [5].

In the literature, methods have been proposed to enhance overall network performance by using BESSs, and the optimal placement, sizing, and operation of the storage units have been studied [6]. The effects of mobile battery systems in battery Electric Vehicles (EV) and plug-in hybrid EVs on the grid were examined in Wong [1]. Optimization has been achieved to solve problems, for instance, by reducing both the power loss and the voltage drop that will occur on the system when the battery system is recharged [1]. In the studies on MBESSs, various optimization methods have been used to obtain optimum results. The Monte Carlo simulation method was used in Abdeltawab and Mohamed [2] during the integration of MBESSs into the network. In Samara [3], using the particle swarm optimization method, the cost analysis of MBESSs on a 41-bus system was performed. Considering the voltage drop and power loss constraints, a system that can work in harmony with the RES has been designed, thanks to the proposed EMS [3]. In Barra [4], an MBESSs with a capacity of 480 kWh and an initial state of charge of 35% was used. Serving 19 customers, the MBESS made an optimum profit of $327/day using the day-ahead forecasting method. In addition to the power loss and voltage drop, which should be considered during the integration of MBESSs into distribution systems, the optimum location, size, and time are important [7]. In Sarıkurt and Balıkçı [8], it was seen that 4% profit was obtained by integrating the MBESSs into the system at the optimum time. It is stated that the algorithm used in this study can be used in large-scale systems.

In Abdeltawab and Mohamed [2], the use of MBESSs is included when the faulty part of the network is isolated from the system and the energy demand is met by distributed generation units. The study focused on reliability analysis. In reliability analysis, the startup time after a fault and the capacity of the storage system are important parameters. It is also assumed that the distribution system is radial, that all switches are reliable, and that two faults do not occur at the same time. Moreover, when the MBESS reaches the fault location, the state of charge is accepted as 50% [2].

Main Points

- The integration of Mobile Battery Energy Storage System (MBESS) into distribution systems has many advantages. However, parameters such as power loss, voltage drop and short circuit must be carefully examined during the integration of MBESSs.
- Optimum MBESSs positioning is very important, especially in short-circuit analysis. It is seen that the short-circuit current changes depending on the location of the MBESSs.
- Since short circuits in electrical distribution systems are instantaneous events, the effects of MBESSs on the current short circuit can be seen more clearly with transient analysis.
- Since loads in a distribution system can vary over time, time series analysis must be made.

The MBESS is connected to different nodes in a simple distribution system in [5]. The effects of MBESSs on the system in case of three-phase fault currents was simulated with the PSCAD/EMTDC program. Considering the test system with four buses, the effects of MBESSs on the system against short circuit faults that may occur in every bus were examined in terms of overcurrent protection [5].

In this study, the MBESSs have been integrated into the 13-bus test system so that analysis can be performed in a larger scale test system. MBESSs were connected to different suitable buses for determining the optimum location. Since power losses and voltage profiles are the most important parameters when designing EMS, the results of these two parameters obtained in case studies were evaluated in the study. In addition, by applying short circuits to different nodes, the behavior of the MBESSs in the system at the time of short circuit was monitored. Most studies in the literature focused on the effect of MBESSs on the energy management system, aiming to optimize the operational cost. In this study, the effect at the time of short circuit has been examined with dynamic analysis.

II. MBESS

In recent years, MBESSs are considered instead of fixed BESSs due to their mobility and easy access to the point of need. The biggest problems seen in BESSs are the high cost and low lifespan. Since small BESSs placed on different load busbars lead to costly undesirable quantities, it may be more advantageous to use a single, large BESSs instead of being placed in pieces. A large BESSs, where determination of the most suitable connection point is much more important, cannot support some parts of the system, especially when the topology of the system is restructured. At this point, MBESSs, which can be transported to the desired area, are more useful than the fixed BESSs [3]. The MBESSs have many benefits, from the manufacturer to the consumer.

A. Benefits for Utility

- High power quality is provided due to the low voltage loss.
- Less power loss and thus high efficiency is achieved.
- When there is high demand, the need for grid power is reduced.
- Optimal usage of grid power is ensured.

B. Benefits for Consumers

- The high cost caused by the load imbalance is reduced.
- In case of faults, reliability is provided with fast intervention.
- The network can be operated in island operating mode.

C. Benefits for Society

- They provide ease of access to remote areas within the distribution network.
- Business efficiency can be increased by reducing interruptions due to faults.

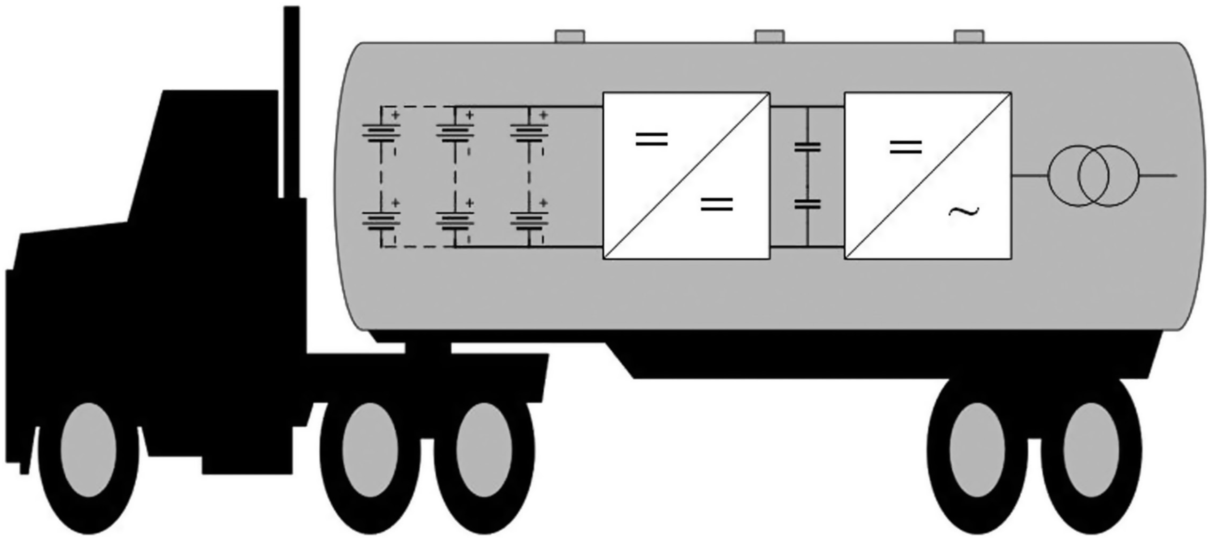

Fig. 1. Representative MBESS.

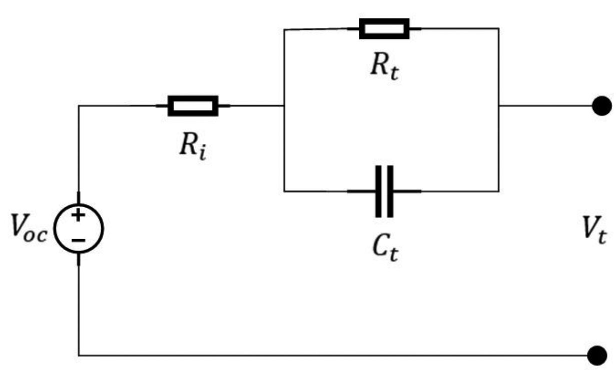

Fig. 2. Battery equivalent circuit model.

- Private individuals/companies enable the development of the free market structure with the operation of MBESSs.
- EVs are encouraged. Thus, a conscious society is formed in order to provide clean energy [8].

The MBESSs consist of two parts, the carrier vehicles and the storage systems, and are connected with the network by first using a DC/DC/AC bidirectional converter. In addition, there is a DC/DC converter, which is a current-controlled Buck–Boost converter, and a control device in the EMS that regulates the power of the battery in charge/discharge situations [3]. The MBESSs, whose general structure is described, can be seen in Fig. 1.

A simple equivalent circuit model of the battery is given in Fig. 2. The model, consisting of internal resistance and a resistor–capacitor block between open circuit voltage and terminal voltage, is used as the general battery model [9].

The idea of Vehicle for Grid (VfG) is becoming widespread. Compared to EVs and the Energy Storage System (ESS), the VfG increases network reliability, is more environment friendly, and provides economic gain to the distribution and production system. Structures with two operating systems, the Vehicle to Grid (V2G) and the Grid to Vehicle (G2V), are separated from the ESSs. The ability to operate in the optimum location and at the optimum time will increase the use of VfGs instead of EVs with external chargers. In an electricity network, the VfGs are MBESSs that provide economic gain in terms of generation and distribution units. They differ from fixed BESSs thanks to their mobile feature. This mobility provides advantages such as load shifting in the network, fast response in case of fault, and island operation [10].

The MBESSs, which are used to provide an island operation feature, can feed the isolated region in case of any fault in the network. The MBESSs act as a temporary buffer until distributed generation units provide energy support again. Some parameters of MBESSs are taken into consideration in long-term dynamic investigations. These are given in Equations 1, 2, and 3 [11]:

$$t_{up\_MBESS} = k_{traff} \frac{D}{S_{MBESS}} + t_{install} \tag{1}$$

where t_{up_MBESS} represents the startup time of MBESSs after fault (*h*), k_{traff} represents traffic condition factor, *D* represents distance between starting location and fault location (*km*), S_{MBESS} represents movement speed (*km/h*) and $t_{install}$ represents installation time (*h*):

$$\Delta E(t) = \int_{t}^{t+\Delta t} \left[P^{Dis\backslash Chr}(t) - \eta_c \left| P^{Dis\backslash Chr}(t) \right| \right] dt \tag{2}$$

where *E* represents the energy stored in the battery (*MWh*), $P^{Dis\backslash Chr}$ represents the charge\discharge power of the battery (*MW*), η_c represents the charge losses (*%*), and Δt represents the time interval (*hs*):

$$SoC(t) = \frac{E(t)}{E_r} \tag{3}$$

where $SoC(t)$ represents the charge level of the battery at time *t* (*%*), *E(t)* represents the energy stored by MBESSs at time *t* (*MWh*), and E_r represents the storage capacity of the MBESSs (*MWh*) [11].

III. EFFECTS OF MBESS ON THE DISTRIBUTION NETWORK

The MBESSs have many effects on distribution systems. Some of the most important effects are on total power loss, voltage drop, and short circuit currents. Reducing the total power loss is one of the most important goals in distribution systems. The power loss in the system can be calculated as in Equation 4:

$$P = \sum_{j=1}^{n} R_j \times I_j^2 \tag{4}$$

where *P* represents the total active power loss on the distribution lines, (*kW*), R_j represents the resistance of the *j*th line (*Ω*), and I_j represents the current of the *j*th line (*A*).

When examining energy distribution systems, another important parameter is the voltage drop. While providing electrical energy to the loads in the network, the voltage values at the nodes must comply with the limits. According to the standards, the voltage range should be between 0.95 and 1.05 pu [12]:

$$\Delta V_{ij} = V_j - V_i \tag{5}$$

where ΔV_{ij} represents the voltage drop on the line between buses *i* and *j* (*V*), V_j represents voltage of the *j*th node (*V*), and V_i represents voltage of the *i*th node (*V*).

The integration of distributed generation units in energy distribution systems can affect the magnitude and direction of the fault current during short circuit. In the literature, although there are studies on balanced fault currents, there are also studies dealing with the effect of unbalanced fault currents. The MBESSs, whose locations can be changed, also have an effect on short circuit currents [13].

IV. CASE STUDY

In the study, the IEEE 13-bus test system was used. The system includes a single feeder, a regulator, two step-down transformers, and nine loads. There are 115, 4.16, and 0.48 kV voltage values in the test system. In addition, a 500 kW MBESS was used in the study [14]. The OpenDSS program was used in the simulation studies. The test system that exists in the software's library is shown in Fig. 3.

Analyses in OpenDSS program were carried out in dynamic mode. Various scenarios have been produced in order to observe the effect of MBESSs on the distribution system. First of all, the battery is examined in scenarios where there is no short circuit fault. Then, the total power loss and maximum voltage drops in the system are determined for the cases in which there is no battery and the battery operates in discharge mode, and at various locations. In addition, by applying two different short circuit types to different locations, the fault current values for different battery locations are determined.

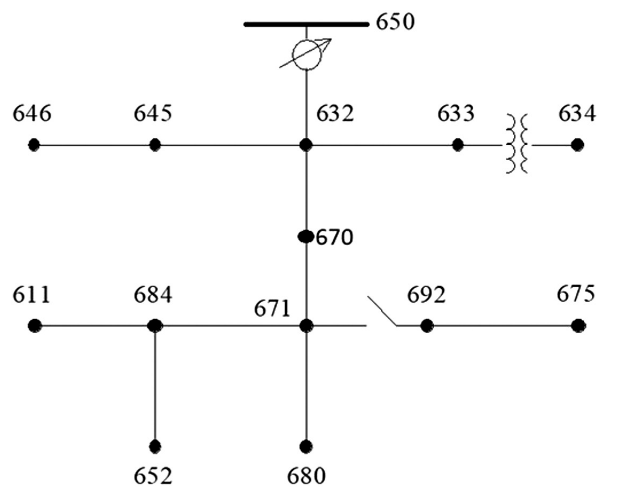

Fig. 3. IEEE 13-bus test system.

The graph representing the total power loss for the scenarios of the basic case, where there is no battery, and the location of the battery to the three-phase buses, is shown in Fig. 4. Batteries are located at three-phase nodes in the distribution system. When Fig. 4 is examined, the power loss in the system in the basic substation without battery is noted as 110.5 kW. As the location of the battery moves away from the feeder, the total power loss in the system decreases. When the battery is located on the bus number 675, which is the node farthest from the feeder, the total power loss in the system is calculated to be at least (85 kW).

The graph of the maximum voltage drops obtained for different scenarios is given in Fig. 5. When Fig. 5 is examined, the maximum voltage drop in the base case without a battery is measured as 2.503%. The battery is operated in the discharge mode, like a generation unit. As the battery system is positioned far from the feeder, the voltage drop decreases, depending on the loads. Accordingly, the least voltage drop is seen whevn the battery is positioned at the farthest point from the feeder, as expected. While the least voltage drop is seen in bus 675, and its value is 1.809%.

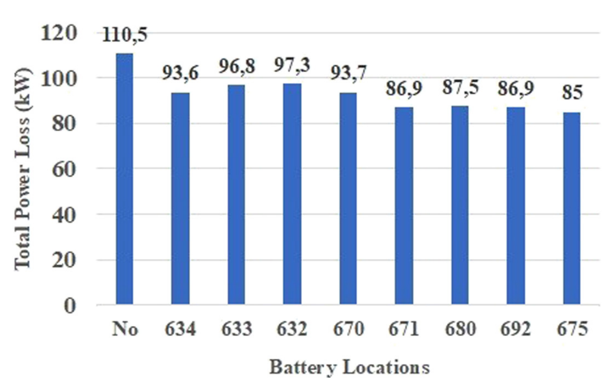

Fig. 4. Total power losses according to battery locations.

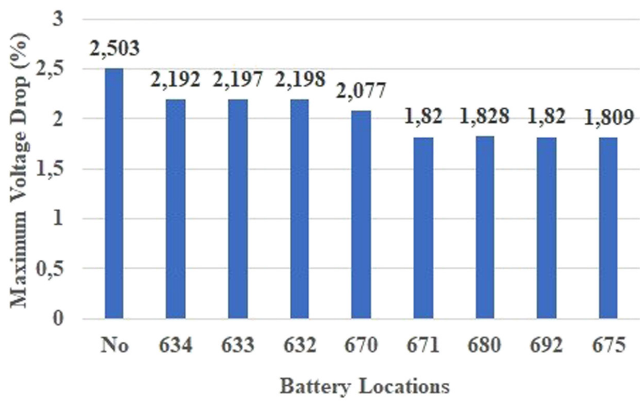

Fig. 5. Maximum voltage drops according to battery locations.

The effect of the change of the battery location on the fault currents are observed when different short circuit faults are applied. For the case where the short circuit fault is in bus 632, the single phase-ground and three-phase fault current values in scenarios with no battery and different battery locations are shown in Fig. 6. As can be seen clearly in Fig. 6, the three-phase short circuit fault current is higher than the single phase-ground short circuit fault current. Positioning the battery close to the fault location slightly increases the fault current.

For the case where the short circuit fault is in bus 671, the single phase-ground and the three-phase fault current values in scenarios with no battery and different battery locations are shown in Fig. 7.

Adding the battery to the system increases the fault current in two different short circuit types. As can be seen in the graph in Fig. 7, the three-phase short circuit fault current is 5746 A in the base case without the battery, and it is calculated as 5787.2 when the battery is connected to bus 634.

In the analysis made with dynamic mode in OpenDSS, the fault current graph in the scenario where the short circuit fault is at 671 and the battery is at 633 is shown in Fig. 8. While a short circuit fault occurs in the system in 0.5 seconds, the protection element separates

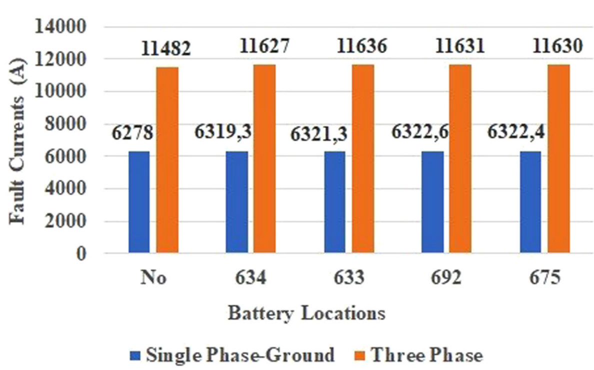

Fig. 6. In case of short circuit faults at 632, fault currents according to battery locations.

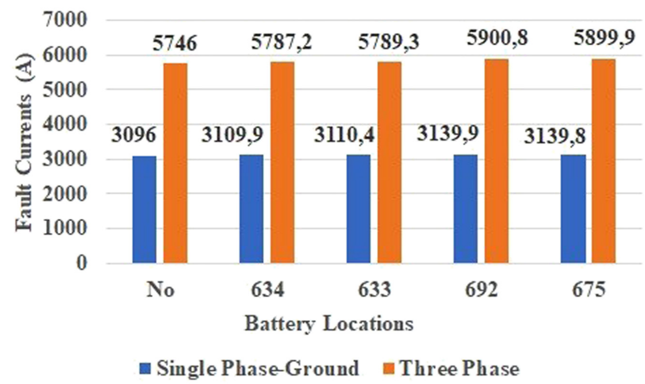

Fig. 7. In case of short circuit faults at 671, fault currents according to battery locations.

the faulty part from the system with a delay of 0.1 seconds. After the faulty part is separated from the feeder network, the effect of the fault current of the battery is seen. In Fig. 8, black represents phase current 1 (I_1), red represents phase current 2 (I_2), and blue represents phase current 3 (I_3).

In the scenario without connecting any battery units, when a short circuit fault occurs in bus 671, the fault current is calculated as 5746 A at most. During the scenario, represented by the graph in Fig. 8, the fault current reaches a maximum of 5789 A. This result shows that the battery has an additional effect of 43 A on the system.

V. CONCLUSION

Most studies in the literature focused on the effect of MBESSs on the energy management system with an aim to optimize the operational cost. In this study, the distribution system with MBESSs has been examined to find the impact of faults on the distribution system. The

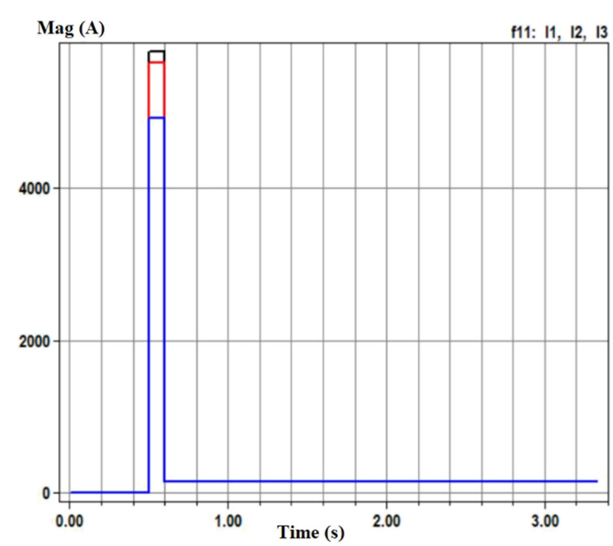

Fig. 8. In case of a short circuit fault at bus 671 and battery at bus 633, the graph of fault current.

integration of MBESSs into electrical distribution systems and their effect on parameters such as power loss, voltage drop, and short circuit current in the distribution system were obtained for different scenarios, tested on the IEEE 13-bus test system.

According to the simulation results obtained using OpenDSS program, the effects of MBESSs on distribution systems in different battery locations are interpreted as follows;

- When the scenarios are analyzed, a maximum decrease of power loss (23.07%) was observed compared to the base case.
- All bus voltages remained within the limits for considered scenarios.
- It has been observed that the location of the battery has little effect on the short circuit current. It is concluded that optimum battery placement is important at this point.

It will be useful to perform a time series analysis to deal with the effects in more detail and to study transient analysis to see the effect of MBESSs on the system in case of abnormal conditions, such as faults and overloads.

Peer-review: Externally peer-reviewed.

Conflict of Interest: The authors have no conflicts of interest to declare.

Financial Disclosure: The authors declared that this study has received no financial support.

REFERENCES

1. Y. S. Wong, L. L. Lai, S. Gao and K. T. Chau, “Stationary and mobile battery energy storage systems for smart grids,” *2011 4th International Conference on Electric Utility Deregulation and Restructuring and Power Technologies (DRPT)*, July, 2011, pp. 1–6, 2011. [CrossRef]
2. Y. Chen, Y. Zheng, F. Luo, J. Wen, and Z. Xu, “Reliability evaluation of distribution systems with mobile energy storage systems,” *IET Renew. Power Generation*, vol. 10, no. 10, pp. 1562–1569, June, 2016. [CrossRef]
3. H. H. Abdeltawab and Y. A. I. Mohamed, "Mobile Energy Storage Scheduling and Operation in Active Distribution Systems," *IEEE Transactions on Industrial Electronics*, vol. 64, no. 9, pp. 6828–6840, March, 2017. [CrossRef]
4. S. M. Samara, M. F. Shaaban and A. Osman, "Management of Mobile Energy Generation and Storage System," *2019 IEEE PES GTD Grand International Conference and Exposition Asia (GTD Asia)*, March, 2019, pp. 450–454, March, 2019. [CrossRef]
5. P. H. A. Barra, G. P. Campos, D. V. Coury, M. Oleskovicz, and M. Biczkowski, “Mobile battery energy storage systems influence on overcurrent protection of distribution networks,” *SBSE 2018 - 7th Brazilian Electrical Systems Symposium*, May, 2018, pp. 1–6, 2018. [CrossRef]
6. H. Abdeltawab and Y. A. I. Mohamed, "Mobile Energy Storage Sizing and Allocation for Multi-Services in Power Distribution Systems," *IEEE Access*, vol. 7, pp. 176613–176623, December, 2019. [CrossRef]
7. Choton K. Das, Octavian Bass, Ganesh Kothapalli, Thair S. Mahmoud, Daryoush Habibi, “Overview of energy storage systems in distribution networks: Placement, sizing, operation, and power quality,” *Renewable and Sustainable Energy Reviews*, vol 91, pp. 1205–1230, August, 2019. [CrossRef]
8. H. Saboori and S. Jadid, “Optimal scheduling of mobile utility-scale battery energy storage systems in electric power distribution networks,” *Journal of Energy Storage*, vol. 31, pp. 101615, October, 2020. [CrossRef]
9. T. Sarıkurt and A. Balıkçı, “A relative capacity estimation method for lithium batteries used in electric vehicle applications,” *Pamukkale University Journal of Engineering Sciences*, vol. 24, no. 5, pp. 809–816, January, 2018. [CrossRef]
10. M. Rahmani-Andebili, “Vehicle-for-grid (VfG): A mobile energy storage in smart grid,” *IET Generation Transmission Distribution*, vol. 13, no. 8, pp. 1358–1368, April, 2019. [CrossRef]
11. Y. Zheng et al., “Optimal integration of mobile battery energy storage in distribution system with renewables,” *Journal of Modern Power Systems and Clean Energy*, vol. 3, no. 4, pp. 589–596, August, 2015. [CrossRef]
12. Eurelectric Union of electrcity industry, “Application guide to the European Standard EN 50160 on ’voltage characteristics of electricity supplied by public distribution systems,” *Electricity Product Characteristics and Electromagnetic Compatibility*. Ref:23002Ren9530, July, 1995.
13. C. Su, Z. Liu, Z. Chen and Y. Hu, "Short circuit analysis of distribution system with integration of DG," 2014 International Conference on Power System Technology, October, 2014, pp. 2921–2926. [CrossRef]
14. D. B. Technology, “*Mobile Energy Storage*”. Accessed date: 15 April 2021. [Online]. Available: https://www.res-group.com/media/342353/mobile_energystorage_28319.pdf

TEPES
TURKISH JOURNAL OF
ELECTRICAL POWER
AND ENERGY SYSTEMS

TEPES Vol 1., Issue. 2, 75-83, 2021 **DOI:** 10.5152/tepes.2021.21018

RESEARCH ARTICLE

Design and Control of a PV-FC-BESS-Based Hybrid Renewable Energy System Working in LabVIEW Environment for Short/Long-Duration Irrigation Support in Remote Rural Areas for Paddy Fields

Kumaril Buts, Lillie Dewan, Modi Pandu Ranga Prasad

National Institute of Technology, Kurukshetra, India

Cite this article as: Buts K, Dewan L, Prasad M. Design and control of a PV-FC-BESS-based hybrid renewable energy system working in LabVIEW environment for short/long-duration irrigation support in remote rural areas for paddy fields. *Turk J Electr Power Energy Syst.* 1(2), 75-83, 2021.

ABSTRACT

The reduction of carbon-based energy consumption is one of the critical challenges of the 21st century. The development of efficient and reliable renewable energy is a significant task of this century. Green revolutions boost agriculture and are responsible for a drastic change in grain production, enhancing energy consumption due to optimum use of the agriculture machinery, basically for irrigation purposes. The scope of this paper is to present a Hybrid Renewable Energy System (HRES) that is capable of replacing the diesel pump commonly used for time-bound irrigation, as in the paddy field for rice production. The proposed experimental HRES system consists of a photovoltaic (PV) generator, a fuel cell (FC), and a battery energy storage system (BESS). This system can provide 0.4 kW, single-phase electrical power, tested under varying solar radiation and load demand conditions, suitable for all-weather electrical irrigation pumps of up to 0.5 HP capacity. Controlling of this hybrid system is carried out in the LabVIEW environment.

Index Terms—Battery energy storage system, controlling, hybrid renewable energy system, irrigation pump.

I. INTRODUCTION

Human development is continuous and is directly proportional to the rate of energy consumption. Green energy supply is a forced demand in this present era. Green revolutions boost agriculture and are responsible for a drastic change in grain production, enhancing energy consumption due to optimum use of the agriculture machinery, basically for irrigation purposes. Agriculture is unique because it accounts for 4 to 8 percent of the total energy demand [1] and is susceptible to energy demand. A very famous quote that is often used, is "Everything can wait, but not agriculture", and this quote is highly justified in rice production. On average, about 2500 L of water need to be supplied for a paddy field to produce 1 kg of rough rice (by rainfall and/or irrigation) [2]. During the rice crop's reproductive stage, a water level of a minimum of 10 cm is required to be maintained in the paddy field for at least 20–30 days [3].

Apart from rainwater, farmers are dependent on other irrigation methods. A diesel pump is one of the options for drawing the water from a deep bored well. Diesel pumps are costly and have an adverse impact on the environmental and ecological systems.

A renewable energy-based hybrid system can deliver a constant power supply at the desired load level and can be used to support irrigation. Various renewable energy genres, including wind systems, photovoltaic (PV) cell, fuel cell (FC) (basically hydrogen fuel cell (HFC)), natural gas-based plant, and battery storage system, are well established and enjoy the advantages of matured technology [4].

PV technology is beneficial for places where ample sunshine is available, and grid-support is not available or limited. However, PV-generators are also installed nowadays in grid-tied distribution areas for reducing coal-linked power demand. The power generated by a PV system is highly dependent on the availability of sunny hours. It isn't easy to store the energy generated for future use (i.e., during cloudy days or at night). For reliable operation, other alternate power sources such as FC systems, hydrogen storage tanks, or battery energy storage systems (BESS) must be integrated with a PV system [5,6].

Corresponding author: Kumaril Buts, Kumaril_61900052@nitkkr.ac.in

Received: March 31, 2021
Accepted: May 4, 2021
Published online: August 27, 2021

The HFC is comparatively an old technology which is now at a mature stage. HFC is beneficial for those areas where days of sunshine are less frequent or insufficient to fulfil the continuous load demand. Of the different FC power plants, such as the solid oxide fuel cell (SOFC), molten carbonate fuel cell (MCFC), phosphoric acid fuel cell (PAFC), proton-exchange membrane fuel cell (PEMFC), and others, the PEMFC power plant is preferred. It has been found very suitable, especially for a hybrid energy system [7,8].

Integrating the FC power plant with a battery storage system is economical, rather than using either of them individually. Without a battery system, the FC system must cater to all power demands, which will increase the FC power plant's size and cost, with a reduction in the performance and life due to overloading. The same holds true when the BESS is used alone. In [9], a detailed dynamic model, the design, and simulation of a hybrid energy system have been discussed, with the conclusion that the battery-supported system has some unique features and advantages over systems without battery support.

A PV system for small-scale applications, such as water pumping, street lighting, and irrigation applications in non-grid-supported remote rural areas, is discussed in Sukamongkol and Chungpaibulpatana [10].

A comprehensive technical analysis related to the combined operation of solar PV, wind power, and HFC has been carried out in Zahedi [4], and suggestions have been offered on some technical difficulties regarding the interconnection of hybrid energy sources and their solutions.

Nowadays, control operations performed in the LabVIEW environment are gaining more attention than other software platforms. in Andreadou and Bonavitacola [11], an efficient method for residential load scheduling and control for smart homes in the LabVIEW environment has been presented. PV generator modeling and simulation, working in the LabVIEW platform for small power supply, is presented in Bendib et al. [12]. User-friendly operation and real-time data availability are some of the inherent features of the LabVIEW environment.

A PV, FC, and BESS-based hybrid system is proposed in this paper to irrigate paddy crops. The proposed hybrid system has been simulated in MATLAB/Simulink and implemented on the hardware available in the School of Renewable Energy & Efficiency (SREE) laboratory, NIT, Kurukshetra, India, in the LabVIEW environment, and tested under varying solar radiation and load demand conditions. The combination of FC-BESS with the PV system is an attractive choice due to the high efficiency, fast load–response, cost-effectiveness and reliable operation.

This paper is organized into five sections: after a brief introduction in section 1, and section 2 describes the configuration and behaviour of the elementary components in the proposed system. Section 3 describes the system, and gives a brief idea about the PV-system, FC system, BESS, DC micro-grid, and their controlling techniques, respectively. Section 4 deals with the system's software and hardware development, followed by a conclusion in section 5, and references.

II. PROBLEM STATEMENTS

A comprehensive field study was carried out with the local farmers' help in the southern area of Bihar, a province of India, where paddy is a major food grain produced during the monsoon season. Some parts of this southern zone are hilly, and are not supported by the national grid. From valuable information provided by the paddy farmers, it is concluded that:

1. The rice crop needs approximately 10 mm of water per day.
2. During the rice crop's reproductive time, it is desirable to maintain a water depth at a minimum of 10 cm for at least 20–30 days in the paddy field.

The water requirement of a rice crop is calculated using simple water balance models [3], which include different inflows and outflows of water in a paddy field.

$$ER + I = ET + P + S + SD + CWS \tag{1}$$

where *ER*, effective rainfall; *I*, irrigation supply; *ET*, evapotranspiration loss; *P*, deep percolation loss; *S*, seepage loss; *SD*, surface drainage or run-off loss; and *CWS*, change in water status.

From Equation 1, it is clear that if adequate rainfall is not available, water balance solely depends on irrigation.

By simple calculation, 1 mL of water is required to maintain 10 cm water depth in a 1-ha area of paddy field. The water pump with performance and technical specifications given in Table I will be sufficient, as it will fulfill the water demand within 2–3 hours. Therefore, an irrigation pump of this capacity can be considered ideal for time-bound paddy field irrigation.

Thus, the problem statement is to design a hybrid renewable energy system (RES) comprising PV, FC, and BESS, producing a 0.4 kW continuous supply (day/night & all-weather) to overcome the diesel pump's irrigation cost and adverse environmental impact. This

TABLE I
PERFORMANCE OF A TYPICAL 0.5HP SINGLE-PHASE IRRIGATION WATER PUMP

Specifications	Descriptions
Power rating	0.5 HP (0.37 kW)
Full load current	4 A
Rated voltage	210 V
Water head	4 m
Discharge	15.5 Liters per second (LPS)

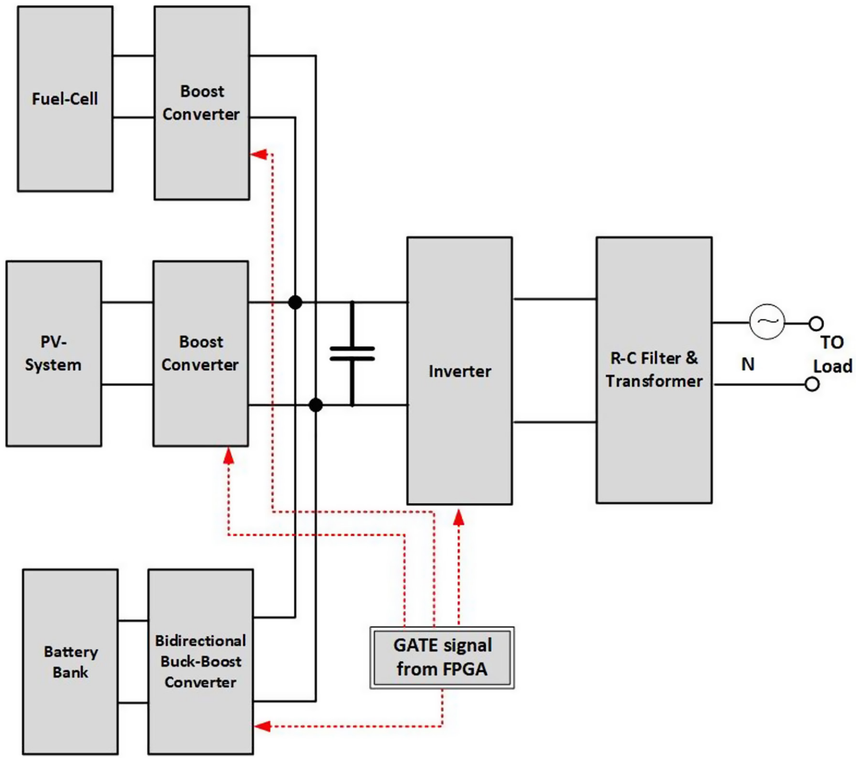

Fig. 1. Line diagram of the hybrid Renewable Energy System (hybrid RES).

system's advantages are that it will be cost-effective, efficient, and reliable for irrigation support, and provide electric power for home illumination when not used for irrigation.

In the next section, a brief description of this hybrid system's components and working is given.

III. SYSTEM DESCRIPTIONS

This proposed hybrid system contains a PV generator, a FC, and a battery system stack. A line diagram of this proposed hybrid system is shown in Fig. 1.

A. The PV System

The illumination of the common junctions between two different materials by photon irradiation, producing electrical potential, is termed a PV effect [13,14]. The electrical characteristics of a PV system can be well illustrated with single- and two-diode models. The single diode model is popular and close to the PV cell's actual behavior [14,15].

Based on the single-diode model, mathematical modeling of the PV system output voltage is expressed as [14],

$$V_{PV} = \frac{N_S n k T}{q} \ln\left[\frac{I_{SC} - I_{PV} + N_P}{N_P I_0}\right] - \frac{N_S}{N_P} R_S I_{PV} \tag{2}$$

where N_S, the number of series cells per string; n, ideality factor; k, Boltzmann constant [J/deg.K]; T, PV cell temperature [deg.K]; q, electronic charge [C]; I_{SC}, short-circuit cell current [A]; I_{PV}, PV cell output current [A]; N_P, the number of parallel strings; I_0, PV cell reverse saturation current [A]; and R_S, series resistance of the PV cell [Ω].

B. The HFC

A FC is an electrochemical device that, like any battery, converts chemical energy into electrical energy [7]. The overall FC is composed of several cells stacked as a single unit [7,15]. An FC power plant uses oxygen and hydrogen as reactants to convert chemical energy into electrical energy.

In the proposed system, mathematical modeling of the HFCs is implemented based on Nernst's instantaneous voltage output equation [7], expressed as:

$$E = N_O\left[E_0 + \frac{RT}{2F}\log\left[\frac{pH_2\sqrt{pO_2}}{pH_2O}\right]\right] \tag{3}$$

where N_O, number of series FCs in the stack; E_0, standard no-load voltage [V]; F, Faraday constant [C/kmol]; R, Universal gas constant [J/kmol K]; T, absolute temperature [K]; pH_2, hydrogen partial pressure [atm]; pH_2O, partial water pressure [atm]; and pO_2, oxygen partial pressure [atm].

C. BESS

A battery is simply an electrochemical cell that produces electrical energy by chemical reactions [16]. A BESS is a stack of cells connected in series or parallel to provide the desired voltage or current level demand.

The battery voltage, V_{Batt}, is calculated separately by two different equations for the charging and discharging modes [17]. The mathematical modeling of the battery characteristics has been accomplished based on equations 4, 5 & 6 [9,17].

$$V_{Batt(charge)} = V_O - \frac{KQ_{max}}{0.1Q_{max} - q} i^* - \frac{KQ_{max}}{Q_{max} - q} it + A\exp(-Bq) \quad (4)$$

$$V_{Batt(discharge)} = V_O - \frac{KQ_{max}}{Q_{max} - 1} i^* - \frac{KQ_{max}}{Q_{max}} t + A\exp(-Bq) \quad (5)$$

where V_O, constant output voltage of the battery [V]; K, the polarization constant [$(Ah)^{-1}$]; Q_{max}, maximum capacity of the battery [Ah]; i^*, reference current [A]; i, measured (actual) current [A]; q, the available capacity of the battery[Ah]; A, exponential voltage [V]; and B, exponential capacity [$(Ah)^{-1}$].

The state of the charge of the battery (SOC_{Batt}) is calculated as:

$$SOC_{Batt} = 100\left(1 - \frac{\int i(t)dt}{Q}\right) \quad (6)$$

where i, instantaneous current [A]; and Q, charge stored [C].

D. DC Micro-Grid

The solar PV system and the HFC act as a DC source and are connected to a DC-link capacitor with a boost converter, while a battery bank also acts as a DC source. It is connected to the DC link via a bidirectional converter.

The voltage source converter (VSC) plays a vital role between the DC-link voltage and the AC loads, acting as a temporary power storage device to provide the voltage source inverter with a steady flow of power. The capacitor's voltage is regulated using a DC-link voltage control loop that balances the capacitor's input and output power. In the proposed hybrid RES system, the VSC controller has a phase-locked loop (PLL) to synchronize the DC power with the load frequency [18,19].

The reference currents and measured currents of the VSC are compared, and are given to relay-based hysteresis controllers. These hysteresis controllers generate the switching logic for the IGBTs of VSC in the manner shown in Table II [20].

TABLE II
SWITCHING LOGIC OF THE HYSTERESIS CONTROLLER

Switching State	Gate Pulse
I^*_{refA}-$i^*_{measuredA}$> upper band	g_1
I^*_{refA}-$i^*_{measuredA}$< lower band	g_4
I^*_{refB}-$i^*_{measureB}$> upper band	g_3
I^*_{refB}-$i^*_{measuredB}$< lower band	g_2

E. Power Converters

In this proposed system, the PV generator and the FC output voltage and current are controlled using a boost converter. The pulse width modulation (PWM)-controlling technique is commonly used to control the boost converters and the inverter's output voltage. A full-bridge voltage–source inverter with four IGBT-based power switches is used here for DC to AC power conversion. A bidirectional buck–boost converter is used for charging and discharging of the battery. The output of this bidirectional converter is connected to the inverter through the DC link.

F. Field-Programmable Gate Array

A field-programmable gate array (FPGA) provides the most convenient way of designing the PWM generator for power converters. FPGAs are like a digital circuit that can be electrically coded to obtain the required modulation signals [21].

In this proposed system, an FPGA-based micro-controller chip is used for generating and controlling the gate pulses with the help of Very High-Speed Integrated Chip Hardware Description Language (VHDL) physical architecture. The VHDL code for the PWM generator is written using the Xilinx ISE 10.1software.

IV. IMPLEMENTATION

The proposed hybrid system is simulated on MATLAB/Simulink2017A and then implemented on the hardware available in the laboratory of SREE, NIT Kurukshetra, India, in the LabVIEW2018environment.

This hybrid system consists of five components: the PV generator, the FC, the BESS system, power converters with specifications given in Table III, and the control section.

The PV system based on four mono-crystalline modules connected in series can generate up to 1 kW. Each module can generate 250 W of peak power. Rating of the PV generator chosen is based on exploiting its maximum benefit within the economic boundary.

The maximum power output of the HFC with a total of 48 cells connected in series is up to 1 kW.

The BESS consists of 12 Li-ion battery units connected in series. The total output capacity of the BESS system is up to 1 kW. The RL load of 0.4 kW active power-drawing capacity equivalent to the load of the desired irrigation pump capacity has been used to verify the performance of the proposed HRES.

A. MATLAB Implementation

The MATLAB Simulation arrangement, as shown in Fig. 2, is developed based on the mathematical modeling, equations from (2) to (6), and the line diagram of the system as shown in Fig. 1. Rating of the components in MATLAB is taken precisely, like that of the hardware setup.

TABLE III
RATINGS OF THE COMPONENTS OF THE HARDWARE SETUP

Field-Programmable Gate Array (FPGA) Box		
1.	Control card technology	FPGA
2.	Pull-up card for inverter gate firing	8 Pulse-Width Modulation (PWM) signals
Single-phase inverter		
1.	Maximum DC input voltage	150 V
2.	Output voltage	100 V AC
3.	Output current	5 A
4.	Switching frequency	10 kHz
LC filter for the single-phase inverter		
1.	Inductor	3 mH, 10A
2.	Capacitor	10 μF
PhotoVoltaic (PV) system specifications and ratings		
1.	Number of channels	2
2.	Short-circuit current per channel	0–20 A
3.	Open-circuit voltage per channel	0–50 V DC
4.	Maximum output power per channel	500 W
Boost converter for PV system		
1.	Input voltage	50 V
2.	Input current	20 A
3.	Output voltage	150 V
4.	Output current	10 A
5.	Switching frequency	20 kHz
Fuel cell components		
1.	Type of the fuel cell	Proton Exchange Membrane (PEM)
2.	Number of cells	48
3.	Rated power	1000 W
4.	Performance	28.8 V and 35 A
5.	Reactants	Hydrogen and air
6.	Maximum stack temperature	65°C
7.	Flow rate at maximum output	13 Liters per minute
Boost converter for fuel cell		
1.	Input voltage	28.8 V at full load
2.	Input current	35 A at full load
3.	Output voltage	150 V
4.	Output current	10 A
5.	Switching frequency	20 kHz
Battery energy storage system (BESS)		
1.	Battery type	Lead-acid
2.	Number of batteries	8, connected in series
3.	Overall output voltage	96 V
4.	Overall capacity	26 Ah
Bidirectional buck-boost converter for BESS		
1.	Input voltage	105 V (battery side)
2.	Output voltage	150 V (inverter side)
3.	Output current	10 A
4.	Switching frequency	20 kHz

B. Hardware Implementation

Based on the MATLAB model, hardware implementation is carried out in the laboratory, under varying solar radiation and load demand conditions, as shown in Fig. 3. The solar radiation and power demand data are based on real-world records.

Controlling the hardware components is carried out in the LabVIEW environment, and a simplified and user-friendly control panel is developed. A personal computer (PC) and an FPGA-based micro-controller placed in the hardware setup communicate with a LAN/ethernet cable.

C. Results and Discussions

The real-time data obtained from the hardware setup with a LabVIEW-based data analyzer and data stored in the Excel sheet is plotted with the help of the graph-plotter.

For power storage or to mitigate the load demands, the battery is operated in charging/discharging mode. Output voltage and current with frequency are captured on a real-time power analyzer (HIOKI 3360 series) during the battery charging and discharging time, respectively.

Comparative analyses (quantitative and qualitative) of the MATLAB simulation and the hardware results, as shown in Fig. 4 and 5, summarized in Table IV, provide the following important information:

- Battery charging/discharging activity during the load change is fast and responsive.
- The system is stable and fulfills the desired load demands.
- Frequency remains within the limit with ± 5% tolerance, which is acceptable.

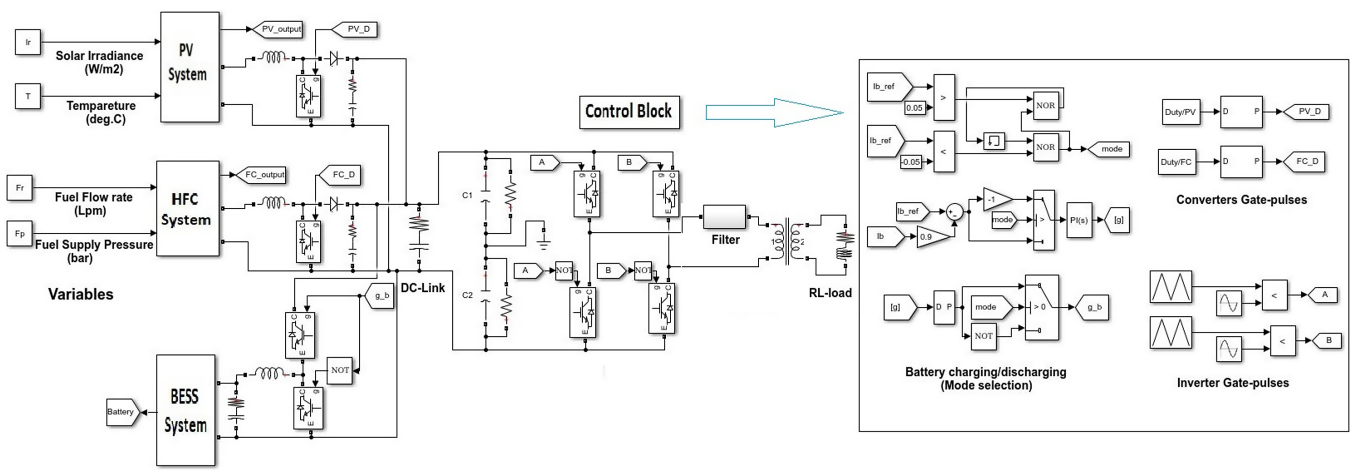

Fig. 2. Simulation arrangement of the hybrid Renewable Energy System.

- MATLAB model of the system mimics the behavior of the actual hardware setup. It can be said that desired system can generate sufficient power to run the irrigation pump.
- From Table IV, it has been observed that the performance of the battery in HRES has good transient and steady-state characteristics.
- The limitation in the system designed is that it provides a limited load demand. However, the design can be expanded to mitigate the higher load by changing the components' rating. During the off-irrigation period, the proposed HRES system can illuminate farms and homes.

V. CONCLUSION

The PV/FC/BESS hybrid power system designed and modeled for irrigation purposes is suitable not only for paddy fields but also for any crop. This hybrid system works in a standalone mode with controlling activity in the LabVIEW environment.

The hybrid system's dynamic behaviors have been tested under varying solar radiation and load demand conditions, where the solar radiation and power demand data are based on real-world records. The LabVIEW-based control strategy for the developed system is efficient and exhibits excellent performance, even for extended periods.

Fig. 3. Hardware setup of the hybrid Renewable Energy System in the lab (a) Converters and inverter setup; (b) Battery stack; and (c) FC & PV emulator connected with the system).

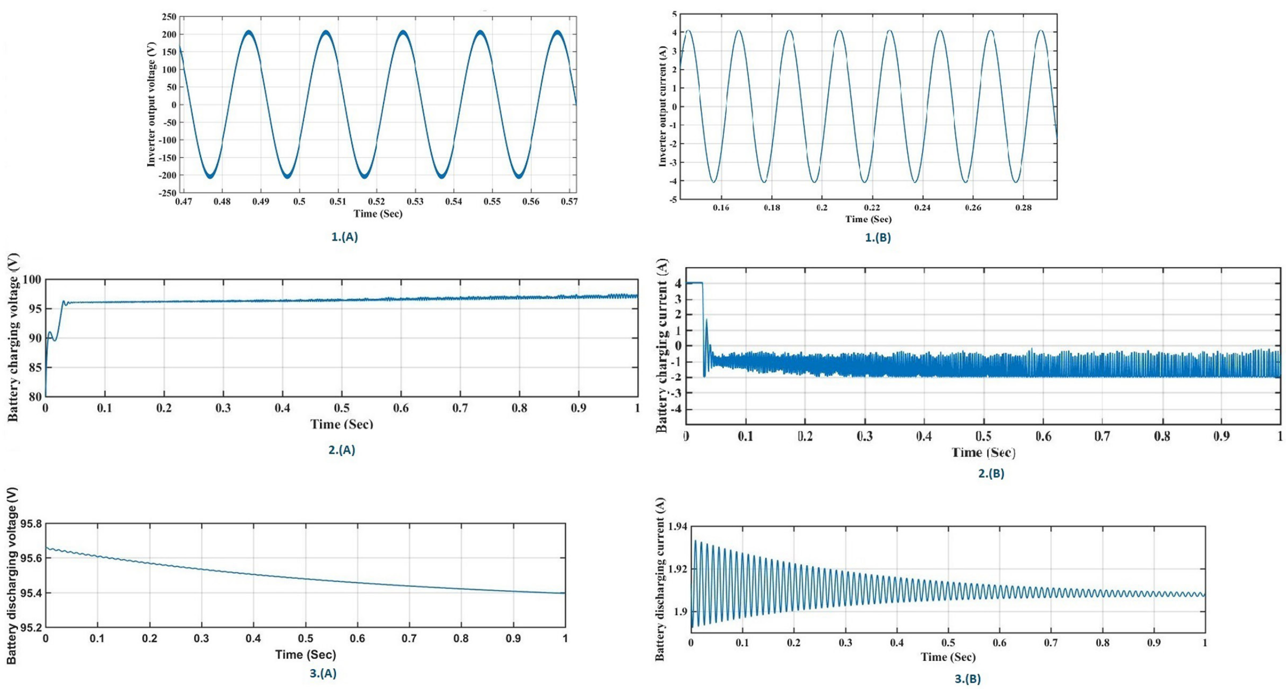

Fig. 4. Simulation results of the MATLAB model of the hybrid Renewable Energy System (1(a) and 1(b): Inverter voltage and current output; 2(a) and 2(b) Battery voltage and current during charging; and 3(a) and 3(b) Battery voltage and current during discharging).

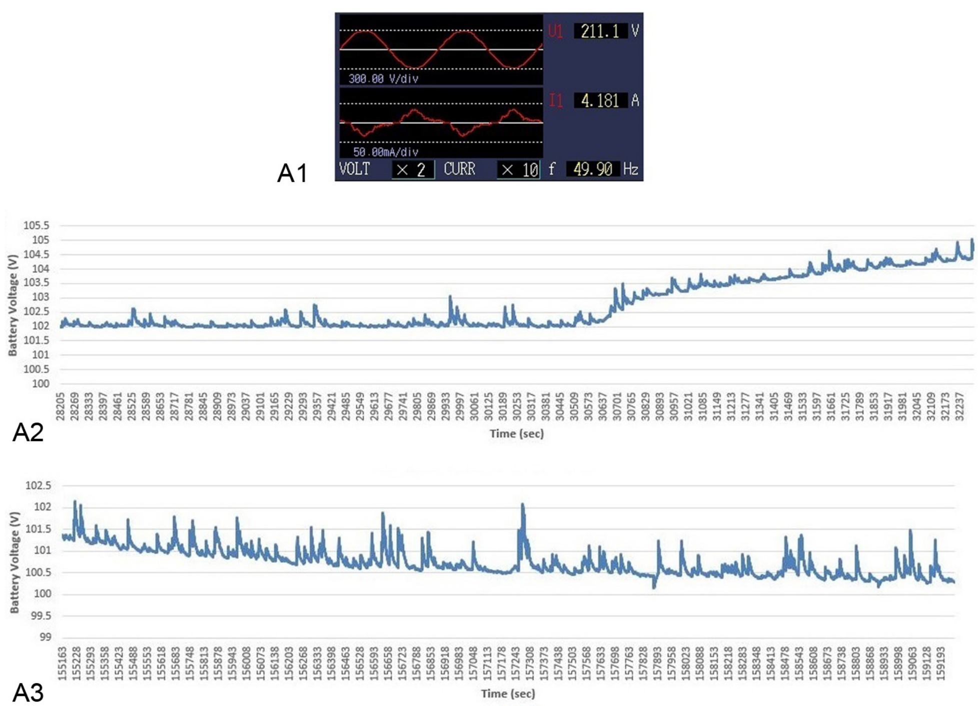

Fig. 5. Results from the hardware setup of the hybrid Renewable Energy System (1(a) and 1(b) Output voltage, current, and frequency from the load-side during charging and discharging of the battery; 2(a) and 2(b) Battery voltage and current during charging; and 3(a) and 3(b) Battery voltage and current during discharging).

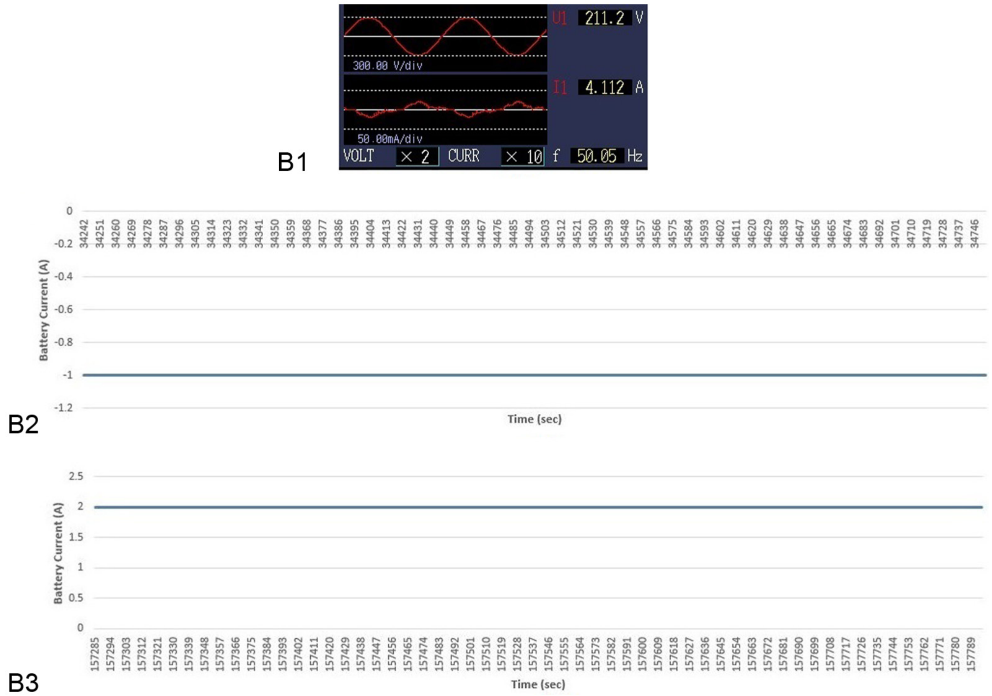

Fig. 5. (*Continued*) Results from the hardware setup of the hybrid Renewable Energy System (1(a) and 1(b) Output voltage, current, and frequency from the load-side during charging and discharging of the battery; 2(a) and 2(b) Battery voltage and current during charging; and 3(a) and 3(b) Battery voltage and current during discharging).

TABLE IV
STEP RESPONSE CHARACTERISTICS OF THE BATTERY CURRENT SIGNALS

Battery Current During Charging		
	Simulation Results	Hardware Results
Rise time (s)	0.271	0.001
Settling time (s)	0.738	0.001
Overshoot	0.03	0
Undershoot	2.1	0
Peak (A)	0.87	1
Battery current during discharging		
	Simulation Results	Hardware Results
Rise time (s)	0.181	0.001
Settling time (s)	0.98	0.001
Overshoot	1.935	0
Undershoot	0.88	0
Peak (A)	1.94	2

Peer-review: Externally peer-reviewed.

Conflict of Interest: The authors have no conflicts of interest to declare.

Financial Disclosure: The authors declared that this study has received no financial support.

Acknowledgment: The hardware implementation was carried out in the School of Renewable Energy and Efficiency (SREE) Lab, NIT, Kurukshetra, India. Thanks to the coordinator, SREE, for providing this opportunity.

REFERENCES

1. Food and Agriculture Organisation, "Annual report on agriculture-2020," related resources. [online] Available: https://www.fao.org. chapter 2: *Energy_for_Agriculture*.
2. Bas Bouman, *Rice Today*. Philippines: International Rice Research Institute, IRRI, Tech. Rep. Jan-Mar issue, vol. 12, no. 1, pp. 38–45, 2009.
3. S. Aryal, "Rainfall and water requirement of rice during growing period," *Journal of Agriculture and Environment*, vol. 13, 2012.
4. A. Zahedi, "Technical analysis of an electric power system consisting of solar PV energy, wind power, and hydrogen fuel cell," in *2007 Australasian Universities Power Engineering Conference*, Perth, WA, Australia, December 09-12, 2007, pp. 1–5. [CrossRef]
5. T. F. El-Shatter and M. N. Eskandar, "Hybrid PV/fuel cell system design and simulation," *Renewable Energy*, vol. 27, no. 3, pp. 479–485, 2002.
6. G. Barchi, G. Miori, D. Moser, and S. Papantoniou, "A small-scale prototype for the optimization of PV generation and battery storage through

the use of a building energy management system," in *2018 IEEE International Conference on Environment and Electrical Engineering and 2018 IEEE Industrial and Commercial Power Systems Europe (EEEIC / I&CPS Europe)*, 2018, pp. 1–5. (doi: 10.1109/EEEIC.2018.8494012)

7. T. Zhou and B. Francois, "Modeling and control design of hydrogen production process for an active hydrogen/wind hybrid power system," *International Journal of Hydrogen Energy*, vol. 34, pp. 21–30, 2009. June 05, 2014.
8. H. Gorgun, "Dynamic modeling of a proton exchange membrane (PEM) electrolyzer," *International Journal of Hydrogen Energy*, vol. 31, no. 1, pp. 29–38, 2006. September, 2018.
9. K. Buts, L. Dewan, and M. P. R. Prasad, "Modeling and implementation of wind-battery storage hybrid power system in LabVIEW environment," in *1st IEEE Conference ICMICA*. NITK, 2020, pp. 1–6. (doi: 10.1109/ICMICA48462.2020.9242826)
10. Y. Sukamongkol and A. Chungpaibulpatana, "A simulation model for predicting the performance of a solar photovoltaic system with alternating current loads," *Renewable Energy*, February 06, 2007, vol. 27, no. 2, pp. 237–58, 2007.
11. N. Andreadou and F. Bonavitacola, "Residential remote load scheduling and control for smart homes with LabVIEW interface," in *IEEE International Conference on Communications, Control, and Computing Technologies for Smart Grids (SmartGridComm)*, Aalborg, Denmark, October 29-31, 2018 February 06, 2007, 2018, pp. 1–7. [CrossRef]
12. B. Bendib, H. Belmili, S. Boulouma, H. Rahmani, and F. Krim, "Modeling and simulation of PV generator characteristics under LabVIEW," In *2018 6th International Renewable and Sustainable Energy Conference (IRSEC)*, Rabat, Morocco, December 05-08, 2018, 2018, pp. 1–6. [CrossRef]
13. R. Luthander and J. Widen, "Photovoltaic self consumption in Buildings: A review," *Applied Energy*, vol. 142, pp. 80–94, January 12, 2015.
14. M. Uzunoglu and O.C. Onar, "Modeling, control and simulation of a PV/FC/UC based hybrid power generation system for stand-alone applications," *Elsevier, Science Direct*, *Renewable Energy*, July 25, 2008, vol. 34, pp. 509–520, 2009.
15. K. Rajashekara, "Hybrid fuel-cell strategies for clean power generation," *IEEE Transactions on Industry Applications*, vol. 41, no. 3, pp. 682–689, 2005. [CrossRef]
16. T. Wei *et al.*, "Battery management and application for energy-efficient buildings," in *2014 51st ACM/EDAC/IEEE Design Automation Conference (DAC)*, June 05, 2014, pp. 1–6. [CrossRef]
17. F. Fan, N. Tai, X. Zheng, W. Huang, and J. Shi, "Equalization strategy for multi-battery energy storage systems using maximum consistency tracking algorithm of the conditional depreciation," *IEEE Transactions on Energy Conversion*, September 2018. vol. 33, no. 3, pp. 1242–1254, 2018. [CrossRef]
18. V. Tipsuwanporn, A. Charoen, A. Numsomran, and K. Phipek, "A single-phase PWM inverter controlling base on PLL technique," in *SICE Annual Conference*, 2011, pp. 1178–1183.
19. Q. Zhang, X. Sun, Y. Zhong, M. Matsui, and B. Ren, "Analysis and design of a digital phase-locked loop for single-phase grid-connected power conversion systems," *IEEE Transactions on Industrial Electronics*, vol. 58, no. 8, pp. 3581–3592, 2011. (doi: 10.1109/TIE.2010.2087295)
20. H. Mao, X. Yang, Z. Chen, and Z. Wang, "A hysteresis current controller for single-phase three-level voltage source inverters," *IEEE Transactions on Power Electronics*, January 02, 2012, vol. 27, no. 7, pp. 3330–3339, 2012. [CrossRef]
21. F. Umer and M. Zied, *Tree-based Heterogeneous FPGA Architectures*. Rabat, Morocco, December 05-08, 2018, Springer, 2012, pp. 8–47.

TEPES
TURKISH JOURNAL OF
ELECTRICAL POWER
AND ENERGY SYSTEMS

TEPES Vol 1., Issue. 2, 84-89, 2021 **DOI:** 10.5152/tepes.2021.21025

RESEARCH ARTICLE

Simulation and Performance Analysis of a Solar Photovoltaic Panel Under Partial Shading Conditions

Abdurrahman Yavuzdeger[1], Burak Esenboga[2], Huseyin Nazligul[1], Fırat Ekinci[1], Tugce Demirdelen[2]

[1]Department of Energy Systems Engineering, Adana Alparslan Turkes Science and Technology University, Adana, Turkey
[2]Department of Electrical and Electronic Engineering, Adana Alparslan Turkes Science and Technology University, Adana, Turkey

Cite this article as: Yavuzdeger A, Esenboga B, Nazligul H, Ekinci F, Demirdelen T. Simulation and performance analysis of a solar photovoltaic panel under partial shading conditions. *Turk J Electr Power Energy Syst.* 1(2), 84-89, 2021.

ABSTRACT

In recent years, the global demand for energy has been increasing due to the rapid population growth, industrialization, technological development, and economic competition among the developed countries. Energy from renewable sources is now being widely used to meet this demand, especially solar or photovoltaic (PV) energy. Photovoltaic energy systems allow the conversion of solar electromagnetic waves of different wavelengths into DC energy in the visible light spectrum. However, the efficiency of the solar PV panel is adversely affected by partial shading conditions (PSCs) such as the shade of trees, leaves, clouds, buildings, or chimneys. One of the potential solutions is to use a bridge diode to increase the energy efficiency of the solar PV panel under PSCs. Therefore, in this study, the performance analyses of 80 W solar PV panels are carried out under six different conditions of partial shading. To present the superiority of the use of a bridge diode, the solar PV panel with bridge diode is analyzed under different intensities of solar radiation by MATLAB/Simulink. In addition, the effects of PSCs on the solar PV panel without bridge diode are evaluated in detail, as part of the experimental application. The results of the analyses under different PSCs reveal that the use of the bridge diode in the solar PV panels has a significant influence on the power produced from the PV system.

Index Terms—Partial shading condition (PSC), photovoltaic (PV) energy, power losses, renewable energy.

I. INTRODUCTION

Recently, the number of applications based on renewable energy sources has increased significantly in an effort to reduce the dependence on fossil fuels. With the rapidly increasing environmental damage attributed to the use of fossil fuels, scientists emphasize the importance of using energy from renewable sources effectively to meet the global energy demand. Among the renewable energy sources, the global installed power capacity of solar energy is increasing considerably day by day. Critical parameters such as temperature, solar radiation, and shading affect the efficiency of photovoltaic (PV) energy systems. Especially, shading conditions dramatically reduce the electrical energy obtained from PV energy systems. Many studies have been conducted to eliminate or minimize the effect of full shading and partial shading conditions (PSCs) on the produced power, as reported in the literature.

The efficiency of PV cells is a vital parameter for solar energy systems. As partial shading significantly reduces the efficiency of the PV cell, different enhanced techniques have been developed to overcome this problem. In this study, the effects of five different PV array configurations on power generation, such as total-cross-tied (TCT), honeycomb (HC), bridged-linked (BL), series-parallel (SP), and series have been investigated using MATLAB/Simulink, under six different shading conditions. According to the simulation results obtained, it is presented that the TCT configuration performs better than other configurations under all PSCs [1]. New PV array topologies have been proposed to increase the output power produced by the solar energy system under eight different shading patterns. The performances of existing and proposed PV array topologies have been comparatively examined using MATLAB/Simulink. According to the performance analysis results, the modified TCT configuration under PSCs approximately doubled the output power compared to the existing TCT topology [2]. Variable environmental conditions adversely affected the production of solar PV energy. Conventional maximum power point tracking (MPPT) techniques under PSCs may not be able to track the correct MPP. To minimize the negative

Corresponding author: Abdurrahman Yavuzdeger, ayavuzdeger@atu.edu.tr

Received: May 12, 2021
Accepted: July 22, 2021
Published online: August 27, 2021

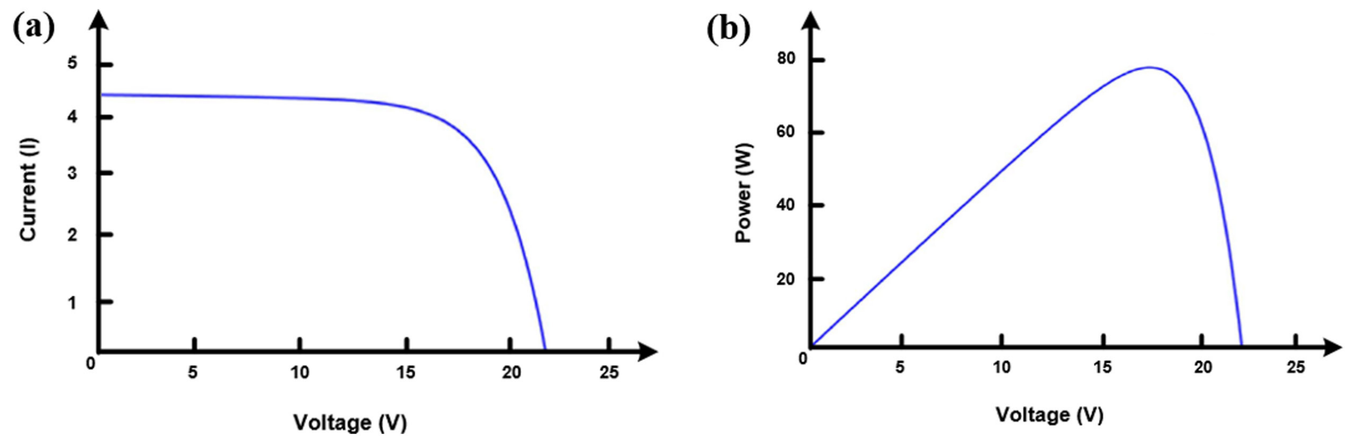

Fig. 1. Solar PV panels used in applied research (a) I–V and (b) P–V characteristics.

impact of partial shading on the generated power, different meta-heuristic techniques have been presented in comparison with the simulation results. The simulation results show the superiority of Gray Wolf Optimization in the speed of convergence and the time to catch global MPP [3]. Various MPPT algorithms which have been widely applied in PV energy systems under PSCs in recent studies are discussed. It has been observed that novel MPPT algorithms as well as hybrid techniques are preferred to increase the efficiency of the PV energy system [4]. A new method has been developed to detect faults such as fire hazards and partial shading using the data of array voltage, array current, and radiation. In addition, experimental studies have been carried out to present the effectiveness of the developed technique [5]. The advantages and disadvantages of MPPT techniques such as Particle Swarm Optimization (PSO), Perturbation and Observation (P&O), Cuckoo Search, Hill-Climbing (HC), Neural Network, Incremental Conductance (IncCond), and Fuzzy-Logic of PV energy systems under uniform radiation and PSCs are discussed in detail [6]. A new method has been developed to obtain P–V and I–V curves of a particular PV energy system under PSCs in different patterns using the standard test condition values of PV modules and the radiation values applied to each module. The simulation results obtained from MATLAB/Simulink show that the electrical properties of PV arrays under partial shading increase the prediction accuracy by including the real effect of bypass and blocking diodes [7]. The MPPT techniques based on bio-inspired algorithms under the changing environmental conditions of PV energy systems have been extensively examined and have contributed to the research in the field of MPPT [8]. PV array configurations are offered to reduce power dissipation under PSCs. Global MPP is readily determined, thanks to the developed method. In addition, it has been compared with the SP and TCT configurations to evaluate the performance of the proposed configurations, and the superiority of the proposed configuration is revealed [9]. A novel hybrid MPPT technique under PSCs is offered. The superiority of the present technique over the standard PSO algorithm and the P&O algorithm has been demonstrated by experimental and simulation results [10]. The behavior of a PV array under PSCs has been examined using MATLAB/Simulink software [11]. Different shading conditions in the PV array have been investigated, and a formula has been developed to determine the critical point from the obtained results [12].

Main Points

- The power obtained from photovoltaic (PV) panels is dramatically reduced due to the decrease in the efficiency of PV cells under different partial shading conditions.
- Shaded modules in the solar PV panels produce many maximum power points in the I–V and P–V curves. The number of those maximum power points has increased because of the increasing number of shaded modules.
- The bridge diode significantly improves the function of the PV panels under different shading conditions. A solar energy system with bridge diodes obtains significant power output compared to a system without these, showing that bridge diodes improve the operating efficiency of solar PV systems.

In the following sections of the paper, solar PV panel characteristics and experimental investigation have been analyzed comprehensively. The performance analysis of the 80 W solar PV panel has been experimentally conducted under six different PSCs. The solar PV panel with bridge diode has been investigated with simulation under the different conditions of solar radiation by using MATLAB/Simulink software, and the results obtained reveal the superiority of the use of bridge diodes.

II. SOLAR PV PANEL CHARACTERISTIC

Photovoltaic solar cells, which have an important place in solar energy systems, convert solar energy directly to DC electrical energy when solar light (in the form of photons) falls on it. The warranty period determined by manufacturers for the smooth operation of solar PV panels is generally 25 years on average. However, it has been stated that the panel power decreases linearly over time. In this study, the performance of the solar PV panel used for the practical study is evaluated with the I–V and P–V curves given in Fig. 1. In addition, Table I presents the parameters of the solar PV panel used for the applied research.

TABLE I
ELECTRICAL PROPERTIES OF THE SOLAR PV PANEL USED IN THE APPLIED RESEARCH

Electrical Characteristics	Value	Electrical Characteristics	Value
Power Rating	80 W	Voltage at maximum power (V_{mp})	17.5 V
Open Circuit Voltage (V_{oc})	21.76 V	Power Tolerances	0% - +5%
Short Circuit Current (I_{sc})	21.76 V	Peak Efficiency	17.6%
Maximum Voltage	1000 V	Current at maximum power (I_{mp})	4.57A

In order to obtain maximum power from the solar PV panels used in PV systems, they are placed at a horizontal angle of inclination and the solar radiation is aimed to fall at a right angle. The level of radiation falling on the panels depends on the latitude and longitude of the location where the panels are placed. The performance of a solar PV panel is affected by many factors. Some of these factors are related to the structure of the panel itself, while others are related to the location and environment in which the panels are installed. The factors are material degradation, solar radiation, panel temperature, parasitic resistances, shade, contamination, and inclination angle.

The shading of solar PV panels is one of the major problems in solar energy systems. Shadow formation significantly reduces the power produced by the solar PV panels, causing huge losses to the customer. Trees, leaves, clouds, buildings, and chimneys can create shadows on the panel, which cause a decrease in the electrical performance of the solar PV panel. The shading effect occurs when the system is not exposed to the same amount of radiation due to some obstacles in the path of light falling on the panel. In this case, solar cells are exposed to lower levels of radiation, and the shading effect reduces system power instead of generating power. Fig. 2 shows the I–V and P–V curves according to the amount of solar radiation reflected on the PV panel, due to shading.

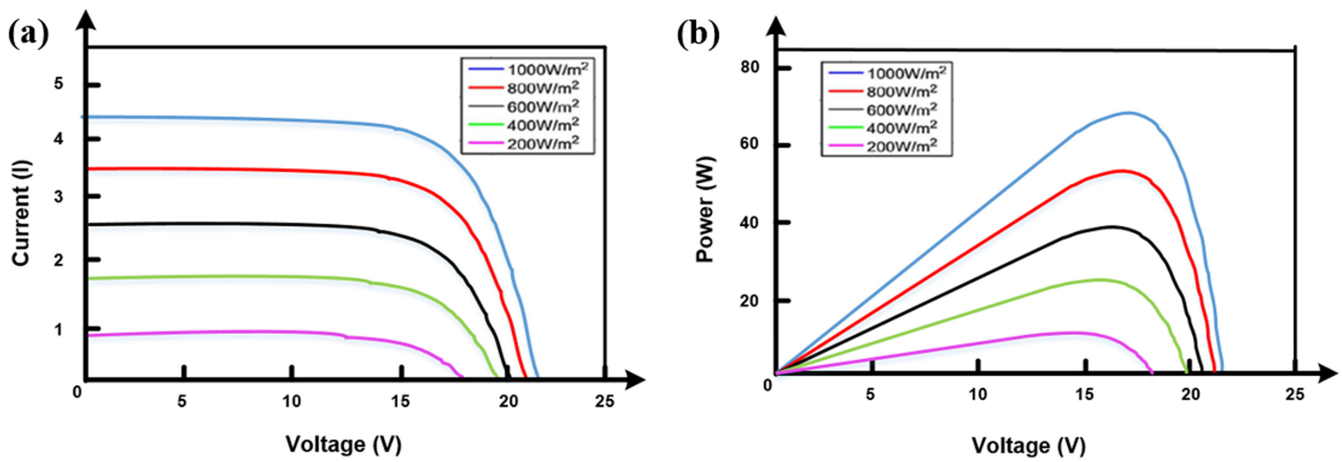

Fig. 2. (a) I–V and (b) P–V characteristics of PV panels at different levels of solar radiation.

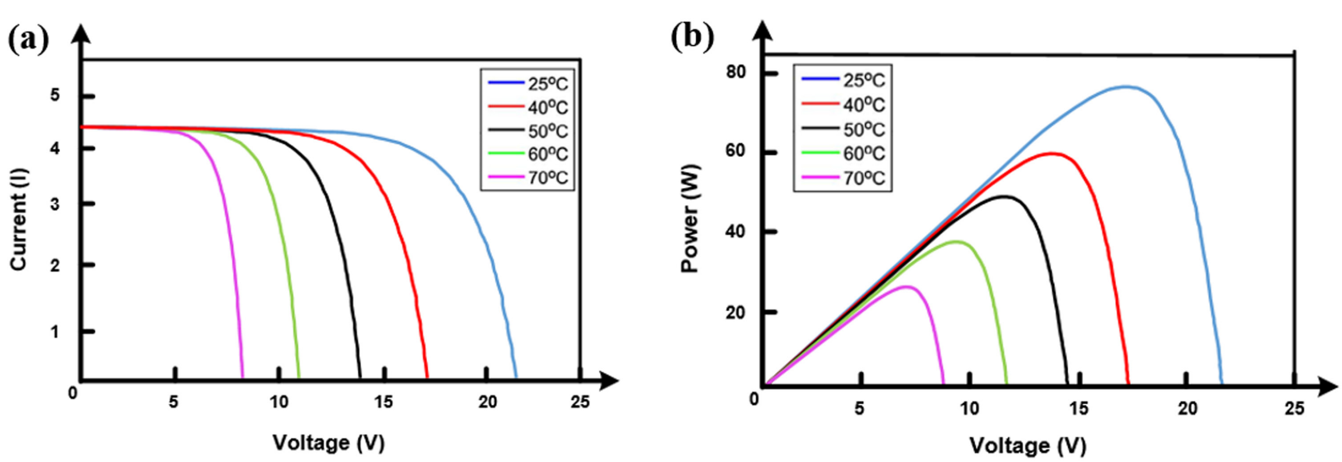

Fig. 3. (a) I–V and (b) P–V characteristics of PV panels at different temperatures.

The output power of a solar PV panel is inversely proportional to the PV panel's temperature. As the temperature of the solar PV panel increases, the power produced by the PV panel decreases. Therefore, the losses caused by temperature are proportional to the solar PV cell temperature. Fig. 3 shows the effect of temperature on the power produced by the solar PV panel.

As the temperature and solar radiation of the solar cell under the shadow change, the produced power decreases. In this case, the shadow results in mismatches of the currents generated from the solar cells of the solar PV panel. Shaded solar cells produce less current than non-shaded chambers. However, since the solar cells in the PV panel are connected in series, the same current must flow through all cells. This situation leads to incompatibilities. Shading the part over one solar cell can significantly reduce the strength of the entire solar PV panel, as if all solar cells are shaded. When a solar cell is under a shadow, the current flow of the shadowed solar cell decreases.

Thus, the total current of the system passes over the shaded solar cell, causing a decrease in the produced power. By operating the bridge diode used for the solar cell under the shadow, the current is provided to pass around the shadowed solar cell. An examination of the bridge diode's effect under partial shading reveals that the presence of a bridge diode in the solar PV panel causes changes in the I–V and P–V curves. If there is a bridge diode in the panel, there is more than one maximum point in the P–V curve of PSCs, while the power value decreases significantly compared to the situation in which there is no shade and no bridge diode. Under partial shading, mismatches owing to the location of the shaded panels and the shape of the shade reduce the power. The dynamic model has been created by MATLAB/Simulink, as shown in Fig. 4.

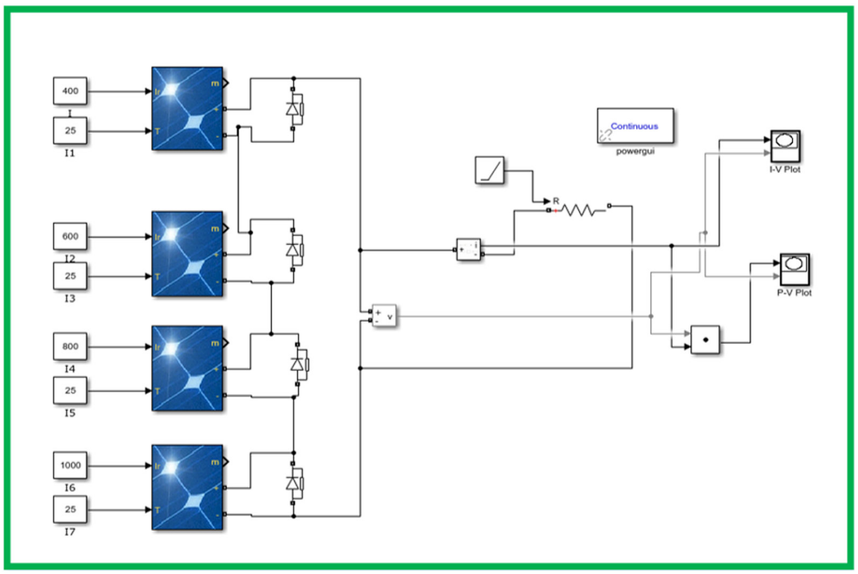

Fig. 4. The dynamic model of the solar PV panel at different levels of solar radiation and temperature.

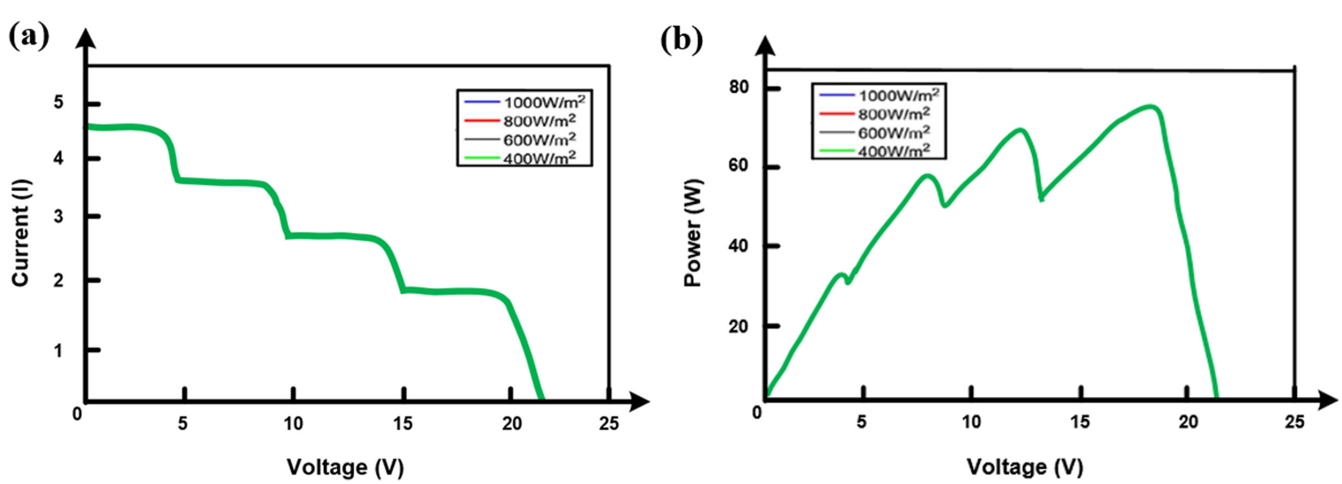

Fig. 5. (a) I–V and (b) P–V characteristics of the bridge diode-connected solar PV panel under the different solar radiation conditions.

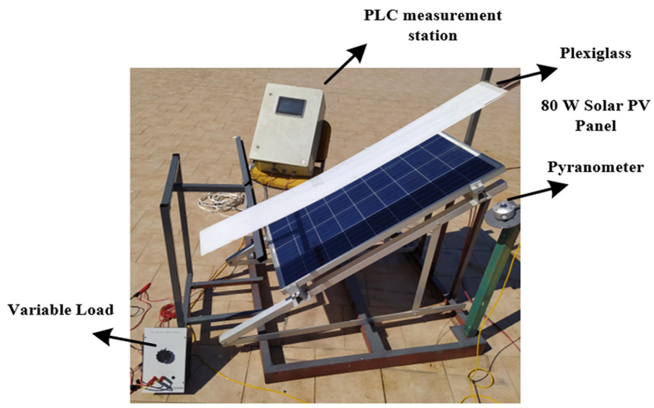

Fig. 6. Experimental setup unit for partial shading conditions of 80 W solar PV panel.

The model shows the shading conditions of the solar PV panel with a bridge diode. The power characteristic of the solar PV panel under the different levels of solar radiation is presented in Fig. 5.

III. EXPERIMENTAL ANALYSIS AND RESULTS

This section details the effect of partial shading on the output power of PV panels, studied by experimental investigation. An experimental test setup was installed on the roof of Alparslan Turkes Science and Technology University in Adana. Experimental studies were performed to investigate the performance of 80 W PV panels under six different partial shading cases. The effect of PSCs on short circuit current and short circuit voltage of PV panels has also been examined. The open circuit voltage and short circuit current values of the 80 W PV panel were recorded by the PLC measurement station. The relationship between the solar radiation level and the produced power was observed by measuring the solar radiation using the pyranometer. The experimental setup unit is shown in Fig. 6.

The solar cells used in the experiment were connected in series, each solar cell having a power of 2.2 W. In order to observe the maximum power point of the 80 W PV panel, experimental studies were carried out at 1000 W/m^2 at 33 °C in the unshaded condition. According to the experimental results in the unshaded condition, the maximum power was 78.8 W at 16.8 V and 4.69 A. The PSCs of the solar PV panels are shown in Fig. 7.

Table II shows the detailed evaluation of the six different conditions. The short circuit current and open circuit voltage, maximum power, and panel temperature under each PSC for the 80 W PV panel are shown comparatively. Significant decrease in output power of PV panel is observed when the performance of the PV panel under

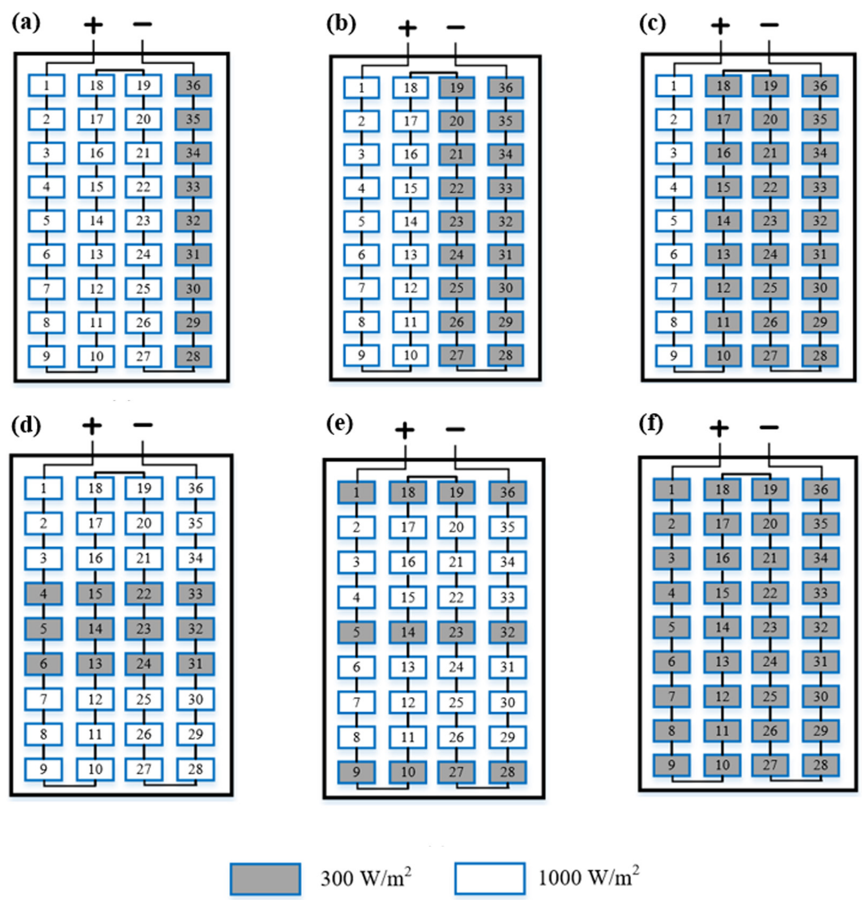

Fig. 7. Partial shading (a) Case 1, (b) Case 2, (c) Case 3, (d) Case 4, (e) Case 5, (f) Case 6.

TABLE II
EXPERIMENTAL ANALYSIS OF THE SOLAR PV PANEL UNDER THE PSCS OF (A) I–V AND (B) P–V CHARACTERISTICS

PSCs	P_{max} (W)	V_{max} (V)	I_{max} (A)	Temperature of the PV panel (°C)
Case 1	19.29	21.3	1.51	31.6–33.2
Case 2	16.38	21.1	1.21	33.5–35
Case 3	19.9	19.9	0.76	36.6–38
Case 4	19.6	21.2	1.09	37.8–38.6
Case 5	18.13	21.0	1.11	38.5–40.2
Case 6	9.20	19.8	0.74	36.2–38.3

PSCs, partial shading conditions; PV, photovoltaic.

shaded and unshaded conditions is compared. An 8.5-fold difference in output power between unshaded and fully shaded conditions was observed experimentally. In the studies in the literature, different photovoltaic array configurations such as TCT, HC, BL, and SP have been proposed to eliminate partial shading problems. In this study, in order to minimize the effect of partial shading on PV performance, the method using the bridge diode has been shown to obtain maximum power from the PV panel. As a result, it has been proven by experimental and simulation results that the panel efficiency of the PV panel without bridge diode is much lower than the PV panel with bridge diode under PSCs.

IV. CONCLUSION

The rapid depletion of fossil fuels makes it necessary to develop and use of alternative energy sources. Among the renewable energy sources, solar energy has come into prominence owing to its many advantages such as being emission-free, eco-friendly, infinite, reliable, preventing global warming, having low maintenance costs, etc. Many critical parameters negatively affect the power produced by PV energy systems. Partial shading is one of the most significant problems that diminish the power obtained from PV energy systems. There are many different approaches such as PV array arrangements and bridge diodes that can be applied in PV energy system designs to minimize partial shading losses. This study has examined the improvement in output power of solar PV panel under PSCs. The performance of 80 W solar PV panels under different shading conditions has been analyzed experimentally and under simulation. It is presented that using a bridge diode increases the performance of the solar PV panel under different PSCs, based on the simulation results obtained from the MATLAB/Simulink software. Hence, the efficiency of the solar PV array strongly depends on the usage of a bridge diode. Moreover, solar radiation levels and different shading conditions affect the efficiency of the solar PV energy system.

Peer-review: Externally peer-reviewed.

Conflict of Interest: The authors have no conflicts of interest to declare.

Financial Disclosure: The authors declared that this study has received no financial support.

REFERENCES

1. M. Kermadi, V. J. Chin, S. Mekhilef, and Z. Salam, "A fast and accurate generalized analytical approach for PV arrays modeling under partial shading conditions," *Sol. Energy*, vol. 208, pp. 753–765, 2020. [CrossRef]
2. M. Mao *et al.*, "A hybrid intelligent GMPPT algorithm for partial shading PV system," *Control Eng. Pract.*, vol. 83, pp. 108–115, 2019. [CrossRef]
3. R. Hariharan, M. Chakkarapani, G. Saravana Ilango, and C. Nagamani, "A method to detect photovoltaic array faults and partial shading in PV systems," *IEEE J. Photovolt.*, vol. 6, no. 5, pp. 1278–1285, 2016. [CrossRef]
4. L. Liu, X. Meng, and C. Liu, "A review of maximum power point tracking methods of PV power system at uniform and partial shading," *Renew. Sustain. Energy Rev.*, vol. 53, pp. 1500–1507, 2016. [CrossRef]
5. A. Mohapatra, B. Nayak, P. Das, and K. B. Mohanty, "A review on MPPT techniques of PV system under partial shading condition," *Renew. Sustain. Energy Rev.*, vol. 80, pp. 854–867, 2017. [CrossRef]
6. O. Bingöl and B. Özkaya, "Analysis and comparison of different PV array configurations under partial shading conditions," *Sol. Energy*, vol. 160, pp. 336–343, 2018. [CrossRef]
7. G. Li, Y. Jin, M. W. Akram, X. Chen, and J. Ji, "Application of bio-inspired algorithms in maximum power point tracking for PV systems under partial shading conditions: A review," *Renew. Sustain. Energy Rev.*, vol. 81, pp. 840–873, 2018. [CrossRef].
8. M. A. Mohamed, A. A. Z. Diab, and H. Rezk, "Partial shading mitigation of PV systems via different meta-heuristic techniques," *Renew. Energy*, vol. 130, pp. 1159–1175, 2019. [CrossRef]
9. D. Prince Winston, S. Kumaravel, B. P. Kumar, and S. Devakirubakaran, "Performance improvement of solar PV array topologies during various partial shading conditions," *Sol. Energy*, vol. 196, pp. 228–242, 2020. [CrossRef]
10. N. Belhaouas *et al.*, "PV array power output maximization under partial shading using new shifted PV array arrangements," *Appl. Energy*, vol. 187, pp. 326–337, 2017. [CrossRef]
11. A. Djalab, N. Bessous, M. M. Rezaouı, and I. Merzouk, "Study of the effects of partial shading on PV array," *IEEE Int. Conf. Commun. Electron.*, pp. 1–5, 2018. [CrossRef]
12. J. C. Teo, R. H. Tan, V. H. Mok, V. K. Ramachandaramurthy, and C. Tan, "Impact of partial shading on the PV characteristics and the maximum power of a photovoltaic string," *Energies*, vol. 11, no. 7, p. 1860, 2018. [CrossRef]

TEPES
TURKISH JOURNAL OF
ELECTRICAL POWER
AND ENERGY SYSTEMS

TEPES Vol 1., Issue. 2, 90-98, 2021 **DOI:** 10.5152/tepes.2021.21028

RESEARCH ARTICLE

Sliding Mode Control Strategy for a Small Hydro Electric Plant-Based DC Microgrid

Ishika Singh, Sheetla Prasad

Electronics and Communication Engineering, Galgotias University, School of Electrical, Uttar Pradesh, India

Cite this article as: Singh I, Prasad S. Sliding mode control strategy for a small hydro electric plant-based DC microgrid. *Turk J Electr Power Energy Syst.* 1(2), 90-98, 2021.

ABSTRACT

With the rapid increase in energy consumption, the demand for small hydro power plants (SHPs) is increasing. The impact of these plants is significant, due to their low environmental damage, low execution cost, and minimum management cost. Moreover, in rural areas, they can also be used to facilitate drinking water and irrigation systems. This study considers a small hydro power plant (SHP) including a turbine with a permanent magnet synchronous generator (PMSG) attached to the DC microgrid through a voltage source converter (VSC) model. In this paper, a sliding mode controller is proposed to minimize the steady state errors and stabilization problems in an SHP-based DC microgrid. The asymptotic convergence of the proposed controller is analyzed using the Lyapunov stability theorem. Based on the Lyapunov stability theorem, the control law derives to ensure the asymptotic convergence to effectively minimize the steady state errors and improve the closed-loop system stabilization. The proposed control law also guarantees stable operation in a short limited time. As results, the proposed controller confirms speedy convergence of steady state error dynamics with negligible oscillations and reduces the limitation of chattering notably, without any loss in control accuracy. The simulation results illustrate the robustness of the proposed controller when subjected to disturbances and system nonlinearities.

Index Terms—Microgrid, permanent magnet synchronous generator (PMSG), sliding mode controller (SMC), small hydro power plant (SHP), voltage source converter (VSC).

I. INTRODUCTION

A microgrid is tiny part of the power distribution system, having components like energy storage devices alongside the distributed generator, and controllable loads which allow increase to a competent energy system. A microgrid as seen from the utility grid perspective is similar to a generator because it is capable of comfortably disconnecting and operating independently after a fault occurs in the main grid [1]. Micrograds attract end users closer to the source generating electricity from distributed energy resources (DERs). These micrograds can work in dual mode, that is, the. islanded mode and the grid-connected mode. In case of any fault, a microgrid can be disconnected from the main grid. As the generation sources are distributed, it can easily work in the islanded mode. Environmental effects, the status of fossil fuels, and economic interest are the three major grounds for the growing awareness toward renewable resources as well as local generation. In the past few years, the evolution of renewable assets in electrical networks is expanding beyond the existing boundaries [2].

The transformation from the use of fossil fuels to sustainable energy resources as power originators in large industries is a major plan of action in reducing the effects of climate change. The carbon footprint on the earth is connected to the history of the huge demand for diesel products, electric power, and water. Moreover, considering their specific power demand, the merger of microgrids with central grid controls in the grading of mining industries is an emerging matter [3].

The microgrid can work both with alternating current (AC) and direct current (DC). The arrangement of the DC system has certain benefits, such as minimizing losses and ease of amalgamation with measures of energy storage, due to which there is a sudden surge in the use of DC microgrids in recent times [4]. Digitalization and the enthusiastic emergence of new ideas offer the thrilling possibilities of a microgrid transactive power system at the disposal level, to bring down transmission losses, reduce infrastructure costs of electrical systems, upgrade credibility, and amplify local energy

Corresponding author: Sheetla Prasad, sheetla.prasad@galgotiasuniversity.edu.in

Received: June 3, 2021
Accepted: September 20, 2021
Published online: October 15, 2021

usage, leading to reduction of electricity bills at the consumer end. Transaction energy, with essential factors such as demand response, distribution of energy resources, the local market for energy, and distributed records of technologies for exposure of dispersed can be framed as a smart grid system [5]. Over the past decade, there has been significant increase in awareness regarding the DC microgrid, as it has shown huge dominance over the AC microgrid in terms of control simplicity, regulation, dependability, ease of integration to renewable energy sources, and DC load connection. However, apart from these numerous benefits, the plotting and execution of a suitable protection system for DC microgrid residue is a remarkable challenge [6].

The combination of distributed energy resources is possible with many platforms, most significantly with the microgrid. However, because of some issues with the blueprint and the absence of machineries, the microgrid is still developing into a wide-ranging and commercialized mix of systems to be integrated with existing electrical systems. There are many challenges concerning irregular values of renewable energy resources (RERs) [7]. The distributed energy resources (DERs) can drive the complex approach of the microgrid operating successfully in an islanded mode, by sincerely controlling it. In the central grid mode, the arrangement requires none or close to zero frequency as well as voltage variations in the middle of the grid and the microgrid project. The options of enhancing the harmonization of power flow into the microgrid structure can be controlled by smart grid technologies in a real-time scenario [8].

Flowing water has a kinetic energy which gives rise to mechanical and electrical energy in the hydropower grid system. The flowing water rotates the hydro turbine and then returns to the water bodies for other uses. The high efficiency (about 60–80%), long life span of the equipment, and absence of pollution or greenhouse gas emission, with low operating cost and maintenance cost are some of the major benefits of the hydropower grid system [9]. The installed power capacities of hydro power plants are distinguished as: pico hydro plants (less than 5 kW), micro hydro plants (5 kW to 100 kW), mini hydro plants (100 kW to 1000 kW), small-scale hydro plants (less than 10 MW), medium-scale hydro plants (10 MW to 100 MW), and large-scale hydro plants (over 100 MW capacity) [10]. The leading method suitable for generating renewable energy is nothing but a small hydropower plant. It is designed to work with low head and flow to drive the hydro turbine, which can be satisfied by a run of river type [11]. The basic components of a small hydro power plant (SHP) are the reservoir, penstock, forebay, intake structure, hydraulic turbine, surge chamber, speed governor, and an electrical generator [12, 13].

The SHP can overcome the problem of instability in power generation and can predict the future production of power. In terms of environmental impact, the SHP has low impact in comparison to photovoltaic power, wind power, and other DERs. The behavior of the SHP is completely nonlinear, and it can be integrated with the utility grid to regulate power flow effectively. For effective control, several controllers are developed [10-13] for the linearized state-space SHP model, which do not consider the nonlinear dynamics of the SHP.

The sliding mode controller (SMC) is based on the discontinuous control law, which is known to be logical, to overcome many problems of robust stability [14-17]. The SMC offers control for a class under actuated systems, which can be seen in a cascade form with external disturbances. The SMC controller will force the motion of state trajectories toward the sliding surface with an exponential approach, enabling the handling of system disturbances and nonlinearities [15].

Due to the nonlinear nature of the SHP and the permanent magnet synchronous generator (PMSG), power flow regulation is a formidable task. Hence, a nonlinear control strategy is the most feasible and capable in regulating power flow within the permissible stability limit. Thus, the present study contributes the following: 1) a nonlinear model of both SHP and PMSG with VSC is considered to minimize steady state errors and achieve faster stabilization using the nonlinear sliding mode control technique; 2) the proposed SMC is used to effectively stabilize nonlinear dynamics with passivity-based desired equilibrium points; 3) based on the Lyapunov stability theorem, the control law derives to ensure the asymptotic convergence on equilibrium points to minimize the steady state errors and improve the closed-loop system stabilization; and 4) as results, the proposed controller ensures speedy convergence of steady state error dynamics with negligible oscillations and reduces the limitation of chattering notably, without any loss in nonlinear control accuracy.

This paper is organized as follows: The nonlinear state-space models of SHP and PMSG are reviewed in Section 2. The sliding mode control-based control strategy is derived, followed by a discussion of Lyapunov's stability convergence analysis in Section 3. The simulation results and demonstrations of the proposed control strategy on SHP and PMSG-based DC microgrid are illustrated in the Section 4, followed by concluding remarks drawn in Section 5.

II. PORTABLE HYDRO POWER PLANT DESCRIPTION

The energy of falling water generates electricity with the use of an SHP [18, 19]. It produces no gloomy effect on the regional stream, leading to a simple reroute of the volume of accessible water, and then returns the water to the stream. Since the stream flows continuously day and night, less battery stock is required in the SHP as compared to other technologies. Despite the stream being far away, it is feasible, as these large distances can be overshadowed by high voltage generators [20]. The periodical stream offers sizable performance using a design combining a hybrid solar and water system. It is always important to study and review the proposed location to check the availability and amount of hydropower present. The components of the SHP are a turbine, a PMSG, and a VSC connected to a DC microgrid. Water is considered to be a renewable energy source, as shown in Fig. 1 [19-21].

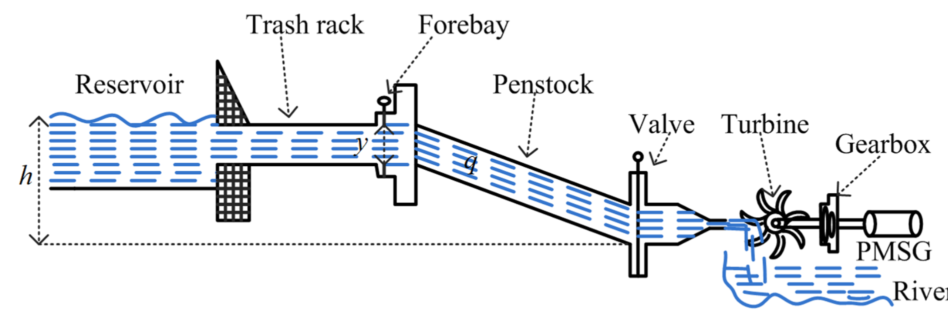

Fig. 1. Representation of an SHP.

A. Hydraulic Turbine Dynamics

The hydraulic turbine is considered to be the main component of the SHP and is also known as the prime mover because of the fact that it converts the kinetic energy of descending water into rotational mechanical energy, eventually generating electrical energy with the use of generators that are attached to the turbines [22]. The turbine is made up of rows of blades that are connected on a rotating shaft or a plate which rotates due to the collision when the water (with velocity and pressure variations) strikes the blades. The model of the hydraulic turbine includes the dynamics of penstock, tunnel, servomotor, and head losses [23]. As in Newton's law, the change in momentum results in generation of a force which is directly proportional to the change which can occur on fluids also. By applying this law, the dynamic model of a tunnel is obtained, resulting from the change of water momentum on the penstock and pressure at the head of the tunnel [19]:

$$T_w \frac{dq}{dt} = 1 - h - k_f q^2 \tag{1}$$

$$h = \left(\frac{q}{y}\right)^2 \tag{2}$$

A servomotor can be considered, which works to achieve rotational or linear motion that is directly proportional to the supplied command signal. In this paper, the servomotor is used to control the flow of water by managing the rotational motion of the spear valve. The spear valve operated by the servomotor is positioned below the penstock and manages the flow of water into the turbine [24]. The general model of the servomotor can be depicted as:

$$T_y \frac{dy}{dt} = u - y \tag{3}$$

The motion of the turbine is transferred into mechanical power and calculated by the multiplication of the water flow and the pressure head. Since everything has certain losses, this equation also includes turbine losses which can be taken into account by subtracting between no-load flow and actual flow, in which the no-load flow is decided by a rated head in the SHP. The per unit turbine power is determined as

$$P_m = A_t h\left(q - q_{nl}\right) \tag{4}$$

The pneumatic turbine blades are maintained against the stream of water, which interchanges its momentum. As the momentum is exchanged, a resulting force is generated, leading to the rotation of the turbine.

In (1) to (4), the terms T_w, T_y, h, q, q_{nl}, y, k_f, u and A_t are described as the time constant of water, time constant of the servomotor, hydraulic head, normalized flow on the penstock, the no-load flow rate of the hydro turbine, gate position, friction losses, input control, and constant of proportionality, respectively.

B. Permanent Magnet Synchronous Generator Dynamics

An alternator is used, similar to a PMSG, which provides the constant excitation field by using a permanent magnet in place of a coil [25]. Here, the rotor and the magnetic field revolve at the same speed. This differs from a normal generator, leading to a voltage drop without an option to regulate when the generator is charged. Therefore, the PMSG converts the mechanical energy obtained from the hydraulic turbine into electrical power, as represented in Fig. 2. To connect the PMSG to a DC microgrid, a VSC is used [26]. The VSC is basically a converter that produces AC voltage from DC voltage, and can be called an inverter, with the ability to transfer power in any direction. The VSC has certain features which enable control of the phase angle, the magnitude, and the frequency of the output voltage [27]. The VSC comprises six insulated-gate bipolar transistors (IGBTs) [19].

The reference frame comprising the dynamic model of PMSG is determined [19] as:

$$L_g \frac{di_{dg}}{dt} = -R_g i_{dg} + L_g w_m i_{dg} - v_d \tag{5}$$

$$L_g \frac{di_{qg}}{dt} = -R_g i_{qg} - L_g w_m i_{dg} + \psi w_m - v_q \tag{6}$$

$$M \frac{dw_m}{dt} = T_m - T_e \tag{7}$$

$$T_m = \frac{P_m}{w_m} = \frac{A_t q^2\left(q - q_{nl}\right)}{y^2 w_m} \tag{8}$$

$$T_e = \psi i_q \tag{9}$$

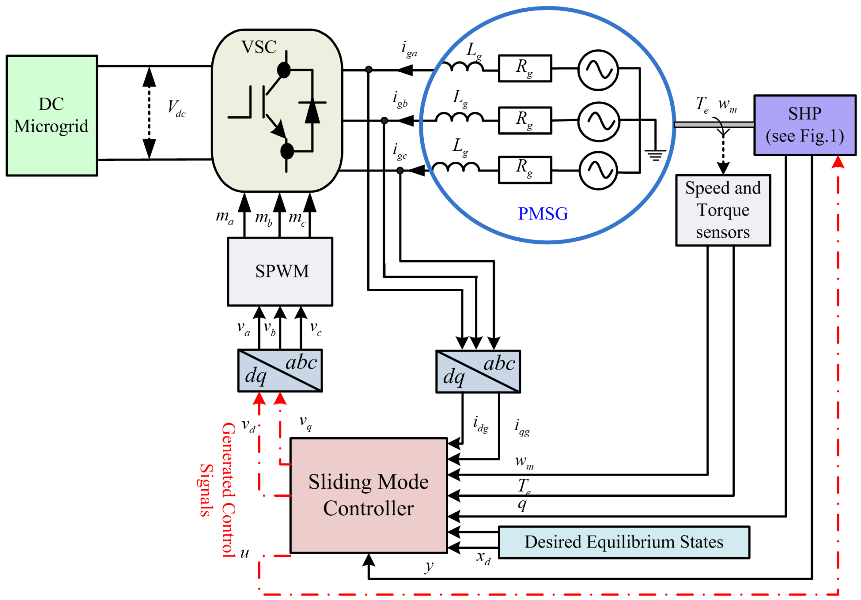

Fig. 2. Proposed control strategy for an SHP-based DC microgrid.

The output voltage of PMSG is given in (10):

$$v_{dq} = m_{dq} v_{dc} \tag{10}$$

where $m_{dq} \epsilon [-1,1]$ is the modulation index and the terms in (5) to (10), that is, T_m, T_e, R, L, v_{dc}, i_{dq}, v_{dq}, w_m, ψ, and M are the mechanical torque, electrical torque, PMSG stator winding resistance, PMSG stator winding inductance, DC link voltage, PMSG output current, PMSG output voltage, rotor speed, permanent magnetic flux produced by the rotor magnets, and moment of inertia of the hydro turbine respectively.

III. CONTROL METHODOLOGY

The SMC has many advantages due to its simplicity and robustness in case of definite unpredictability and disturbances, which are well recognized, but also has a few limitations like chattering and brutalness of control forces, which are also well known [28]. To overcome these limitations, certain procedures can be followed, like the computational intelligence technique, neural network, fuzzy system, variable damping ratio strategy, and evolutionary computation. The main merits of a sliding mode controller are the achievement of desired control through the selection of a suitable sliding manifold, which reaches the manifold and can be maintained there afterward through a discontinuous control to compel the system state remains in stable region. Hence, The SMC designs are categorized into two modes: the reaching phase, before entering the sliding manifold; and the sliding mode phase, where the system is compelled to stay in that mode after the reaching phase [29]. The SMC techniques are productive tools to discard the system uncertainties. Accordingly, the main assets of SMC are inconsiderate to internal and external variations and the overlapping of the sliding parameter to zero in a limited time [30-32]. Hence, the sliding mode control scheme is considered here, as shown in Fig. 2, to enhance the closed-loop system dynamics of the SHP-based DC microgrid against disturbances.

The load disturbance and system uncertainties in the dynamics of the reaching phase are highly preferable for the selection of sliding (switching surface) and are chosen in (11):

$$\sigma = c\left(x - x_d\right) = \begin{bmatrix} 0 & 1 & 0 & 0 & 0 \\ 0 & 0 & 1 & 0 & 0 \\ 0 & 0 & 0 & 1 & 0 \end{bmatrix} \left(\begin{bmatrix} q \\ y \\ i_{dg} \\ i_{qg} \\ w_m \end{bmatrix} - \begin{bmatrix} x_{d1} \\ x_{d2} \\ x_{d3} \\ x_{d4} \\ x_{d5} \end{bmatrix} \right) \tag{11}$$

where, x_{d1}, x_{d2}, x_{d3}, x_{d4} and x_{d5} are stable equilibrium points of the SHP and PMSG dynamics. All equilibrium points are taken from passivity-based control approach [19, 33] and the above equilibrium points are considered here in (12):

$$\begin{aligned} x_{d1} &= \left(\frac{k_1 q - 1}{k_1 - q\left(k_f - \frac{1}{y}\right)} \right), \\ x_{d2} &= \sqrt{\frac{A_t x_{d1}^2 \left(x_{d1} - q_{nl}\right)}{P_d + R_g \left(i_{dg} + i_{qg}\right)^2}}, \\ x_{d3} &= 0, \\ x_{d4} &= \frac{T_m + k_2\left(x_{d5} - w_m\right)}{\psi}, \\ x_{d5} &= w_m \end{aligned} \tag{12}$$

The SMC design process is broadly classified into two modes, the reaching and sliding mode. The states trajectories (1), (3), and

(5)–(7) are considered to obtain equivalent dynamics after application of the reaching condition ($\sigma = 0$) in (11):

$$\begin{bmatrix} y \\ i_{dg} \\ i_{qg} \end{bmatrix} - \begin{bmatrix} x_{d2} \\ x_{d3} \\ x_{d4} \end{bmatrix} = 0 \tag{13}$$

Now the system trajectories slide on the switching surface after reaching it. Hence, sliding condition ($\dot{\sigma} = 0$) is applied on (11) and written in (14):

$$\begin{bmatrix} \frac{dy}{dt} \\ \frac{di_{dg}}{dt} \\ \frac{di_{qg}}{dt} \end{bmatrix} - \begin{bmatrix} \frac{dx_{d2}}{dt} \\ \frac{dx_{d3}}{dt} \\ \frac{dx_{d4}}{dt} \end{bmatrix} = 0 \tag{14}$$

From (3), (5), (6), and (12), the dynamics of (14) becomes equal to the desired stable equilibrium states and slide on the switching surface. Hence, (14) can be written in (15):

$$\begin{bmatrix} u \\ v_d \\ v_q \end{bmatrix} = \begin{bmatrix} x_{d2} \\ \frac{R_g}{L_g} x_{d3} - x_{d5} x_{d4} \\ \frac{R_g}{L_g} x_{d4} - x_{d5} x_{d3} - \psi x_{d5} \end{bmatrix} \tag{15}$$

Theorem 1: To reach and slide on the switching surface within the bounded region, the system trajectories should be equal to stable equilibrium states using the SMC control law in (16):

$$\begin{bmatrix} u \\ v_d \\ v_q \end{bmatrix} = \begin{bmatrix} x_{d2} + k_3 sign(\sigma_1) \\ \frac{1}{v_{dc}} \left(\frac{R_g}{L_g} x_{d3} - x_{d5} x_{d4} + k_4 sign(\sigma_2) \right) \\ \frac{1}{v_{dc}} \left(\frac{R_g}{L_g} x_{d4} - x_{d5} x_{d3} - \psi x_{d5} + k_5 sign(\sigma_3) \right) \end{bmatrix} \tag{16}$$

Where, tuning terms k_1, k_2, k_3, k_4 and k_5 are positive scalars.

Proof: The asymptotic convergence criteria are proved using Lyapunov's function in (17):

$$\vartheta = \frac{1}{2} \sigma^T \sigma \tag{17}$$

The above (17) is differentiated, and after substitution from (3), (5), (6), and (12), it can be written in (18):

$$\frac{d\vartheta}{dt} = \sigma^T \begin{pmatrix} y - u \\ \frac{R_g}{L_g} i_{dg} - w_m i_{qg} - v_{dc} v_d \\ \frac{R_g}{L_g} i_{qg} - w_m i_{dg} - \psi w_m - v_{dc} v_q \end{pmatrix} \tag{18}$$

Using SMC control law (16), the above equation in (19):

$$\frac{d\vartheta}{dt} = \sigma^T \begin{pmatrix} y - x_{d1} - k_3 sign(\sigma_1) \\ \frac{R_g}{L_g} [i_{dg} - x_{d3}] - \left(w_m i_{qg} - x_{d5} x_{d4} \right) - k_4 sign(\sigma_2) \\ \frac{R_g}{L_g} \left(i_{qg} - x_{d4} \right) - \left(w_m i_{dg} - x_{d5} x_{d3} \right) - \psi \left(w_m - x_{d5} \right) - k_5 sign(\sigma_3) \end{pmatrix} \tag{19}$$

The closed-loop dynamics of the SHP-based DC microgrid with SMC law converges asymptotically on the desired stable equilibrium states. Hence, the above equation is simplified in (20):

$$\frac{d\vartheta}{dt} \le -\sigma^T \left[k_3 sign(\sigma_1) \quad k_4 sign(\sigma_2) \quad k_5 sign(\sigma_3) \right]^T \tag{20}$$

However, the SMC law converges asymptotically on desired stable equilibrium states for $k_3 > 0$, $k_4 > 0$, and $k_5 > 0$ respectively. This completes the proof.

IV. RESULTS AND DISCUSSION

In this section, the robustness of the proposed control scheme is validated on SHP-based DC microgrid systems. The nonlinear state-space dynamics of the SHP-based DC microgrid systems is simulated

TABLE
SYSTEM PARAMETERS AND VARIABLES [20]

Components	Parameters	Values (in unit)
PMSG	P	20 kW
	v_{dc}	480 V
	w_m	2π34 rad/s
	R_g	0.05 pu
	L_g	0.08 pu
	ψ	1.50 pu
	M	25.0 pu
SHP	T_w	4 sec
	q_{nl}	1.25
	T_y	0.3 sec
	k_f	$1.7*10^{-4}$ pu
	A_t	1.25 pu
Controller tuning parameters	k_1	1.5 pu
	k_2	2.0 pu
	k_3	0.3 pu
	k_4	4.0 pu
	k_5	0.9 pu

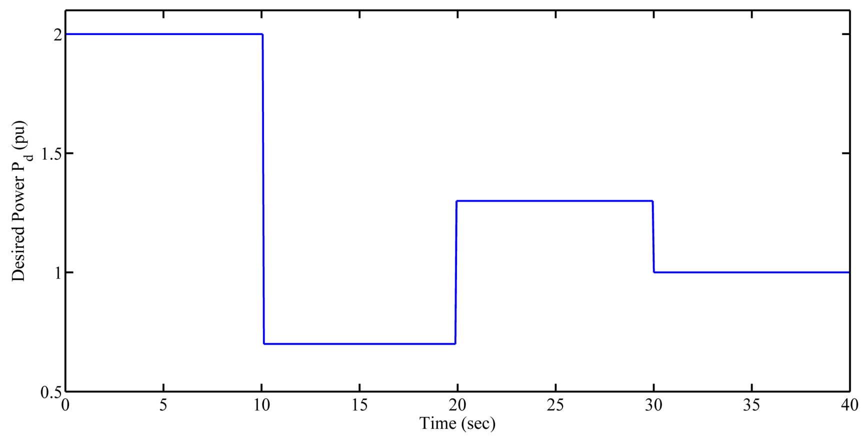

Fig. 3. Desired active power disturbance pattern in SHP.

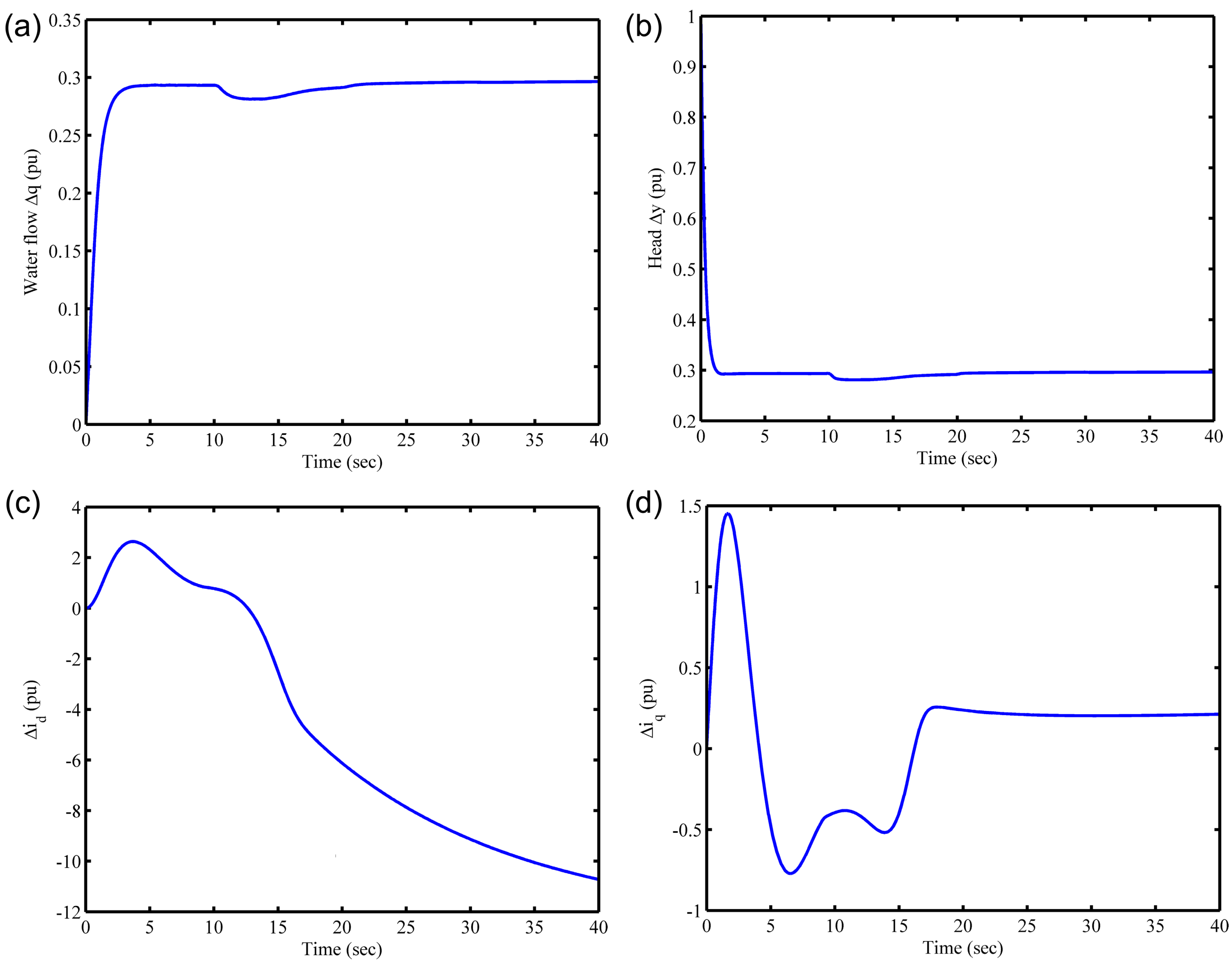

Fig. 4. (a) Normalized water flow of the SHP; (b) water head of the SHP; (c) d-axis current response of the PMSG; and (d) q-axis current response of the PMSG.

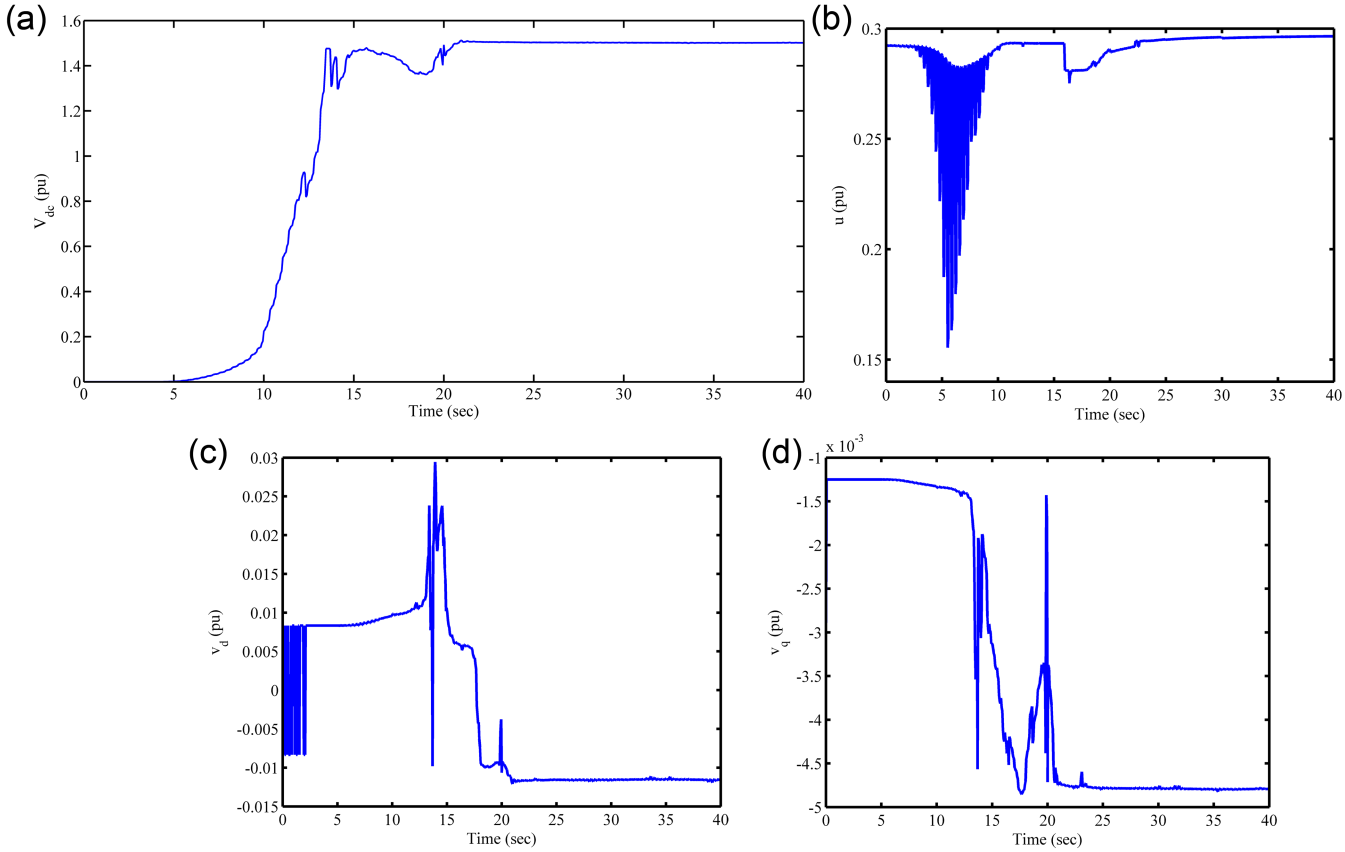

Fig. 5. (a) DC microgrid voltage; (b) control effort of the SHP; (c) d-axis control effort of the PMSG; and (d) q-axis control effort of the PMSG.

using MATLAB© software, as shown in Fig. 2. The SHP-based DC microgrid system parameters are given in the appendix in Table. The microgrid model under discussion contains a PMSG having values of 20 kW, an SHP, a 480 V DC grid, a hydraulic turbine, and a VSC.

The performance of the sliding mode controller is demonstrated in presence of [01001] initial condition and random uncertainties in the desired active power reference in SHP, as shown in Fig. 3 respectively. The deviations in normalized water flow and water head in the reservoir in SHP, and d-axis and q-axis currents in PMSG dynamics are shown in Fig. 4(a-d) respectively. It is seen that deviations in normalized water flow and water head in the reservoir in SHP are negligible, with very short time interval, due to presence of random uncertainties in the desired active power reference in SHP.

The trajectories of the PMSG dq-axis currents are also shown in Fig. 4(a-d) and found within the limit range. Hence, the proposed control structure converges the SHP system trajectories on the desired stable equilibrium point effectively, which remains in the stable region.

The DC voltage deviation at the VSC output terminal, SHP control effort, and PMSG dq-axis voltage control efforts are given in Fig. 5(a-d) respectively. It is evident that the oscillations in DC voltage and chattering in the controlled signals are minimum due to the robust quality of the proposed control strategy, even in the presence of arbitrary random desired active power reference in SHP. Hence, the proposed controller confirms speedy convergence of system dynamics on the equilibrium point, with negligible oscillations; and it improves steady state error responses simultaneously with reduction in the chattering against input uncertainty.

The PMSG rotor angular speed deviation and generated active power deviation are shown in Fig. 6(a-b) respectively, in the presence of arbitrary random desired active power reference in SHP and initial state perturbations. It is evident in the said figure that the PMSG rotor angular speed and active power both have minimum steady state errors with negligible oscillations.

It is observed that the sliding mode-based control scheme converged the SHP and PMSG system nonlinear dynamics on the equilibrium point effectively and is insensitive even in presence of uncertainties in the desired parameters. Thus, the proposed control scheme has negligible steady state error and faster stabilization.

V. CONCLUSION

The microgrid plays an important role in the electric power system because it can provide reduced reliance on the local utility microgrid, better service reliability, and also an enhanced economy. In this paper, a sliding mode controller is proposed to minimize the steady state errors and stabilization problems in an SHP-based DC microgrid. The nonlinear model of both SHP and PMSG with VSC

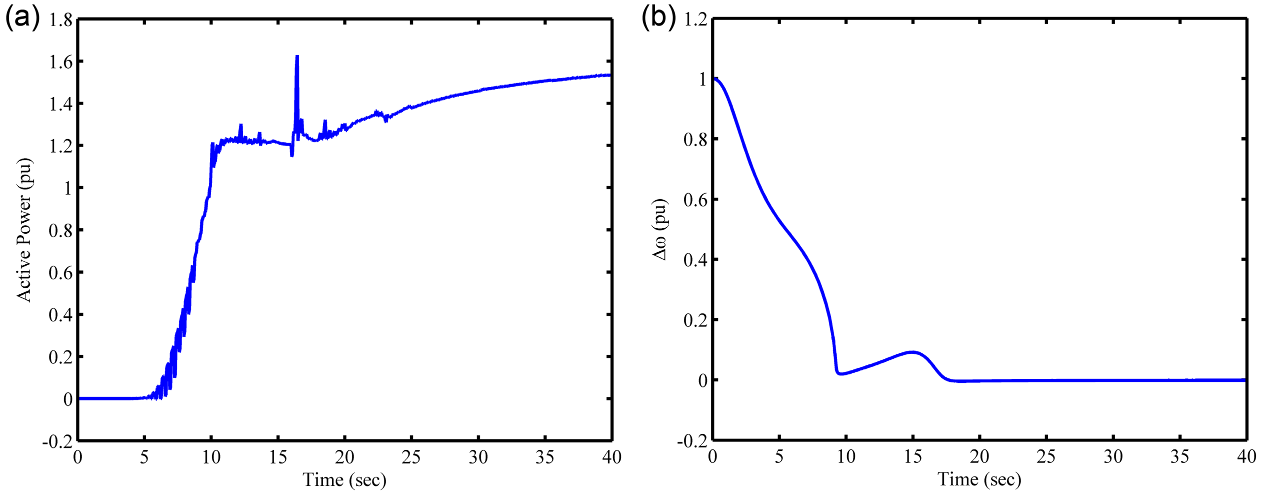

Fig. 6. (a) Deviations in the PMSG angular speed; and (b) generated DC power.

was considered to minimize the SHP-based DC microgrid issues. The proposed controller design effectively interpreted the steady state errors and stabilization challenges in the SHP-based DC microgrid. Based on the Lyapunov stability theorem, the control law was derived to ensure the asymptotic convergence to minimize the steady state errors and improve the closed-loop system stabilization effectively. The proposed control law also guaranteed stable operation in a short limited time. As results, the proposed controller confirmed the speedy convergence of steady state error dynamics with negligible oscillations and reduced the limitation of chattering notably, without any loss in control accuracy. In future, the integration of the microgrid with the live grid will be analyzed using a centralized controller in the presence of communication delays.

Peer-review: Externally peer-reviewed.

Conflict of Interest: The authors have no conflicts of interest to declare.

Financial Disclosure: The authors declared that this study has received no financial support.

REFERENCES

1. A. Cagnano, E. De Tuglie, and P. Mancarella, "Microgrids: Overview and guidelines for practical implementations and operation," *Appl. Energy*, vol. 258, p. 114039, 2020. [CrossRef]
2. M. A. Jirdehi, V. S. Tabar, S. Ghassemzadeh, and S. Tohidi, "Different aspects of microgrid management: A comprehensive review," *J. Energy Storage*, vol.30, p. 101457, 2020. [CrossRef]
3. J. S. Gómez *et al.*, "An overview of microgrids challenges in the mining industry," *IEEE Access*, vol. 8, pp. 191378–191393, 2020. [CrossRef]
4. F. Gao, R. Kang, J. Cao, and T. Yang, "Primary and secondary control in DC microgrids: A review," *J. Mod. Power Syst. Clean Energy*, vol. 7, no. 2, pp. 227–242, 2019. [CrossRef]
5. S. M. Altunkaya and M. Özcan, "Emerging financing tools for renewable energy investments," *Turk. J. Electr. Power Energy Syst.*, vol. 1, pp. 33–41, 2021. [CrossRef]
6. S. Beheshtaein, R. M. Cuzner, M. Forouzesh, M. Savaghebi, and J. M. Guerrero, "DC microgrid protection: A comprehensive review," *IEEE J. Emerg. Sel. Top. Power Electron.*, 1–1. [CrossRef]
7. N. T. Mbungu, R. M. Naidoo, R. C. Bansal, and V. Vahidinasab, "Overview of the optimal smart energy coordination for microgrid applications," *IEEE Access*, vol. 7, pp. 163063–163084, 2019. [CrossRef]
8. T. Kerdphol, F. S. Rahman, Y. Mitani, M. Watanabe, and S. K. Küfeoğlu, "Robust virtual inertia control of an islanded microgrid considering high penetration of renewable energy," *IEEE Access*, vol. 6, pp. 625–636, 2018. [CrossRef]
9. M. K. Mishra, N. Khare, and A. B. Agrawal, "Small hydro power in India: Current status and future perspectives," *Renew. Sustain. Energy Rev.*, vol. 51, pp. 101–115, 2015. [CrossRef]
10. D. Sharma, S. Mishra, and J. Nanda, "Micro-grid operation and control of Photo-Voltaic power with canal-based small hydro power plant," in IEEE Region 10 Conference (TENCON), 2016, pp. 1289–1293.
11. D. Borkowski, "Analytical model of small hydropower plant working at variable speed," *IEEE Trans. Energy Convers.*, vol. 33, no. 4, pp. 1886–1894, 2018. [CrossRef]
12. W. J. Gil-González, A. Garces, O. B. Fosso, and A. Escobar-Mejía, "Passivity-based control of power systems considering hydro-turbine with surge tank," *IEEE Trans. Power Syst.*, vol. 35, no. 3, pp. 2002–2011, 2020. [CrossRef]
13. H. S. Sachdev, A. K. Akela, and N. Kumar, "Analysis and evaluation of small hydropower plants: A bibliographical survey, " *Renew. Sustain. Energy Rev.*, vol. 51, pp. 1013–1022, 2015. [CrossRef]
14. M. R. A. R. Santabudi, A. S. Rohman, and H. F. Prasetyo, "Speed control implementation of BLDC motor using sliding mode two-steps LMI design," in IEEE 3rd International Conference on Science in Information Technology (ICSITech), 2017.
15. R. P. Vieira, L. T. Martins, J. R. Massing, and M. Stefanello, "Sliding mode controller in a multiloop framework for a grid-connected VSI with LCL filter," *IEEE Trans. Ind. Electron.*, vol. 65, no. 6, pp. 4714–4723, 2018. [CrossRef]
16. C. Yin, X. Huang, Y. Chen, S. Dadras, S.-M. Zhong, and Y. Cheng, "Fractional-order exponential switching technique to enhance sliding mode control," *Appl. Math. Modell.*, vol. 44, pp. 705–726, 2017. [CrossRef]
17. A. Oveisi and T. Nestorovic, "Robust observer-based adaptive fuzzy sliding mode controller," *Mech. Syst. Signal Process.*, vol. 76–77, pp. 58–71, 2016. [CrossRef]
18. I. Alagöz, M. Bulut, V. Geylani, and A. Yıldırım, " Importance of real-time hydro power plant condition monitoring systems and contribution to electricity production," *Turk. J. Electr. Power Energy Syst.*, vol. 1, no. 1, pp. 1–11, 2021. [CrossRef]

19. W. Gil-González, O. D. Montoya, and A. Garces, "Modeling and control of a small hydro-power plant for a DC microgrid," *Electr. Power Syst. Res.*, vol. 180, p. 106104, 2020.
20. D. K. Maina, M. J. Sanjari, and N. C. Nair, "Voltage and frequency response of small hydro power plant in grid-connected and islanded mode," in Australasian Universities Power Engineering Conference (AUPEC), pp. 1–7, 2018.
21. S. Camal, F. Teng, A. Michiorri, G. Kariniotakis, and L. Badesa, "Scenario generation of aggregated wind, photovoltaics and small hydro production for power systems applications," *Appl. Energy*, vol. 242, pp. 1396–1406, 2019. [CrossRef]
22. B. Guo, A. Mohamed, S. Bacha, and M. Alamir, "Variable speed micro-hydro power plant: Modelling, losses analysis, and experiment validation," in IEEE International Conference on Industrial Technology (ICIT), 2018, pp. 1079–1084.
23. A. Y. Hatata, M. M. El-Saadawi, and S.Saad, "A feasibility study of small hydro power for selected locations in Egypt," *Energy Strategy Rev.*, vol.24, pp.300–313, 2019. [CrossRef]
24. B. d. A. Regina, M. J. R. Agular, and A. A. Ferreira, "Comprehensive and didactic DC servomotor control platform," in IEEE 15th Brazilian Power Electronics Conference and 5th IEEE Southern Power Electronics Conference (COBEP/SPEC), 2019, pp. 1–6.
25. E. Ebrahimzadeh, F. Blaabjerg, X. Wang, and C. L. Bak, "Harmonic stability and resonance analysis in large PMSG-based wind power plants," *IEEE Trans. Sustain. Energy*, vol. 9, no. 1, pp. 12–23, 2018. [CrossRef]
26. L. P. Kunjumuhammed, B. C. Pal, R. Gupta, and K. J. Dyke, "Stability analysis of a PMSG-based large offshore wind farm connected to a VSC-HVDC," *IEEE Trans. Energy Convers.*, vol. 32, no. 3, pp. 1166–1176, 2017. [CrossRef]
27. W. Gil-González, A. Garcés, and O. B. Fosso, "Passivity-based control for small hydro-power generation with PMSG and VSC," *IEEE Access*, vol. 8, pp. 153001–153010, 2020. [CrossRef]
28. X. Yu and O. Kaynak, "Sliding mode control made smarter: A computational intelligence perspective," *IEEE Syst. Man Cybern. Mag.*, vol. 3, no. 2, pp. 31–34, 2017.
29. H. Ye, M. Li, and W. Luo, "A novel reaching law of sliding mode control design and analysis," in Chinese Automation Congress (CAC), 2017, pp. 1803–1807.
30. S. Prasad, S. Purwar, and N. Kishor, "Non-linear sliding mode load frequency control in multi-area power system," *Control Eng. Pract.*, vol. 61, pp. 81–92, 2017. [CrossRef]
31. S. Prasad, S. Purwar, and N. Kishor, "H-infinity based non-linear sliding mode controller for frequency regulation in interconnected power systems with constant and time-varying delays," *IET Gener. Transm. Distrib.*, vol. 10, no. 11, pp. 2771–2784, 2016. [CrossRef]
32. S. Dong, C. L. P. Chen, M. Fang, and Z. G. Wu, "Dissipativity-based asynchronous fuzzy sliding mode control for T–S fuzzy hidden Markov jump systems," *IEEE Trans. Cybern.*, vol. 50, no. 9, pp. 4020–4030, 2020. [CrossRef]
33. O. D. Montoya, A. Garces, S. Avila-Becerril, G. Espinosa-Pérez, and F. M. Serra, "Stability analysis of single-phase low-voltage AC microgrids with constant power terminals," *IEEE Trans. Circuits Syst. II*, vol. 66, no. 7, pp. 1212–1216, 2019. [CrossRef]

cigre Turkey

TEPES
TURKISH JOURNAL OF
ELECTRICAL POWER
AND ENERGY SYSTEMS

TEPES Vol 1., Issue. 2, 99-107, 2021 **DOI:** 10.5152/tepes.2021.21043

RESEARCH ARTICLE

A Comparative Study on the Performances of Power Systems Load Forecasting Algorithms

Titus Oluwasuji Ajewole[1], Abdulsemiu Alabi Olawuyi[2], Mutiu Kolawole Agboola[3], Opeyemi Onarinde[1]

[1]Department of Electrical and Electronic Engineering, Osun State University, Osogbo, Nigeria
[2]Department of Electrical and Electronic Engineering, Osun State Polytechnic Iree, Osun State, Nigeria
[3]Department of Electrical and Electronics Engineering Technology, Federal Polytechnic Ede, Osun State, Nigeria

Cite this article as: Ajewole Titus O, Olawuyi Abdulsemiu A, Agboola Mutiu K, Onarinde O. A comparative study on the performances of power systems load forecasting algorithms. *Turk J Electr Power Energy Syst.* 1(2), 99-107, 2021.

ABSTRACT

In this study, the efficiencies of three different neural network load forecasting algorithms are compared to determine the best performance. The algorithms—Levenberg–Marquardt, gradient descent, and gradient descent with momentum and adaptive learning rate backpropagation are used to train a neural network (NN) model for energy demand prediction on a power system. Prior loads, weather parameters (temperature, relative humidity, and precipitation), and customer population of the supplied region are employed as training inputs. To ascertain the accuracy of the predictions, mean absolute error and mean square error are used as evaluation indices, and the algorithm with the least index values is deployed on a transmission substation. The Levenberg–Marquardt algorithm was found to be the most efficient candidate, and this algorithm is therefore recommended for adequate and proper system management, planning, and expansion, to enhance the efficiency, effectiveness, and accessibility of power supply.

Index Terms—Algorithm, comparison, load forecasting, model training, neural network, transmission substation.

I. INTRODUCTION

The ever-increasing human population and the need for industrialization have led the human race to a dire need for stable and quality electrical energy [1, 2]. Proper planning for adequate electrical energy is therefore an absolute necessity. Load forecasting is an important planning practice in power system industries, as its relevance stems from both the energy perspective and the economic angle [3]. Accurate load forecasting has many benefits, both managerially and economically. In the absence of efficient and effective forecasting of load, wastage is inevitable. Thus, robust forecasting is absolutely essential for the stakeholders in the energy sector [3]. Electrical load forecasting plays a key role for energy providers, economic consortia, and other corporations in the domain of electrical energy [4]. However, for a load forecast to best serve its ultimate purpose, it must be accurate, fast, and robust [5]; and the loss function should be optimally minimized [6].

There has been a lot of attention on load forecast studies using different methods with various time bounds [7]. While some studies have used statistical techniques [8-10], there are others that have used the artificial intelligence (IA) algorithms or machine learning models [11, 12]. One of the machine learning models that has gained a lot of relevance in load forecasting is the neural network (NN), which is a machine learning pattern that mimics the working function of the brain [13]. Machine learning uses data and produces a model to perform a task [14].

Load forecast in a power system is generally classified into short-term load forecast (STLF), medium-term load forecast (MTLF), and long-term load forecast (LTLF) [4]. However, [5] presents a fourth type, with the addition of very-short-term load forecast (VSTLF). The VSTLF has the least time of forecast, as [6] highlights that the period of this forecast is from one minute to one day. Conversely, [4] proposed that the range of VSTLF is from a few minutes to an hour ahead. The time range given by the latter is worth noting because if the time range extends to a day, then it is STLF [15]. The predictions of load for various time horizons are noted for various operations [10]. Very-short-term load forecast is significant because it helps the electric utilities and grid operators in making important decisions on real-time scheduling of electricity generation, real-time operation,

Corresponding author: Abdulsemiu Alabi Olawuyi, abdulsemiuolawuyi@gmail.com

Received: August 18, 2021
Accepted: September 20, 2021
Published online: October 15, 2021

demand–response, security assessment, sensitivity analysis, and load frequency control [3]. Furthermore, it is also helpful in real-time control of the electrical power system [4]. While [16] proposes that load prediction from a few hours to a few days is STLF, the authors in [4, 8–10] are more specific that STLF is often between an hour and one week. Short-term load forecast also gives hourly forecast results and is useful in power system decision making in overload condition and in spinning reserve planning [6]. It also plays an important role in grid stability [16], and moreover, [15] add that STLF provides useful notifications for power system administrators to enhance load usage. In the case of MTLF, the range is mostly between 7 days and 12 months [3, 13, 14], and its significance includes providing the power system stakeholders with adequate notification for system expansion, power system equipment requirements, and employment of staff [17]. Any load prediction that is for more than a year is grouped as LTLF [18], which lasts years and even decades, and is useful for future expansion, planning, as well as recruitment of staff [15, 19].

Considering its numerous aspects of importance in power systems, load forecasting needs to be efficient and effective. The various techniques used in forecasting power system loads are grouped into three, namely, the statistical or classical or parametric method, the machine learning or non-parametric method, and the hybrid method [1]. Because electrical loads are affected by several factors like class of consumers, variation in the calendar, holidays, the time of day, economic activities, random activities like sports and festivals, meteorological parameters, and so on, load-prediction techniques need to be compared for optimal choice. Among the meteorological factors, temperature is the most important and most common input [16, 17]. In an evaluation of the statistical methods as presented in [8], three analytical techniques are employed to address the MTLF problem, with mean absolute percentage error and root mean square error used as evaluation metrics. A comparison of the three techniques shows that the technique of linear regression performs better than both compound growth and quadratic regression techniques. The NN is employed by [1] to predict a power system, with mean square error (MSE) and mean absolute error (MAE) used as evaluation indices in the work which compares the backpropagation neural network (BPNN) and the radial basis function neural network (RBFNN). The BPNN has a better model, with ten hidden neurons, while the RBFNN has better architecture, with 15 neurons. In the work, the Levenberg–Marquardt (LM) algorithm performed better than the GD with momentum and adaptive learning rate backpropagation (GD+) algorithm. Meanwhile, the shortcoming in the work relates to the large values of the performance metrics. In Ref [19], NN performed better than the support vector machine, k-nearest neighbors, generalized regression neural network, and the Gaussian process regression and recurrent neural network; with the least value of 1.5 during the validation process, while the other machine learning methods had values greater than 1.5.

In this present study, three different algorithms are compared, as they are employed to train the artificial neural network (ANN) and to ascertain the one that performs optimally. To ascertain the accuracy of the predictions, MAE and MSE are used as evaluation indices. The optimal algorithm is consequently used for electrical load prediction in a transmission substation and then recommended for adequate and proper system management, planning, and expansion, to enhance the efficiency, effectiveness, and accessibility of power supply. The rest of this paper is structured as follows: while Section II presents the methodology of the study, the results obtained and the analyses of same are contained in Section III, and Section IV concludes the study.

II. MATERIALS AND METHODS

Performances of Levenberg–Marquardt (LM), GD, and gradient descent with momentum and adaptive learning rate backpropagation (GD+) are compared to ascertain the optimal algorithm, as the three are used in the training of ANN. The best performing one is thereafter deployed for load prediction on a transmission substation. The Osogbo Substation in Southwest Nigeria is strategically located very close to the National Control Centre; therefore, the Transmission Company of Nigeria uses the substation for grid stability. Electrical load data were obtained from the Regional Control Centre, while information on weather parameters was obtained from the National Aeronautics and Space Administration (NASA), and the population data were obtained online. As shown in Fig. 1, feed-forward backpropagation is employed in modeling the NN, with six inputs—temperature, relative humidity, precipitation, population, actual load of year 2011 and actual load of year 2012—feeding the model. While Table I shows the values of the input parameters, Fig. 2 shows that there are 15 neurons in the hidden layer of the model, with hyperbolic tangent as the activation function.

The target of the model is the actual load for year 2013, which is the model's output. The MSE and MAE are used to evaluate the network, and are described as [1]:

$$\text{MSE} = \frac{1}{N}\sum_{i=0}^{N}\left(y-y\right)^{2} \tag{1}$$

$$\text{MAE} = \frac{1}{N}\sum_{i=0}^{N}\left|y-y\right| \tag{2}$$

For design and training of the NN, the perceptron and the algorithms are described. Shown in Fig. 3 is the block diagram of the perceptron, while Fig. 4 depicts a single-layer NN.

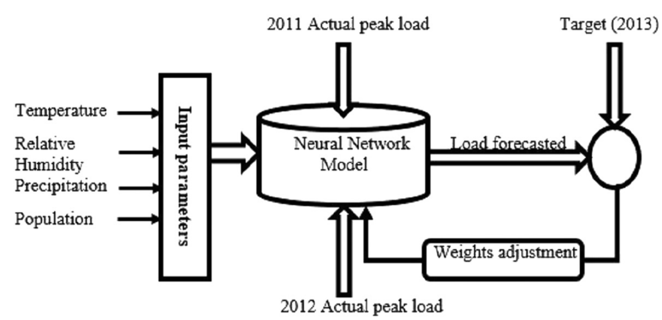

Fig. 1. ANN block diagram representation.

TABLE I
INPUT PARAMETERS OF THE NEURAL NETWORK

Input Parameters of the Neural Network						
Months	***T*** **(°C)**	**Relative Humidity**	**Precipitation (mm)**	**Population**	**2011 Peak Load (MW)**	**2012 Peak Load (MW)**
January	24.18	70.90	31.98	614917	66.1	65.2
February	25.73	77.81	47.31	615834	63.7	66.2
March	26.14	84.09	60.72	616750	66.8	68.9
April	25.69	84.15	138.97	617667	69.4	68.9
May	25.02	87.72	209.95	618583	70.9	72.1
June	24.35	88.58	204.55	619500	60.4	77.5
July	23.60	89.26	214.75	620416	62.1	77.5
August	23.39	88.86	182.19	621333	65.1	79.6
September	24.14	89.25	370.49	622249	60.7	67.9
October	24.81	88.39	203.07	623166	56.4	68.7
November	24.96	83.43	72.98	624083	68.9	79.0
December	24.45	70.68	28.27	625000	66.1	78.4

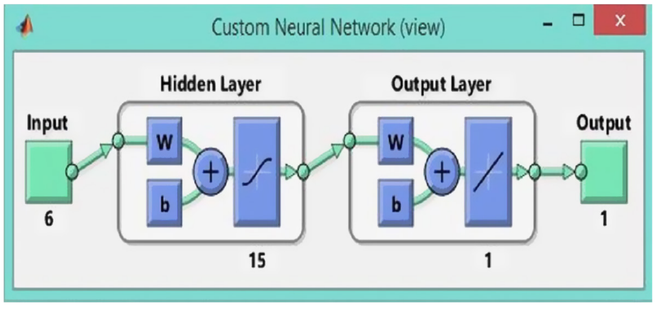

Fig. 2. Neural network architecture.

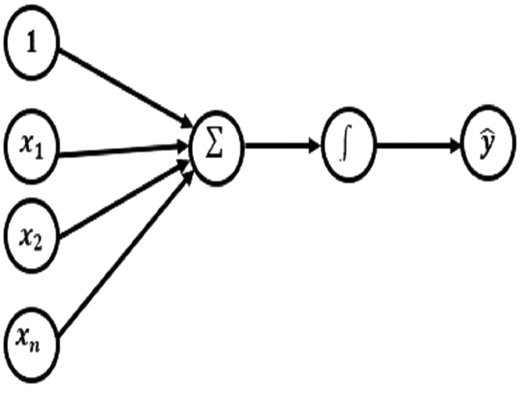

Fig. 3. A perceptron.

For the perceptron:

$$y = g\left(w_0 + X^T W\right) \tag{3}$$

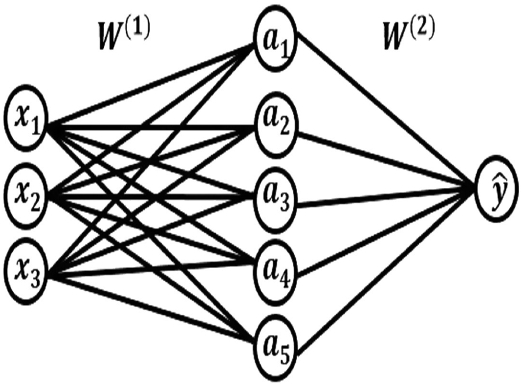

Fig. 4. Single-layer neural network.

where y is the output, g is the activation function, w_0 is the bias, X is the inputs matrix, and W is the network weights [6].

In the NN, the weights that separate the inputs and the hidden stratum are $W^{(1)}$, while those weights that separate the hidden stratum and the final stratum are $W^{(2)}$. As given in [6], the hidden layer is described as:

$$a_i = w_{0,i}^{(1)} + \sum_{j=1}^{m} x_j w_{j,i}^{(1)} \tag{4}$$

Thus, the hidden layer output will be $g(a_i)$ which corresponds to the inputs that feed the output layer:

$$y = g\left(w_{0,i}^{(2)} + \sum_{j=1}^{d1} g\left(a_j\right) w_{j,i}^{(2)}\right) \tag{5}$$

Therefore,

$$y = g\left(w_{0,1}^{(2)} + g(a_1)w_{1,1}^{(2)} + g(a_2)w_{2,1}^{(2)} + g(a_3)w_{3,1}^{(2)} + g(a_4)w_{4,1}^{(2)} + g(a_5)w_{5,1}^{(2)}\right) \tag{6}$$

The algorithms of this study are LM, GD, and GD+. While LM is a modification of Newton's method [20], GD is a classical algorithm for weight updates in the NN [21], and extension to GD produces the GD+ [22].

A. Levenberg–Marquardt

Being a modification of Newton's method, LM is represented using Newton's equation [23]:

$$x_{k+1} = x_k - H[x_k]^{-1} g_k \tag{7}$$

where H is the Hessian matrix, x_k the current value of x, g is the gradient, and x_{k+1} is the updated value of x. The Hessian matrix may not be positive definite. Hence, the LM modification addresses this shortcoming by adding $\mu_k I$ to the Hessian matrix. I is an identity matrix and $\mu_k \geq 0$. Thus,

$$x_{k+1} = x_k - \left(H(x_k) + \mu_k I\right)^{-1} g_k \tag{8}$$

And by introducing a step size, α_k (8) becomes,

$$x_{k+1} = x_k - \alpha_k \left(H(x_k) + \mu_k I\right)^{-1} g_k \tag{9}$$

Furthermore, when $\mu_k \to 0$, the LM modification tends to behave like the pure Newton's method. Also, when $\mu_k \to \infty$, the algorithm attains a pure GD with a small learning rate. The LM algorithm is, on the other hand, obtained from the Gaussian method [20] in (10):

$$x_{k+1} = x_k - \left(J^T J\right)^{-1} J^T e \tag{10}$$

The Jacobian matrix is denoted by J and e stands for network errors. Therefore,

$$x_{k+1} = x_k - \left(J^T J + \mu_k I\right)^{-1} J^T e \tag{11}$$

B. Gradient Descent

For the GD algorithm, the loss function is minimized by calculating the slope, which is used in updating the weights, and is mathematically modeled as [24]:

$$x_{k+1} = x_k - \alpha_k g_k \tag{12}$$

From (12), α_k is the learning rate, and in the NN, the weights are updated to optimize the errors; x_k denotes the previous weights, while x_{k+1} denotes the updated weights; and g_k is the derivative of the loss function with respect to the weights. During training, the LM algorithm moves from being close to GD to being close to Newton's method. This shows that the LM algorithm is the hybridization of GD and Newton's method

C. Gradient Descent with Momentum and Adaptive Learning Rate Backpropagation

Produced by extension to the GD, the GD+ algorithm ensures elimination of the possibility of being trapped in the local minimum during the training process, by adding a momentum constant to the GD algorithm as [22].

$$x_{k+1} = x_k - \alpha_k V_t \tag{12}$$

Where,

$$V_t = \beta V_{t-1} + (1-\beta) g_k \tag{13}$$

Where, β is momentum constant, taking values $0 < \beta < 1$. When $\beta = 0$, (13) becomes $V_t = g_k$. Therefore, when the momentum constant is zero, GD is obtained. The default value of β is 0.9 [25].

III. RESULTS AND DISCUSSION

A. Correlation Analyses of the Inputs Variables

Fig. 5–8 represent the correlation plots of the input variables in the NN with respect to electrical load, in order to verify the effects of the inputs on the load. The temperature has a positive correlation of 0.3606 as shown in Fig. 8, which implies that an increase in temperature will lead to an increase in electrical load in the supplied region. Moreover, relative humidity, precipitation, and population have corelation coefficients of –0.3458, –0.4394 and –0.2533, respectively. They all have negative correlation with respect to the load. However, the correlation of population shows that an increase

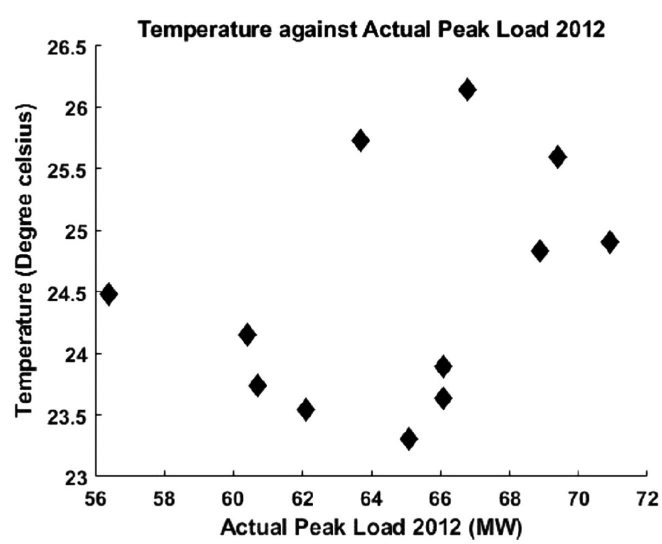

Fig. 5. Scatter plot of temperature (OC) against actual peak load (MW) of 2012.

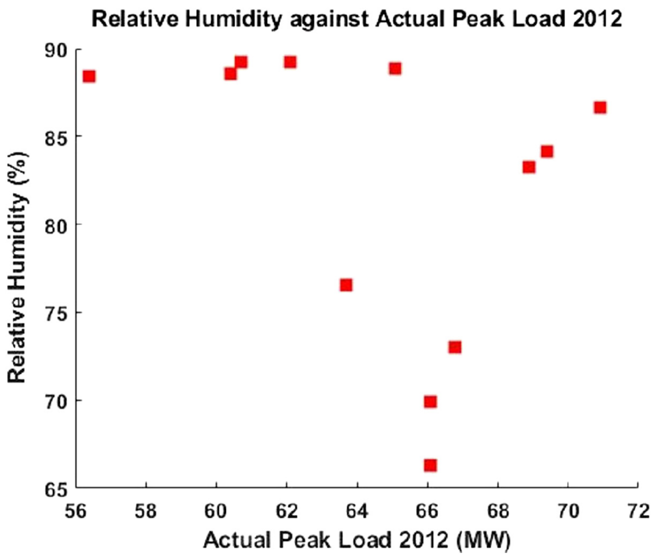

Fig. 6. Scatter plot of relative humidity (%) against actual peak load (MW) of 2012.

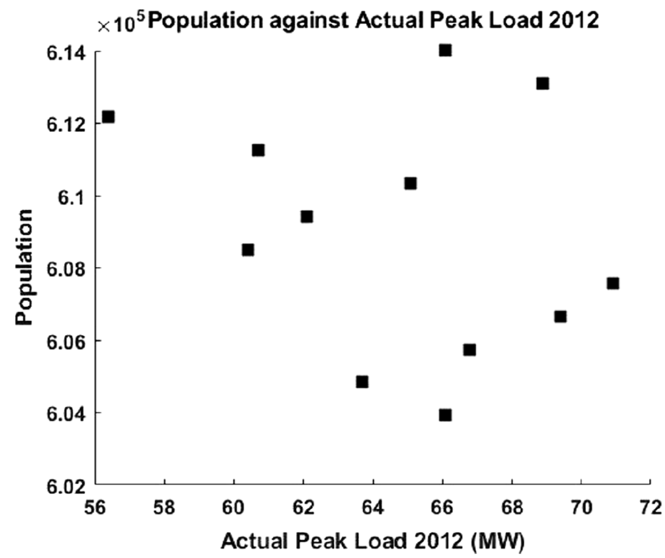

Fig. 8. Scatter plot of population against actual peak load (MW) of 2012.

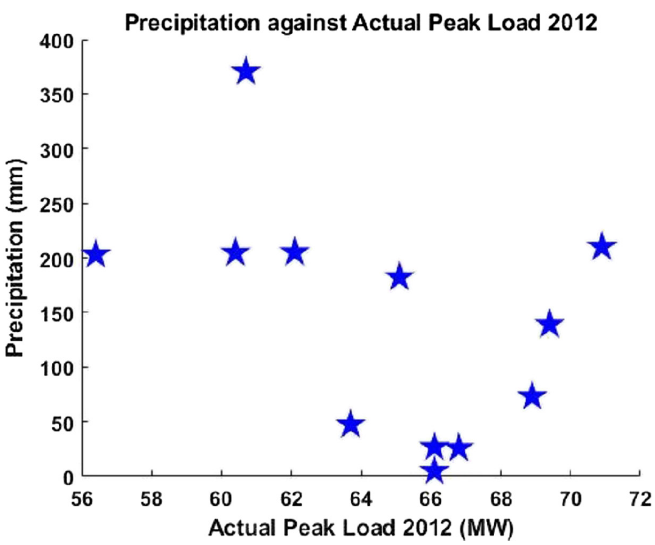

Fig. 7. Scatter plot of precipitation (mm) against actual peak load (MW) of 2012.

in population does not translate to increase in electrical load in the region under study. This problem could be mitigated by using renewable energy [26]. The stakeholders ought to look at this aspect critically to enhance the development needed in Osogbo, because the availability and accesibililty of elecrtrical load are synonymous with development.

B. Regression Analyses

The datasets used for the simulation were divided into 70% for training and 15% each for validation and testing of the NN model. The regression plots for the three algorithms have been presented in Fig. 9–11. Each of the plots has the output against the target. The closer the target to the output, the better the regression plots. Likewise, the more the regression value is to 1, the better. The output value represents the equation of a straight line. The coefficient of the target is the gradient and the constant value is the intercept on output axis. Also, the more the slope is to unity and the intercept to zero, the better the regression plot. Each of the algorithms has four different plots; the training, the validation, the test, and the all plots. The plots of the LM algorithm are shown in Fig. 9. The algorithm was well trained and so has regression value of 1, while the GD and GD+ algorithms have values of 0.9968 and 0.98741 respectively. All the three algorithms performed well during validation and testing, as each has a regression value of unity. However, the all plots give the overall best performing algorithm. The LM, GD, and GD+ algorithms have values of 0.96799, 0.83317 and 0.93658 respectively. These results mean that the LM algorithm has the best performance during the training, because its value of 0.96799 is the closest to 1.

C. Performance Metrics of the Algorithms During Training

The best performing algorithm was also validated using the evaluation metrics. The MAE and MSE functions in the MATLAB Neural Network toolbox were used to evaluate the performance of the three algorithms during the training process. The MAE and MSE of the algorithms are shown in Fig. 12. The LM algorithm has the least values of MAE and MSE, 0.602 and 2.0768 respectively, while GD has the highest values, 1.4559 and 9.9834 respectively, and GD+ performed better than GD because of the momentum it adds and because its learning function could adapt better. The work of [1] also proved that LM is better than GD+. Theoretically, both GD and GD+ are first-order algorithms while LM is a second-order algorithm [23],

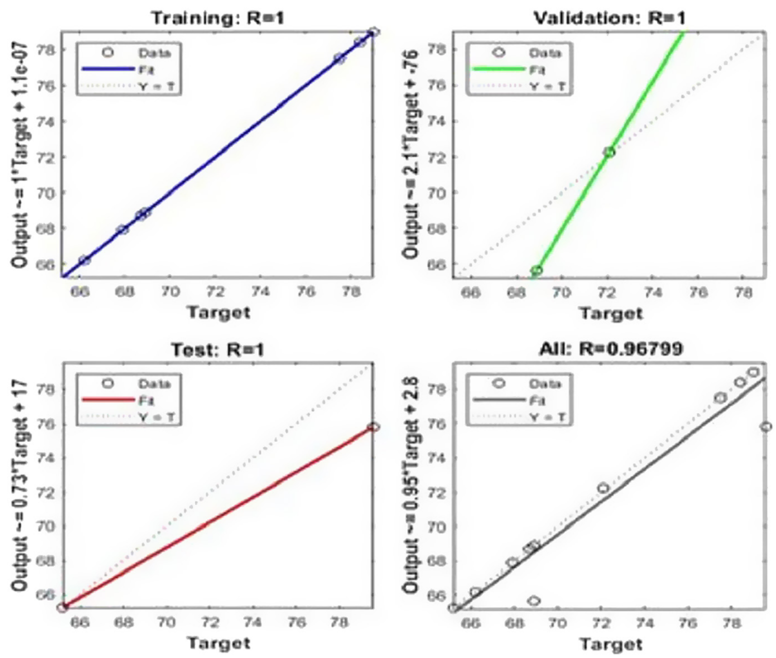

Fig. 9. Levenberg–Marquardt algorithm regression plots.

which can solve more complex problems. Consequently, LG was deployed as the forecasting algorithm in this study.

D. Training and Prediction of the LM Algorithm

Fig. 13 shows the plots of LM during training. The graph illustrates that the target loads are equal to the output loads, except for the months of March and August. The overall errors are nearly zero. This showcases the good performance of the LM algorithm during training process of the NN model. This model was then used for prediction as presented in Fig. 14, which shows that the forecasted load is closest to the actual load for the months of April, May, and September. The errors are between the range 10 and –10, while the

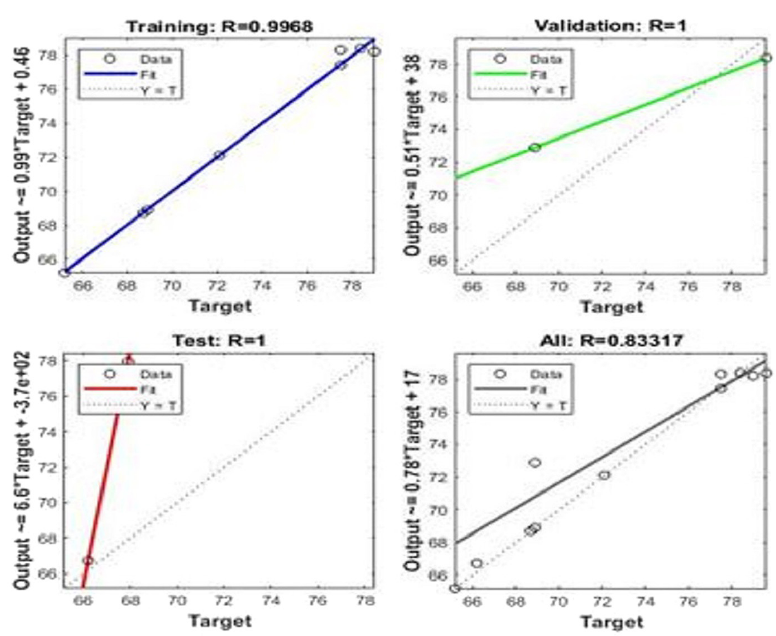

Fig. 10. Gradient descent algorithm regression plots.

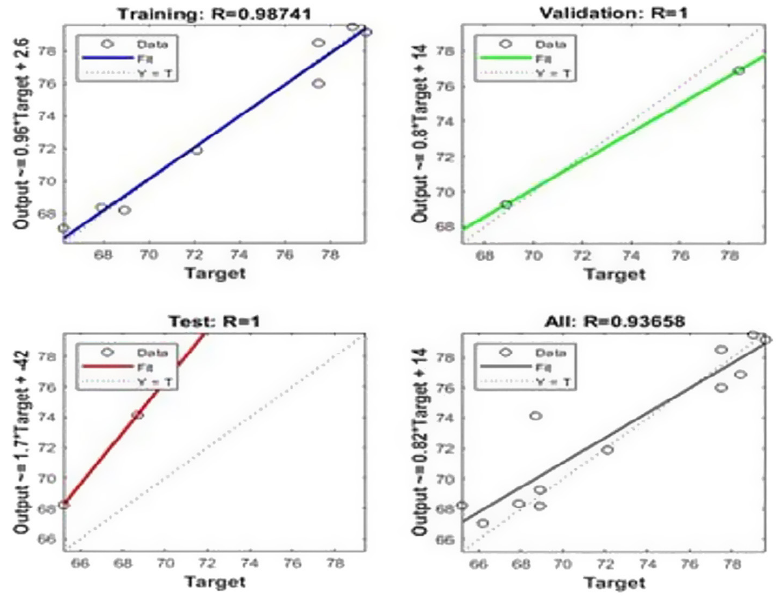

Fig. 11. Gradient descent algorithm with momentum and adaptive learning rate regression plots.

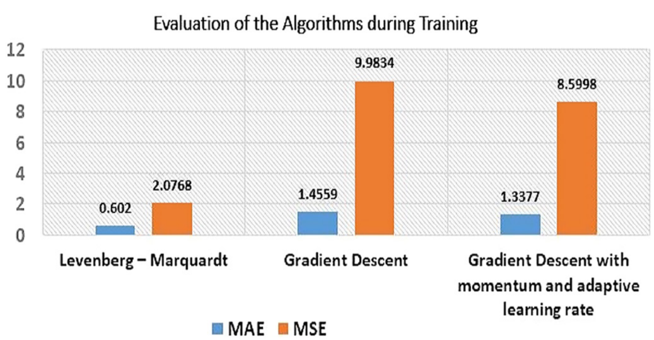

Fig. 12. Evaluation of the algorithms during training.

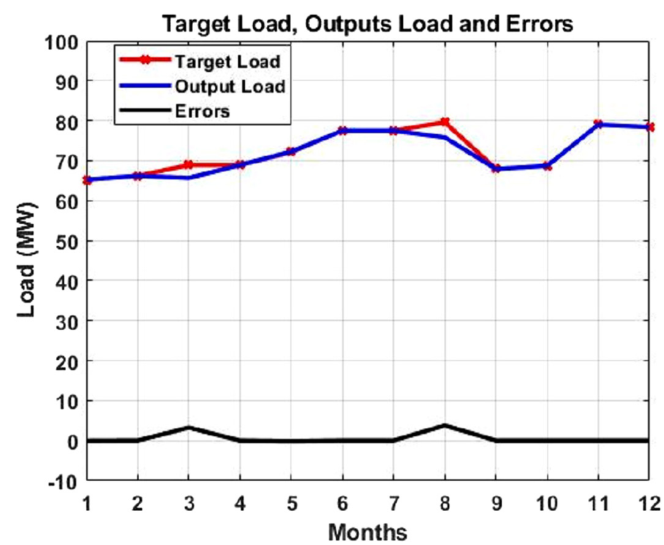

Fig. 13. Target load, output load, and errors using the Levenberg–Marquardt algorithm.

average prediction error is –2.05301. The LM algorithm has relatively good performance in this study, as illustrated in Table II which shows MAE to be 6.4675 and MSE 57.9962. The value of MSE is always greater than MAE because MSE penalizes errors more than MAE, as shown in (1) and (2).

IV. CONCLUSION

Three different NN algorithms have been compared for their electrical load forecasting efficiencies. A NN model was developed for energy demand prediction on power systems, and the Levenberg–Marquardt, gradient descent, and gradient descent with momentum and adaptive learning rate algorithms were used to train the model. The training inputs were prior loads, weather parameters (temperature, relative humidity, and population), and population of the supplied region. From the correlation study of the inputs, it is found that the temperature has a positive correlation of 0.3606, implying that an increase in the temperature will lead to increase in electrical load in the supplied region. In addition, relative humidity, precipitation, and population have a negative correlation of –0.3458, –0.4394, and –0.2533 respectively. The correlation of the population shows that an increase in population does not translate to an increase in electrical load in the region under study. The accuracy of the prediction was appraised using MAE and MSE as evaluation indices; and the algorithm with the least index values was considered the best. Levenberg–Marquardt was found to be the most efficient technique, and was recommended

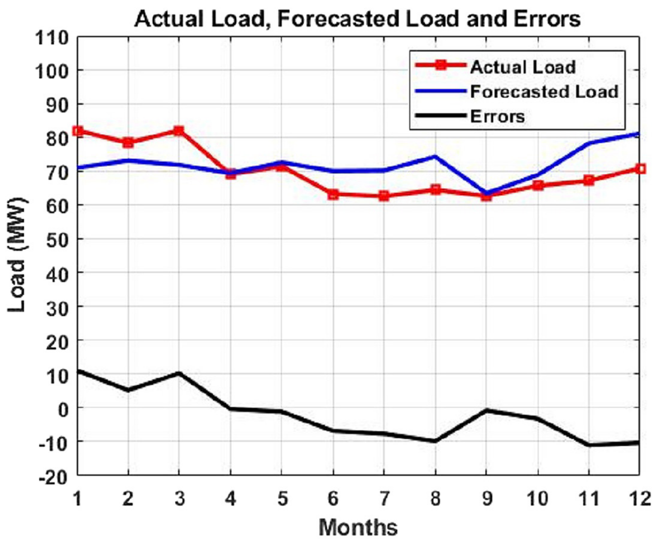

Fig. 14. Actual load, forecasted load, and errors with the Levenberg–Marquardt algorithm.

TABLE II
PERFORMANCE FUNCTION OF THE LM ALGORITHM DURING PREDICTION

Indices	LM Algorithm
MAE	6.4675
MSE	57.9962

for adequate and proper system management, planning, and expansion, to enhance the efficiency, effectiveness, and accessibility of power supply.

Peer-review: Externally peer-reviewed.

Acknowledgments: The authors thank the Regional Control Center, Osogbo, for providing the necessary data on the electrical load utilization of the area from 2011 to 2015. The authors also appreciate the National Aeronautics and Space Administration (NASA), for providing the weather parameters needed for the study.

Conflict of Interest: The authors have no conflicts of interest to declare.

Financial Disclosure: The authors declared that this study has received no financial support.

REFERENCES

1. E. A. Feilat, D. T. Al-Sha'abi and M. A. Mo-mani, "Long-term load forecasting using neural network approach for Jordan's power system," *Eng. Press*, vol. 1, no. 2, pp. 43–50, 2017.
2. T. O. Ajewole, O. D. Momoh, O. D. Ayedun and M. O. Omoigui, "Optimal component configuration and capacity sizing of a mini integrated power supply system," *Environ. Qual. Manag.*, vol. 28, no. 4, pp. 57–62, 2019. [CrossRef]
3. R. Patel, M. R. Patel and R. V. Patel, "A review: Introduction and understanding of load forecasting," *J. Appl. Sci. Comput.*, vol. 4, pp. 1449–1457, 2019.
4. W. Aribowo and S. Muslim, "Long-term electricity load forecasting based on cascade forward backpropagation neural network," *J. Telecommun. Electron. Comput. Eng.*, vol. 12, no. 2, pp. 1449–1457, 2020.
5. P. Dixit, "Daily peak load forecast using artificial neural network," *Int. J. Electr. Comput. Eng.*, vol. 9, no. 4, p. 2256, 2019.
6. A. Amini, "6S191_MIT_DeepLearning_L1.pdf - Introduction to Deep Learning Alexander Amini MIT," *6.S191 Introduction to Deep Learning | Course Hero*, 2020. [Online]. Available: https://www.coursehero.com/file/54813875/6S191-MIT-DeepLearning-L1pdf/.
7. S. Singh, S. Hussain and M. A. Bazaz, "Short-term load forecasting using artificial neural network," in Fourth International Conference on Image Information Processing (ICIIP), 2017, pp. 1–5.
8. O. Olabode, O. Amole, T. Ajewole and I. Okakwu, "Medium-term load forecasting in a Nigerian electricity distribution region using regression analysis techniques," in International Conference in Mathematics, Computer Engineering and Computer Science (ICMCECS), 2020, pp. 1–5.
9. H. Matsila and P. Bokoro, "Load forecasting using statistical time series model in a medium voltage distribution network," in IECON 2018-44th Annual Conference of the IEEE Industrial Electronics Society, 2018, pp. 4974–4979.
10. A. Y. Saber and A. R. Alam, "Short-term load forecasting using multiple linear regression for big data," in IEEE Symposium Series on Computational Intelligence (SSCI), 2017, pp. 1–6.
11. A. Baliyan, K. Gaurav and S. K. Mishra, "A review of short-term load forecasting using artificial neural network models," *Procedia Comput. Sci.*, vol. 48, pp. 121–125, 2015. [CrossRef]
12. S. Khatoon and A. K. Singh, "Effects of various factors on electric load forecasting: An overview," in 6th IEEE Power India International Conference (PIICON), 2014, pp. 1–5.
13. Z. Zhang, "A gentle introduction to artificial neural networks," *Ann. Transl. Med.*, vol. 4, no. 19, p. 370, 2016. [CrossRef]
14. S. H. Han, K. W. Kim, S. Kim and Y. C. Youn, "Artificial neural network: Understanding the basic concepts without mathematics," *Dement. Neurocogn. Disord.*, vol. 17, no. 3, pp. 83–89, 2018. [CrossRef]
15. T. Anwar, B. Sharma, K. Chakraborty and H. Sirohia, "Introduction to load forecasting," *Int. J. Pure Appl. Math.*, vol. 119, pp. 1527–1538, 2018.
16. G. M. U. Din and A. K. Marnerides, "Short-term power load forecasting using deep neural networks," in International Conference on Computing, Networking and Communications (ICNC), 2017, pp. 594–598.
17. S. M. Elgarhy, M. M. Othman, A. Taha and H. M. Hasanien, "Short-term load forecasting using ANN technique," in Nineteenth International Middle East Power Systems Conference (MEPCON) [Internet]. Cairo: IEEE Publications, 2017, pp. 1385–1394. Available: http://ieeexplore.ieee.org/document/8301364/.
18. N. Ammar, M. Sulaiman and A. F. M. Nor, "Long-term load forecasting of power systems using artificial neural network and ANFIS," *ARPN J. Eng. Appl. Sci.*, vol. 13, no. 3, pp. 828–834, 2018.
19. H. Sangrody, N. Zhou, S. Tutun, B. Khorramdel, M. Motalleb and M. Sarailoo, "Long-term forecasting using machine learning methods," in IEEE Power and Energy Conference at Illinois (PECI), 2018, pp. 1–5.
20. M. Buhari and S. S. Adamu, "Short-term load forecasting using artificial neural network," in Proceedings of the International Multi-Conference of Engineers and Computer Scientists, Hongkong, vol. 1, pp. 1–71, March 14–16, 2012.
21. X.-S. Yang, "Optimization techniques and applications with examples," *Optim. Tech. Appl. Examples*, 2018.

22. S. H. Haji and A. M. Abdulazeez, “Comparison of optimization techniques based on gradient descent algorithm: A review,” *PalArchs J. Archaeol. Egypt Egyptology*, vol. 18, no. 4, pp. 2715–2743, 2021.
23. H. Yu and B. M. Wilamowski, “Levenberg–Marquardt training,” in *Intelligent systems*. Boca Raton: CRC Press, 2018, pp. 12–11.
24. P. Netrapalli, “Stochastic gradient descent and its variants in machine learning,” *J. Indian Inst. Sci.*, vol. 99, no. 2, pp. 201–213, 2019. [CrossRef]
25. MathWorks. *MATLAB (R2018a)*. USA: MathWorks, 2018.
26. M. O. Lawal, T. O. Ajewole and O. S. Babalola, “Fortification of the 330-KV Nigerian network using renewable energy resources,” *Niger. J. Eng.*, vol. 26, no. 1, pp. 33–40, 2019.

TEPES
TURKISH JOURNAL OF
ELECTRICAL POWER
AND ENERGY SYSTEMS

TEPES Vol 1., Issue. 2, 108-117, 2021 **DOI:** 10.5152/tepes.2021.21024

RESEARCH ARTICLE

Optimization and Prototyping of a Brushless DC Motor for Torque Ripple Reduction Using the Shifted Hammersley Sampling Method

İsmail Topaloğlu

Department of Electrical and Electronics Engineering, Çankırı Karatekin University, Faculty of Engineering, Çankırı, Turkey

Cite this article as: Topaloglu I. Optimization and prototyping of a brushless DC motor for torque ripple reduction using the shifted hammersley sampling method. *Turk J Electr Power Energy Syst.* 1(2), 108-117, 2021.

ABSTRACT

The recent developments in permanent magnet technology and its increased usage in areas involving brushless direct current (BLDC) motors have increased the interest in this motor type. In the study, a 24/8 pole 3 kW brushless direct current motor was designed, simulations were carried out using the finite element analysis (FEA) method, and an optimization study was carried out using the shifted Hammersley sampling method. Efforts were made to improve the torque ripple and back electromotive force (EMF) values originating from the permanent magnet and the motor design in the BLDC motors. The efficiency of the shifted Hammersley method was validated by the experimental study. The designed BLDC is suitable for applications over a wide range of speeds. The experimental and optimization results both showed that the back EMF harmonics and torque ripples of the BLDC motor under load condition were reduced.

Index Terms—Brushless motor, Hammersley sampling, optimization, torque ripple.

NOMENCLATURE

C_S, C_{PM}, C_R, C_W	**Cost of magnetic steel, Cost of magnet material, Cost of rotor steel, Cost of copper ($)**
d_i, d_o, Ts, P	Stator inner radius, Stator outer radius, Stator length (mm), Number of pole pairs
W_t, W_{sb}, W_{sh}, W_s	Tooth width inside radius, Shoe width inside radius, Slot width inside radius, Slot opening width inside radius (mm)
$\rho_s, \rho_R, \rho_{PM}$	Stator steel density, Rotor steel density, Magnet material density (kg/m^3)
$N_{ph}, N_c, N_s, N_{sp}, N_p$	Phase number, Number of conductors per slot, Number of stator slots, Number of slots/poles/phases, Number of parallel circuits per phase
$P_n, U_{sef}, R_s, L_s, J_m, \varphi$	Rated power (W), RMS voltage in stator (V), Resistance in stator (Ohm), Inductance in stator (H), PMSG inertia moment (kg·m^2), Induced magnetic flux (Weber)
$d_s, L_m, T_m, \tau_m, t_{rs}$	Required slot depth, Mean length per turn, Magnet axial thickness, Magnet spacer thickness, Rotor steel thickness (mm)
$d_{sh}, d_1, d_2, t_r, k_s$	Shaft diameter (mm), Stator slot wedge depth (mm), Stator slot tip depth, Number of wires per square, Lamination stacking factor
$W_{Total}, W_W, W_S, W_R, W_{PM}$	Total active material weight, Wire weight, Stator weight, Rotor weight Magnet weight (kg)
$W_l, r_{rb}, r_{ri}, N_m, N_w$	Wire length (mm), rotor yoke outer radius (mm), rotor inner radius (mm), Number of magnets, Number of wires

I. INTRODUCTION

A. Motivation

Brushless direct current motors typically have 85–90% efficiency, whereas brushed motors are typically 75–80% efficient. Brushes wear down over time, resulting in hazardous sparking and reduction in the lifespan of brushed motors. The BLDC motors are quieter, lighter, and last considerably longer than the traditional DC motors. Brushless direct current motors are frequently employed in modern electronics

Corresponding author: Ismail Topaloglu, itopaloglu@karatekin.edu.tr

Received: May 12, 2021
Accepted: October 3, 2021

since they generate low noise and low heat; hence, they are particularly suitable for systems that operate continuously. They might potentially be the primary source of power for service robots, which necessitate meticulous force management for safety reasons. Brushless motors require far less maintenance than brushed motors. The brushes must be cleaned often, making them unsuitable for use in many fields including medicine. Brushless motors also have the advantage of being able to reach higher torques. Brushes generate friction, which slows down the motor; however, BLDC motors do not have this problem. All these factors necessitate further developments in this type of motor.

B. Literature Review

Brushless direct current motors can produce high torque at low speeds, which is preferred in many applications today [1-7]. Meanwhile, the characteristics of these types of applications relate to several parameters which include, but are not limited to cost, efficiency, and ease of control. The optimization of industrial motors is very important because it directly affects their efficiency and cost. The performance and disturbing effects are also directly affected by the design. There are many studies in the literature regarding the design and optimization of this type of motor [8-17], some of which focus on optimizing the machine's geometric dimensions [18-21], while the others concern control [22-25]. In the literature, a BLDC motor consists of a stator core and windings, rotor and permanent magnets, and a shaft [26]. Fig. 1 shows the initial cross-sectional view of the geometry of the designed BLDC motor.

Many types of motor structures have been designed in previous studies [27-33]. The optimization objectives and functions of the BLDC motor developed are presented in the paper, between (1) and (9). Some researchers have used different optimization techniques for weight reduction or harmonics elimination [34]. Some other researchers have investigated the optimization of the back EMF waveform and the microcontroller-based sensorless BLDC motor drive, with respect to winding configurations and torque ripple reduction, respectively [35]. There are many methods and algorithms for the design and optimization of permanent magnet machines in the literature [36, 37]. Some researchers have searched for a solution with a single objective function, while others have searched for a solution with two or more objective functions [38, 39]. The main purpose here is to present a design where maximum efficiency can be obtained with minimum cost and minimal running problems. However, some undesirable effects arise from the permanent magnet in this type of motor, for example, the torque ripple and back EMF harmonics. Many studies in the literature have tried to reduce these disturbing effects [40].

The literature clearly reveals that some of the techniques used in the optimization of these types of motors are quasi-Newton, nonlinear programming, sequential programming, and genetic and hybrid algorithms [41]. These optimization algorithms seek results to improve one or more objective functions within certain constraints. Torque ripple occurs as part of the interaction between the magneto-motive force and the air-gap flux harmonics [42], and its value is directly affected by the permanent magnet angle, number of poles and slots, pole embrace, pole shape, pole offset, magnet thickness, air-gap length, and skewing.

C. Contribution

In this study, optimization studies were conducted using the shifted Hammersley sampling method and finite element analysis (FEA). The comparison between the experimental results and other results has been presented in the study. Thanks to the optimization technique used, there has been a decrease in torque ripples. The study presents the design of a BLDC motor, the cost, weight, and volume equations to be used in the optimization function, and the optimization results. The experimental studies have been discussed in a separate section.

Main Points

- Optimization and prototyping of a BLDC motor for torque ripple reduction using the shifted Hammersley sampling method were carried out and experimental results were obtained.
- A back EMF sensing circuit was developed and applied for BLDC.
- Torque ripple reduction was achieved by structural design optimization.
- An experimental test system was established for the loaded and unloaded states of the BLDC motor.

II. DESIGN OF A BLDC MOTOR

The designing of BLDC motors involves highly complex processes [6]. In this section, the basic motor design parameters are discussed. One of the main purposes of the study is to reduce the cost of the motor. To achieve this, it is necessary to actively reduce the amount of material used, without reducing the efficiency. For this, it is necessary to create a suitable design model within the ideal solution set.

The optimized motor has reached the desired voltages and currents under load. This shows that when the motor is under load, phase current reaches 50 A, so it is under the maximum loaded current. The winding pattern of the motor is aimed at achieving a reduction to the third harmonic. The winding is designed for short pitch and not full pitch, due to its reduction of the harmonic content in the motor. Due to the short pitch and the distributed winding, the main wave and harmonics are slightly decreased, as seen in

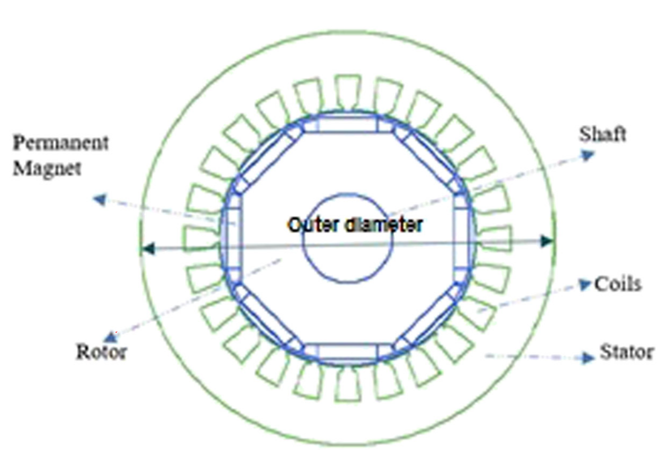

Fig. 1. Brushless direct current motor designed in the study.

Fig. 2. The diagram illustrates the slot star as the phasor, which will be the induced voltage in each of the slots. When coils are delivered to the slots, the voltages of the distributed coils are taken as the sum of the slot star phasors from the winding ends.

In the motor design, the air-gap originating from the permanent magnets has been designed to reduce magnetic flux harmonics. The design is presented in Fig. 2. Here, thanks to this winding design, the torque ripple and harmonics have been decreased. A double layer and short-pitched winding have been used in the motor.

Fig. 3 presents the mapping of induction levels in order to verify that the ferromagnetic parts are not too saturated. It can be seen that the saturation level is acceptable for this full-load operation. Saturations above two Tesla are solely in some local areas such as the saturation bridges and at the ends of the magnets and teeth. A 1/8 model of the motor is used in the simulation due to the motor pole symmetry.

The graph of the total motor volume and the change in iron and copper losses are presented in Fig. 4. The high rate of increase in the total volume directly increases the copper losses significantly. The results deserve some comments. First, it can be remarked that at the expense of the average coupling, it is possible to improve all other parameters, both at low speed and at high speed, as in in Fig. 4. Thus, the author succeeds in reducing all back EMF harmonics at low and high speeds. In addition, the third harmonic is always at a low value regardless of the speed, which is very advantageous for having coupling risk of zero-sequence currents as delta configuration [33]. Thus, the zero-sequence current would be much lower than for the original machine and additional copper losses will be reduced. Regarding the joule losses, values are greatly reduced at low speed and slightly at high speed. The iron losses directly depend on the machine size. Therefore, this machine will provide a higher efficiency than the original motor.

III. OPTIMIZATION OF BLDC

The purpose of the process described in this section is to minimize the fundamental of the back EMF induced. This criterion is very important for security constraints (safety requirements). Indeed, in case of loss of control at high speed, it is necessary to have a low value of the to avoid fundamental electrical arcing effects. Optimization is realized for one operating point, which is at 1500 rpm. The number of iterations is nine, with a total duration of about 111 seconds. Performances are presented in Fig. 8 and 9. The improvements and degradations introduced by optimization are illustrated in green and red respectively. Regarding the results, it can be said that the optimization process is very fast and the results converge rapidly. Moreover, the objective—in terms of reduction of the fundamental back EMF—is achieved with a decrease of over 16 per cent compared to the initial machine. For some other values, we also notice improvements such as volume, joule losses at 1500 rpm, and harmonics, which are lower. However, it may be noted that at 3000 rpm, the performance is worse than that initially for harmonics values and losses. This is because the optimization has taken into account only the operating point at low speed. Thus, the performances of this operating point are at the best value but can be at the expense of high-speed operations. To overcome this result, it is necessary to optimize at least two operating points. Besides, it would be interesting to optimize not just one objective but several objectives, in order to achieve a better compromise between

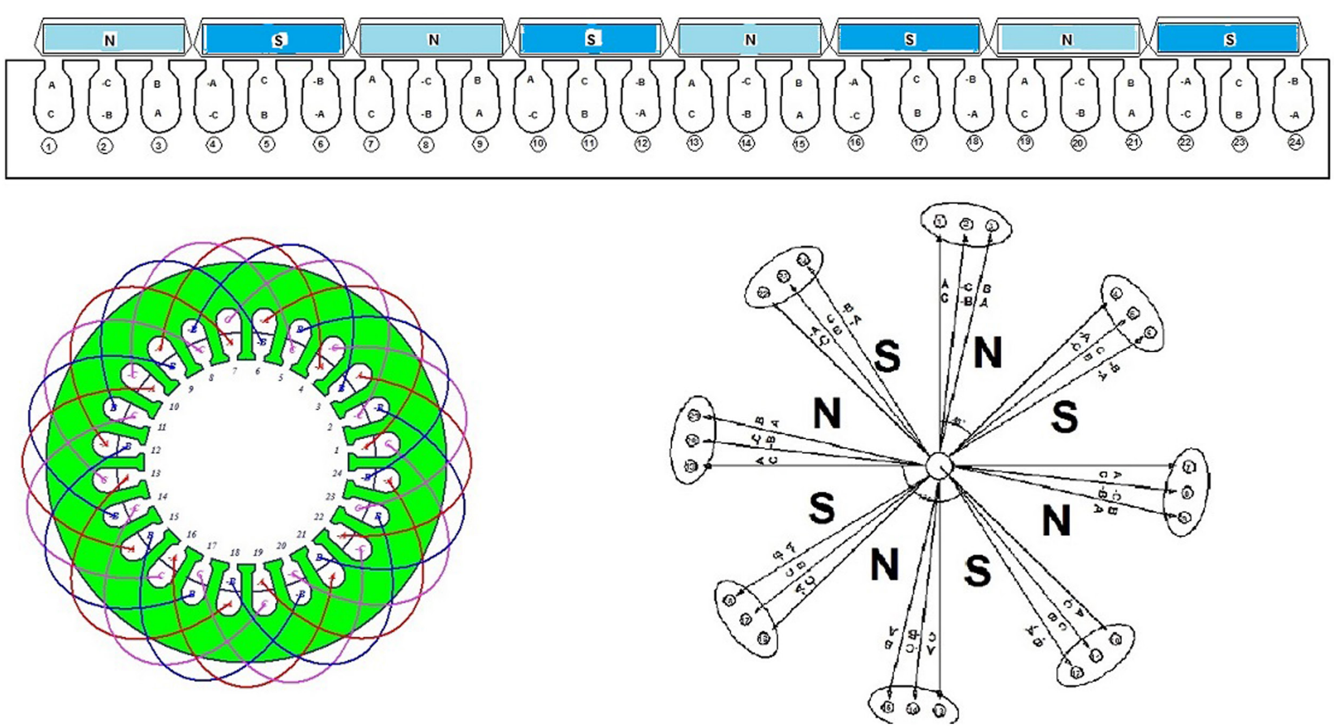

Fig. 2. Winding pattern of PM brushless DC motor. (a) Representation of slots and coil-sides. (b) Coil distribution in slots. (c) Representation of slot star.

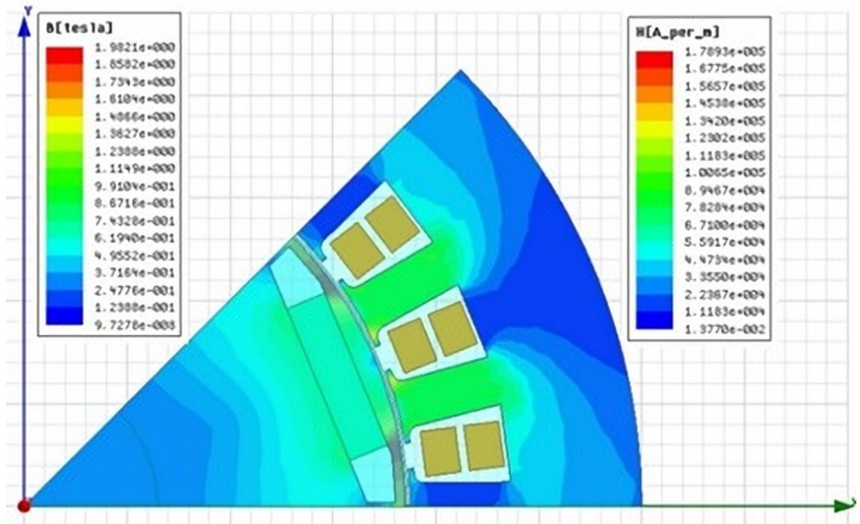

Fig. 3. Mapping of induction levels of 24/8 optimized machine.

two conflicting objectives [33-35]. Therefore, the next section proposes multi-objective optimization, taking into account the two operating points (low and high speed).

The performance of the 24/8 machine on two operating points has been optimized, namely, at 1,500 rpm and 3000 rpm. These two end points allow optimization to converge to optimal solutions over the entire operating range. Since the model simulates two operating points, the computation time of the Jacobian matrix is longer (4.2 seconds + 15.7 seconds, or about 20 seconds per iteration).

The goal in this optimization will be threefold: (1) Minimizing the volume of the machine; (2) minimizing the joule losses; and (3) significantly limiting back EMF harmonics for the two operating points. To do this, the author performed a weighted analysis (with the same coefficients) of the two objectives—to minimize the weight and joule losses—and also constrained the values of the back EMF harmonics in order to maintain them under 15% of the fundamental value. In this case, the number of iterations was 13, with a total duration of about 220 seconds.

An examination of the motor geometry clearly shows that the stator consists of stator teeth and stator yoke:

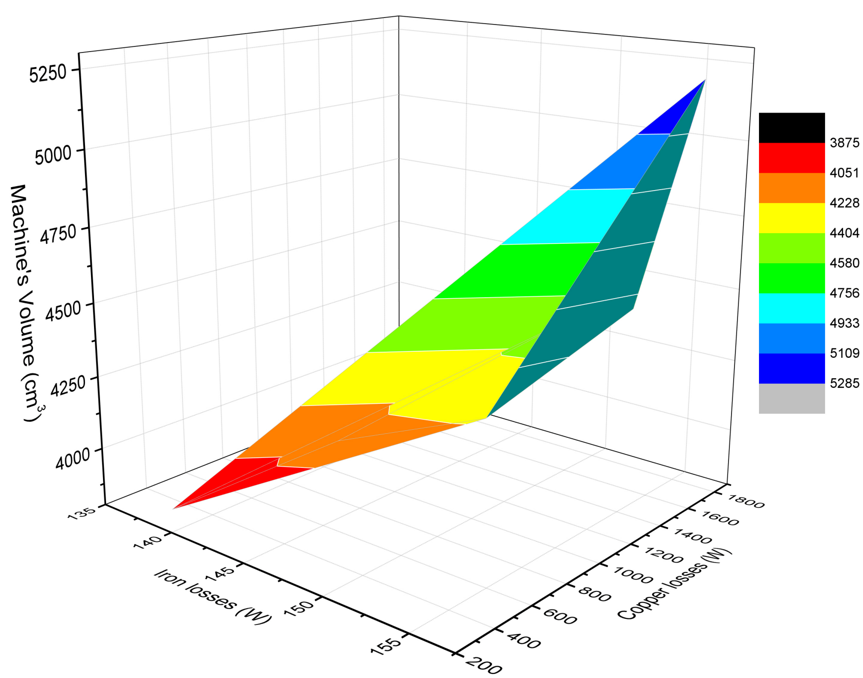

Fig. 4. Results of iron losses, copper losses, and machine volume.

$$\text{Stator teeth volume} = V_t = \left(d_0^2 - d_i^2\right)\left(\left(d_s\left(\pi\left(d_0 + d_i\right)N_h N_m N_{sp}\right)\right)\right) + \left(\left(\left(W_{sh} d_l\right) + \left(W_{sh} + W_{sb}\right)\frac{d_2}{2}\right)0.001\right)L_s N_h N_m N_{sp} \tag{1}$$

$$\text{Stator yoke volume} = V_b = \pi\left(d_0^2 - d_i^2\right)\left(T_s - \left(d_s + \left(d_1 + d_2\right)0.001\right)\right) \tag{2}$$

By calculating the stator teeth volume and stator yoke volume, the total stator volume can be calculated. Equations 1 and 2 represent stator teeth volume and stator yoke volume, respectively:

$$\text{Stator iron volume} = V_s = V_t + V_b \tag{3}$$

$$\text{Weight of stator} = W_s = 2V_s\rho_s \tag{4}$$

Equations 3 and 4 represent the stator iron volume and weight of the stator, respectively. Equation 5 expresses the magnet weight of the motor. Equations 6 and 7 represent the rotor steel weight and wire weight, respectively:

$$\text{Magnet weight} = W_{PM} = 2\rho_{PM}\left(d_0^2 - d_i^2\right)\pi T_M \tag{5}$$

$$\text{Rotor steel weight} = W_R = \left[\left((r_{rb}^2 - r_{ri}^2)\cdot\pi\right)L_s k_s\right]\rho_R \tag{6}$$

$$\text{Wire weight} = W_W = \frac{2N_{ph}N_p N_w N_c N_{sp} L_m W_l}{48000} \tag{7}$$

Here, the total active material weight and total cost function can be found using (1)–(7). Equations 8 and 9 represent the total active material weight and total active material cost, respectively:

$$\text{Total active material weight} = W_{\text{Total}} = W_S + W_{PM} + W_W + W_R \tag{8}$$

$$\text{Total active material cost} = C_{\text{Total}} = W_S C_S + W_{PM} C_{PM} + W_W C_W + W_R C_R \tag{9}$$

A. Shifted Hammersley Sampling Method

The screening (shifted Hammersley sampling) calculation is utilized for pattern creation [7]. The customary Hammersley sampling calculation is a semi arbitrary number generator, which has extremely low inconsistency and is utilized for semi Monte Carlo re-enactments [11]. A low-error arrangement is characterized as a succession of foci that estimate the equidistrubution in a multi-dimensional solid shape in an ideal manner. This implies that the designing space is populated consistently by these arrangements and that dimensionality is not an issue in light of the innate properties of Monte Carlo sampling. The number of foci does not increase dramatically with an expansion in the quantity of information boundaries. The regular Hammersley examining calculation is built by utilizing the extreme reverse capacity.

The total active material weight and total active material cost are our optimization goal functions. These functions consist of weight of stator, weight of rotor, weight of wire, and weight of magnet. The main purpose in using these functions includes the geometrical dimension parameters of motors, especially magnet shape. The most common methods are random or regular sampling. However, these may provide unwanted noisy results, which is why we have used the Hammersley calculation, to yield smoother and noiseless results. Hammersley mapping points provide uniformly distributed vectors. These vectors lead to better results from other techniques. The implementation of this technique obviously depends on the approximation method of the selected goal functions. If the parameters of goal functions include wide ranges of noise and the input parameters are too complex, then the selected method needs a large number of samples to obtain reliable results. Therefore, we should choose the objective functions according to the parameter to be increased or decreased, and avoid large sampling. This study aimed to reduce torque ripples; for this, the total active weight—including magnet parameters—was chosen as one of the main objective functions.

M_{lg} is magnet width in Fig. 5. The initial geometry has an M_{lg} of 18.8 mm; after the optimization process, M_{lg} is 16 mm. This will directly affect the machine volume and machine weight. M_{lg} is used for the optimization parameters in the optimization process.

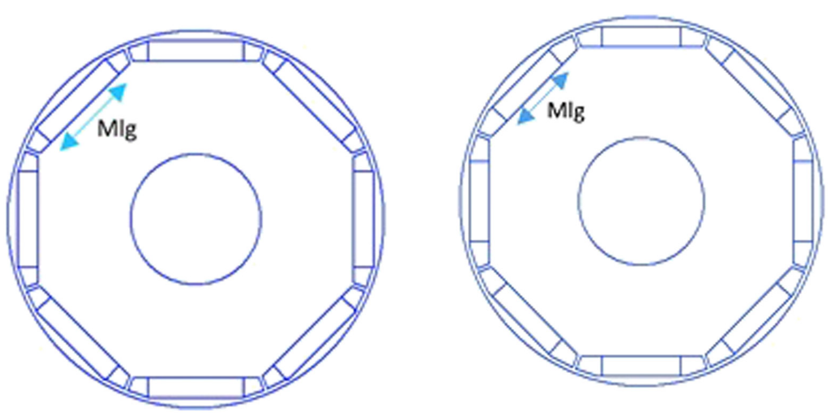

Fig. 5. Geometry presentation of motor. (a) Initial geometry. (b) Optimized geometry.

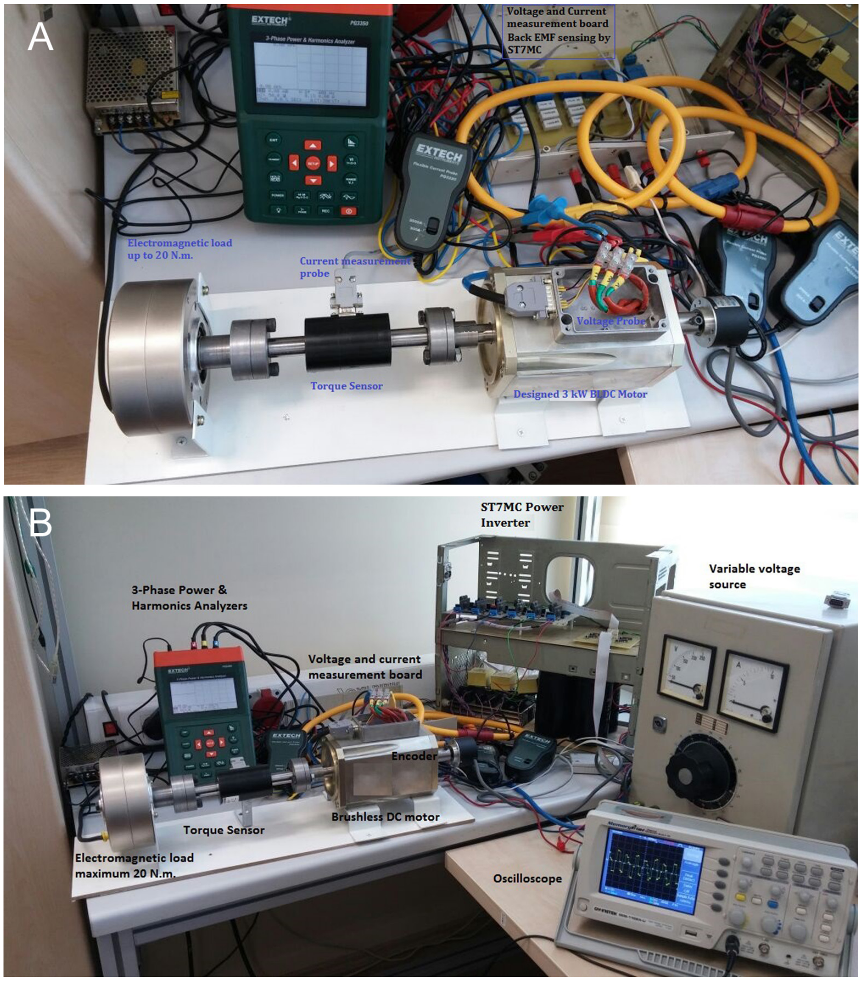

Fig. 6. Experimental study set up representation. (a) General experimental system. (b) Measurement equipment.

IV. EXPERIMENTAL STUDY OF BLDC

Based on given the geometric and material characteristics, the performances of a designed BLDC are analyzed. Loaded and unloaded situations are tested under different motor speeds, at 1500 rpm and 3000 rpm. The experimental study set up and measurement system set up have been presented in Fig. 6 (a) and (b) respectively.

The LA-25 current transducer was used for current measurement in the system. The rating of the designed motor was 3 kW, 48 V, 50 A, and 3000 rpm. A variable voltage source fed the test system. The electromagnetic load allowed up to 20 Nm. The EXTECH P03350 three-phase power and harmonic analyzer were used for measuring harmonics. Back EMF was measured with the ST7MC microcontroller, which is shown in Fig. 7. In Fig. 7, the values of the resistors are $R4 = 16$ kΩ, $R5 = 16$ kΩ, $R6 = 16$ kΩ, $R7 = 240$ kΩ, $R8 = 18$ kΩ, $R9 = 12$ kΩ, $R4a = 100$ kΩ, $R4b = 100$ kΩ, $R4c = 100$ kΩ, $R5a = 100$ kΩ, $R5b = 100$ kΩ, and $R5c = 100$ kΩ, respectively.

The designed current, torque, voltage, and back EMF, and the harmonics circuit scheme and its implementation have been presented in Fig. 6 and 7, respectively.

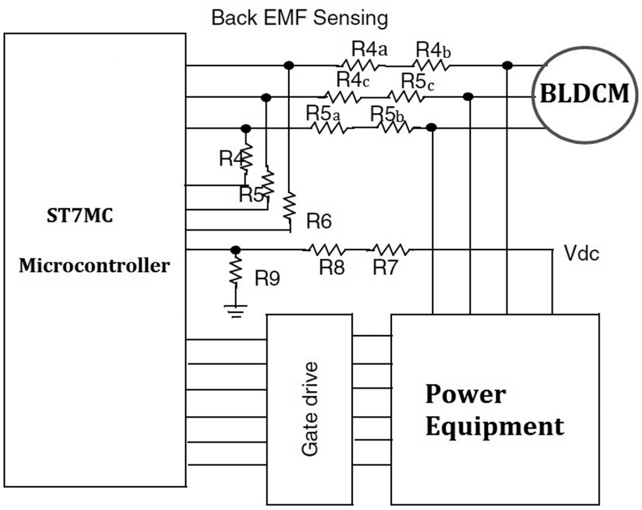

Fig. 7. Back EMF sensing scheme. EMF, electromotor force.

V. RESULTS AND DISCUSSION

The results of the optimization, simulation, and experimental test are presented in this section. All values are compared with each other and the results are discussed. Torque ripple reduction is obtained under different speeds, at 1500 rpm and 3000 rpm.

The flux harmonics consist mainly of third, fifth, seventh and eleventh harmonics. The optimized results, both 1500 rpm and 3000 rpm, are better than FEA. However, the experimental study shows that the obtained torque ripple value is very close to the optimized results, and the main difference is only approximately 1.42%. When the motor speed is increased to 3000 rpm, main torque ripple difference is decreased, at 1.19%, as seen in Fig. 8.

Note that H_n designates the *n*th order harmonic of the output parameter. The torque of the BLDC motor is strongly affected by back EMFs and phase current waveforms [35]. The first is the main wave of EMF. The third, fifth, and seventh are back EMF harmonics. The fifth is the biggest measured harmonic in the motor, as shown in Fig. 9.

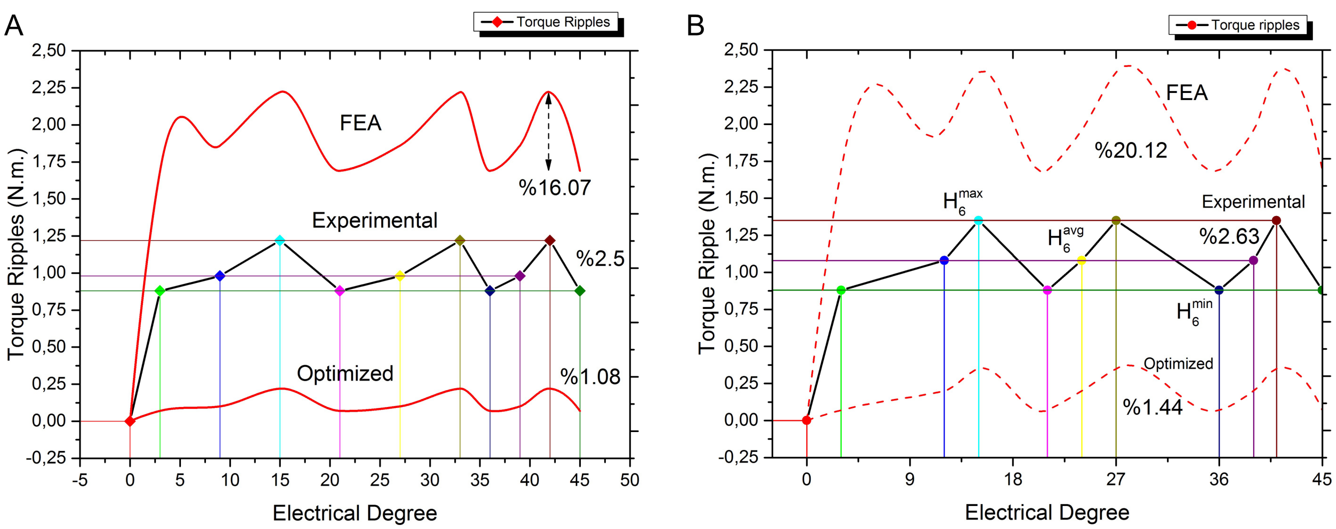

Fig. 8. Torque ripple reduction in BLDC motor. (a) At 1500 rpm. (b) At 3000 rpm. BLDC, brushless direct current.

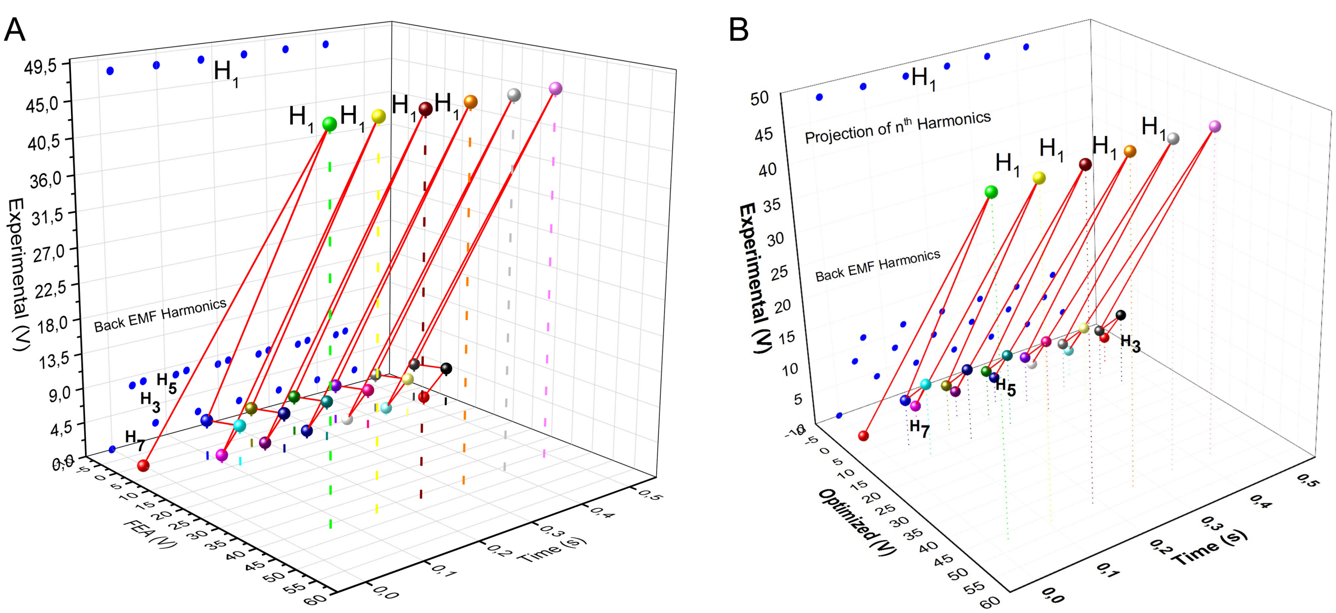

Fig. 9. Comparison of back EMF FEA, optimization, and experimental results. (a) FEA and experimental results. (b) Experimental and optimization results. EMF, electromotor force; FEA, finite element analysis.

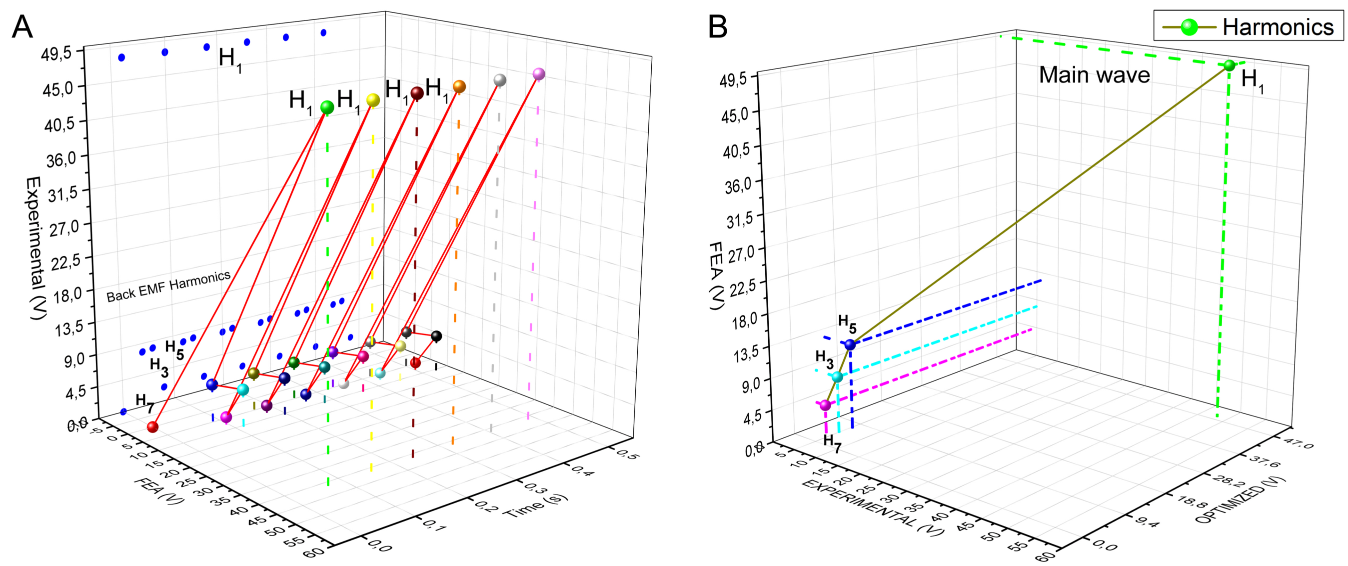

Fig. 10. Back EMF harmonics at 3000 rpm and comparison of FEA, optimized geometry, and experimental study. (a) Experimental FEA. (b) Experimental FEA in optimized geometry. EMF, electromotor force; FEA, finite element analysis.

The results show that the optimized and experimental study has achieved very close numerical values, but the FEA result is a very high value, except for the main wave. Particularly, the fifth and third are bigger than in the experimental study.

It can be seen in Fig. 10 that the third is lower than the fifth, because the third harmonic is reduced with the winding technique applied while designing the motor. Nevertheless, the fifth harmonic continues to have the highest effect on torque ripples.

The reliability of the results is verified between the simulation and experiment in Fig. 11. Fig. 11(b) and (d) show the back EMF waveform (main wave) under loaded conditions. The impacts of the magnets on the back EMF voltage can be seen from these waveforms. The back EMF waveform is shown in Fig. 11(a) and (c). The measured back EMF waveform and simulation results have been compared in Fig. 11. The comparison shows a close match.

The main purpose of this motor design and the optimization process is to provide decreased torque ripple for industrial applications. To achieve this goal, back EMF-induced torque formations in the motor should also be examined. For this, a special measuring circuit has been designed and implemented. Torque values at different motor speeds were obtained. The results of the FEA and the experimental results were compared with each other. In the phase harmonic values measured, some non-reducible effects remain, apart from the design-induced reduction effects.

Finally, the results have demonstrated the powerful side of the methodology used for the optimization based on RN modeling. The results have been obtained with good accuracy, since the optimizations have taken place within a few minutes. Moreover, the methodology has the advantage of being generic. It is relatively easy to change the patterns of the stator and rotor reluctances to optimize with different technological choices. For optimal results, future works have to include finer RN models in order to obtain better resolution and results that are closer to FEA. Likewise, optimization has to be performed on more operating points for optimal solutions that are valid for the entire operating range. Lastly, the inclusion of the calculation for mechanical losses and constraints, heat losses through a nodal model, and ventilation losses will help designer to obtain much more realistic results with such multiphysics models.

VI. CONCLUSION

The optimization, prototyping, and analysis of BLDC motors were performed using Hammersley sampling. In addition, experimental verification was provided via a laboratory setup. The FEA simulations, optimization results, and experimental results are compared. The comparison shows a close match.

In a first step, the machine 24/8 was optimized on an operating point at low speed. These first results have given better performance compared to the initial machine. However, given that the optimization takes place only for a single operating point, the other operating points have been degraded. Therefore, in a second step, another optimization, taking into account two operating points (low speed and high speed), was performed. In this case, the optimal machine furnished much higher performances on most criteria.

A back EMF measurement card was designed and used to measure in the experimental studies. FEA simulations were performed with Ansys, using a static magnetic module. The results obtained in the measurements were compared with the simulation results, and it was observed that the torque ripples were reduced after the Hammersley method optimization.

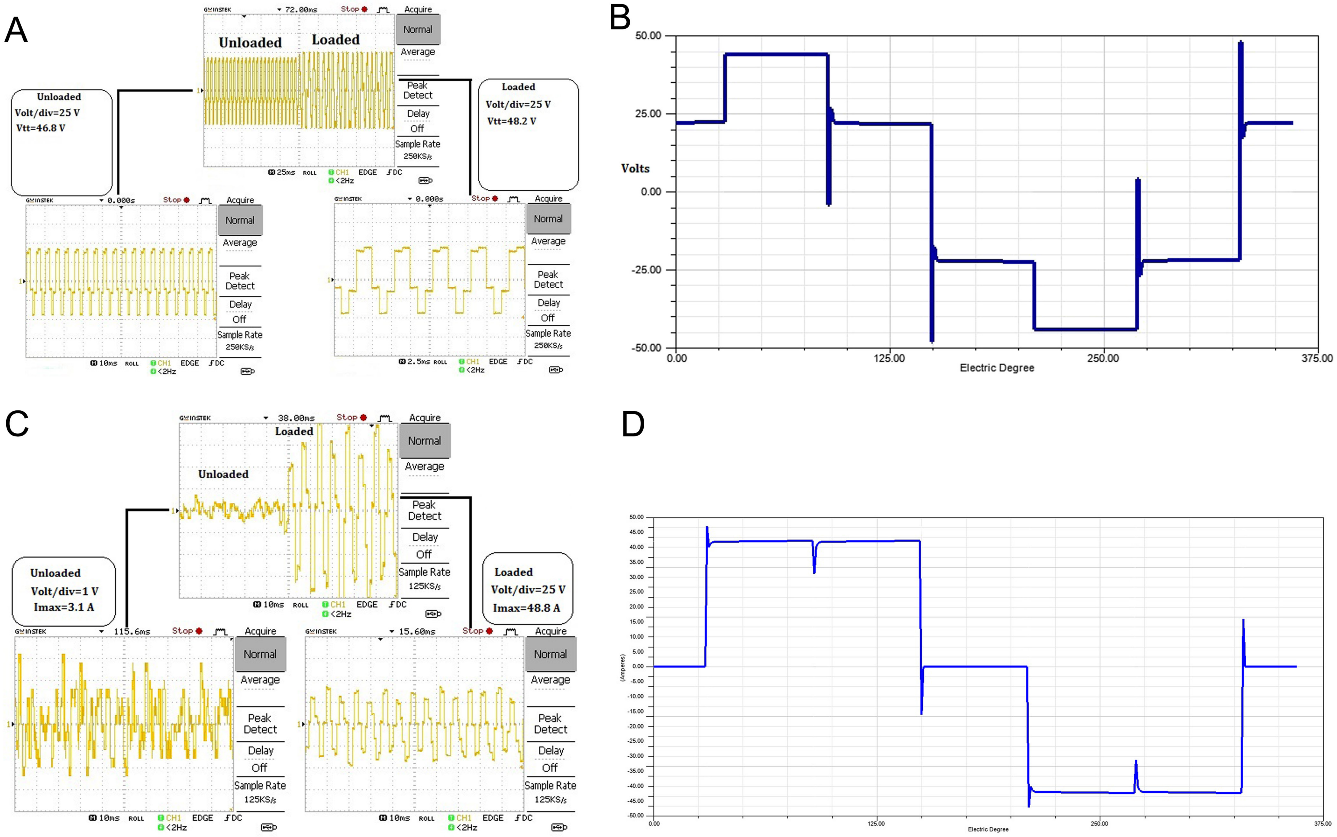

Fig. 11. Optimized motor potential and currents under load. Fig 11 (a) and (c) are experimental results under loaded and unloaded conditions. Fig 11 (b) and (d) are simulation results under loaded condition.

Peer-review: Externally peer-reviewed.

Conflict of Interest: The authors have no conflicts of interest to declare.

Financial Disclosure: The Scientific Research Projects Unit of Cankiri Karatekin University under Grant (MF050315B15) supported this work.

REFERENCES

1. H. Shang, L. Zhao and T. Wang, "Torque ripple reduction for permanent magnet synchronous motor based on learning control," in *2nd Int. Conf. Inf. Sci. Control Eng.*, 2015, pp. 1001–1005.
2. H. M. Kim, Y. Kim and S. Jung, "Torque ripple and back EMF harmonic reduction of IPMSM with asymmetrical stator design," in *20th Int. Conf. Electr. Mach. Syst. (ICEMS)*, Sydney, NSW, 2017, pp. 1–4. [CrossRef]
3. H. Kim and S. Bhattacharya, "A novel current control strategy based on harmonic voltage injection for power losses reduction of PMSMs with non-sinusoidal back-EMF," *IEEE Ind. Appl. Soc. Ann. Meet.*, Baltimore, MD, USA, 2019, pp. 1–6. [CrossRef]
4. L. Liu, G. Götting and J. Xie, "Torque ripple reduction using variable DC-link voltage technique for permanent magnet synchronous motor in battery electric vehicle," *IEEE 29th Int. Symp. on Industrial Electronics (ISIE)*, Delft, Netherlands, 2020, pp. 374–379. [CrossRef]
5. H. Kim, Y. Han, K. Lee and S. Bhattacharya, "A sinusoidal current control strategy based on harmonic voltage injection for harmonic loss reduction of PMSMs with non-sinusoidal back-EMF," *IEEE Trans. Ind. Appl.*, vol. 56, no. 6, pp. 7032–7043, 2020. [CrossRef]
6. H. Liu, I. Kim, Y. J. Oh, J. Lee and S. Go, "Design of permanent magnet-assisted synchronous reluctance motor for maximized back-EMF and torque ripple reduction," *IEEE Trans. Magn.*, vol. 53, no. 6, Art no. 8202604, pp. 1–4, 2017. [CrossRef]
7. A. G. de Castro *et al.*, "Improved finite control-set model-based direct power control of BLDC motor with reduced torque ripple," *IEEE Trans. Ind. Appl.*, vol. 54, no. 5, pp. 4476–4484, 2018. [CrossRef]
8. G. Li, J. Wang, B. Li and T. Zhang, "A current optimization strategy for torque ripple reduction of brushless DC motor with nonideal back electromotive force," in *22nd Int. Conf. Electr. Mach. Syst. (ICEMS)*, Harbin, China, 2019, pp. 1–6. [CrossRef]
9. M. Sumega, S. Zossak, P. Varecha, P. Rafajdus and M. Stulrajter, "Adaptive algorithm to reduce acoustic noise and torque ripple in low-cost PM motors," in *Int. Aegean Conf. Electr. Mach. Power Electron. (ACEMP) & 2019 Int. Conf. Opt. Electr. Electron. Equip. (OPTIM)*. Istanbul, Turkey, 2019, pp. 100–107. [CrossRef]
10. M. Sumega, P. Rafajdus, S. Kocan and M. Stulrajter, "Torque ripple reduction in PM motors using current harmonics controller," in *ELEKTRO*, Taormina, Italy, 2020, pp. 1–6. [CrossRef]
11. M. Sumega, M. Štulrajter and P. Rafajdus, "Torque Ripple Reduction in PM Synchronous Motor - FEM simulation," in *Int. Conf. on Electr. Mach. (ICEM)*, Gothenburg, 2020, pp. 1239–1245. [CrossRef]

12. C. Chillet and J. -Y. Voyant, “Design-oriented analytical study of a linear electromagnetic actuator by means of a reluctance network,” *IEEE Trans. Magn.*, vol. 37, no. 4, pp. 3004–3011, 2001. [CrossRef]
13. H. Dogan *et al.*, “Multistatic reluctance network modeling for the design of PMSM,” *IEEE Trans. Magn.*, vol. 49, no.5, pp.2347–2350, 2013. [CrossRef]
14. T. Raminosoa, I. Rasoanarivo, F. Meibody-Tabar and F. -M. Sargos, “Time-stepping simulation of synchronous reluctance motors using a nonlinear reluctance network method,” *IEEE Trans. Magn.*, vol. 44, no. 12, pp. 4618–4625, 2008. [CrossRef]
15. B. D. Peloux, L. Gerbaud, F. Wurtz, V. Leconte and F. Dorschner, “Automatic generation of sizing static models based on reluctance networks for the optimization of electromagnetic devices,” *IEEE Trans. Magn.*, vol. 42, no. 4, pp. 715–718, 2006. [CrossRef]
16. L. D. Sousa and B. Silvestre, ““A combined multiphase electric drive and fast battery charger for electric vehicles,” in *IEEE Vehicle Power and Propulsion Conf.*, Lille, France, 2010. [CrossRef]
17. M. Liwschite-Garik and C. C. Whipple, *Electric Machinery*. New York, USA: D. Van Nostrand Company Inc., 1946.
18. D. C. Haneslman, *Brushless Permanent-Magnet Motor Design*. New York, USA: McGraw-Hill Inc., 1994.
19. R. A. Hawsey and J. M. Bailey, “Ultra-high speed permanent magnet axial gap alternator with multiplestators,” U.S. Patent Number 4.996.457, 1991.
20. O. Olorunfemi, “Multiobjective optimum design of electrical machines for variable speed motor drives,” in *IEEELAS Ann. Meet. Conf. Rec.*, 1991, vol. 1, pp. 163–168. [CrossRef]
21. N. Boules and H. Wey, “Machine constants and design consideration of a high power synchronous machine of the disc construction type,” *Electr. Mach. Electromagn.*, vol. 5, pp. 25–37, 1980.
22. R. Krishan and A. S. Baradwaj, “A comparative study of various motor drive systems for aircraft applications,” in *IEEEAAS Ann. Meet. Conf. Rec.*, 1991, pp. 252–258. [CrossRef]
23. H. R. Bohon, Y. D. Liu and M. M. Mallinson, “Investigation into a class of brushless DC motor with quasisquare wave voltages and currents,” *IEEE Proc. B*, vol. 133, no. 2, pp. 103–111, 1986. [CrossRef]
24. C. C. Chan, “Axial field electrical machines design and applications, ” *IEEE Trans. Energy Convers.*, vol. EC–2, no. 2, pp.294–300, 1987. [CrossRef]
25. G. R. Slemon, “On the design of high performance PM motors,” in *IEEE-iIAS Ann. Meet Conf. Rec.*, 1992, pp. 279–285. [CrossRef]
26. N. Boules, “Design optimization of permanent magnet DC machines,” in *IEEEiIAS Ann. Meet. Conf. Rec.*, 1987, pp. 27–34.
27. G. A. J. Amaratunga, P. P. Acarnley and P. G. McLaren, “Optimum magnetic circuit configuration for permanent magnet aerospace generators,” *IEEE Trans. Aerosp. Electron. Syst.*, vol. AES–21, no. 2, pp. 230–255, 1985. [CrossRef]
28. M. Hippner and R. G. Harley, “Looking for an optimal rotor for high speed permanent magnet synchronous machine, ” *IEEEAAS Ann. Meet. Conf. Rec.*, 1992, pp. 265–270. [CrossRef]
29. R. Wang and J. Gieras, “Analysis of characteristics of a permanent magnet hybrid linear stepping motor,” in *Proc. of ICEM*, Istanbul, Turkey, 1998, vol. 2–4, pp. 833–838. [CrossRef]
30. P. Silvester, “Network analog solution of skin and proximity effect problems, ” *IEEE Trans. Power Apparatus Syst.*, vol. PAS–86, no. 2, pp. 241–247, 1967. [CrossRef]
31. P. Sewell *et al.*, “Dynamic reluctance mesh modelling of induction motors, ” in *Proc. of ICEM*, Istanbul, Turkey, 1998, pp. 1324–1329. [CrossRef].
32. C. Rasmussen and E. Ritchie, “Improved reluctance-mmf network for calculation of magnetic field distribution in surface-mounted permanent-magnet motors,” *Electromotion*, vol. 4, pp. 55–61, 1997.
33. I. Topaloglu and O. Gürdal, “Design of linear electromagnetic launcher system and dimension optimization using equivalent circuit model of linear electromagnetic launchers to improve launching performance,” *J. Fac. Eng. Archit. Gazi Univ.*, vol. 28, no. 1, pp. 103–113, 2013.
34. I. Topaloglu and O. Gürdal, “A second order sensitivity analysis based numerical approach developed for dimension optimization, in electric machine design by electromagnetic design programme,” *J. Fac. Eng. Archit. Gazi Univ.*, vol. 25, no. 2, pp. 363–369, 2010.
35. I. Topaloglu, F. Korkmaz, H. Mamur and R. Gürbüz, “Closed-loop speed control of PM-BLDC motor fed by six step inverter and effects of inertia changes for desktop CNC machine,” *Electronics and Electrical Engineering*, Kaunas: Technologija, vol. 19, no. 1, pp. 7–10, 2013. [CrossRef]
36. J. Perho, “Reluctance Network for Analyzing Induction Machines,” *Ph.D. Thesis*, Helsinki University of Technology, Finland, 2002.
37. J. Ye, B. Bilgin and A. Emadi, “An Offline Torque Sharing Function for Torque Ripple Reduction in Switched Reluctance Motor Drives,” *IEEE Trans. Energy Convers.*, vol. 30, no. 2, pp. 726–735, 2015.
38. A. Sapena-Ba˜no and M. P. Sanchez, “Harmonic Order Tracking Analysis: A Novel Method for Fault Diagnosis in Induction Machines,” *IEEE Trans. Energy Convers.*, vol. 30, no. 3, pp. 833–841, 2015.
39. H. M. Hasanien, A. S. Abd-Rabou and S. M. Sakr, “Design optimization of transverse flux linear motor for weight reduction and performance improvement using response surface methodology and genetic algorithms,” *IEEE Trans. Energy Convers.*, vol. 25, no. 3, pp. 598–605, Sep. 2010.
40. W. Hua, M. Cheng, Z. Q. Zhu and D. Howe, “Analysis and optimization of back-EMF waveform of a flux-switching permanent magnet motor,” *IEEE Trans. Energy Convers.*, vol. 23, no. 3, pp. 727–733, Sep. 2008.
41. J. T. Chen and Z. Q. Zhu, “Winding configurations and optimal stator and rotor pole combination of flux-switching PM brushless AC machines,” *IEEE Trans. Energy Convers.*, vol. 25, no. 2, pp. 293–302, Jun. 2015.
42. J. T. Chen, “An Improved Microcontroller-Based Sensorless Brushless DC (BLDC) Motor Drive for Automotive Applications,” *IEEE Trans. Indus, App.*, vol. 42, no. 5, pp. 1216–1221, Jun. 2006.

cigre Turkey

TEPES
TURKISH JOURNAL OF
ELECTRICAL POWER
AND ENERGY SYSTEMS

TEPES Vol 1., Issue. 2, 118-128, 2021 **DOI:** 10.5152/tepes.2021.21019

REVIEW

Electricity Energy Forecasting for Turkey: A Review of the Years 2003–2020

Nalan Özkurt, Hacer Şekerci Öztura, Cüneyt Güzeliş

Department of Electrical and Electronics Engineering, Yaşar University, İzmir, Turkey

Cite this article as: Özkurt N, Öztura H, Güzeliş C. Electricity energy forecasting for turkey: A review of the years 2003–2020. *Turk J Electr Power Energy Syst.* 1(2), 118-128, 2021.

ABSTRACT

This paper provides a comprehensive review of the studies on electricity energy forecasting for Turkey during the years between 2003 and 2020. The review analyzes the forecasting studies in terms of the methods that are applied for forecasting, the profiles of the researchers and their institutions, and the years and location information about the data for which the forecasting is implemented. The search that is presented in this paper covers almost all related works that are published in the literature. Forecasting of electricity energy has been always a tool for energy demand–supply planning and has become indispensable due to increasing needs for the prediction of electricity production and consumption in the management of smart grid systems. Therefore, development of competencies in electricity energy forecasting is a must for all nationwide actors who have responsibilities in the management of smart grids. This paper may be used to identify the already developed competencies in electricity energy forecasting by the individual researchers on their own, and the institutions of Turkey. Thus, it may constitute a base for future works to build up new competency centers to meet Turkey's need on short-, medium-, and long-term forecasting of electricity production and consumption.

Index Terms—Turkish electricity market, machine learning, statistical methods, electricity forecasting.

I. INTRODUCTION

Electricity has special properties, from generation to consumption. It needs to be maintained at a constant balance between demand and supply, and it is non-storable. Therefore, consumption forecasting is obligatory for electricity generation. The Ministry of Energy and Natural Resources (MENR) accomplished some forecasting studies by using simple methodologies during the late 1970s. The milestone of energy estimation related to future demands and energy planning was the introduction of the simulation models by the State Planning Organization (SPO) and the MENR in 1984. Energy marketing studies were started at the beginning of the 2000s. Fig. 1 shows the historical development of energy marketing in Turkey [1]. After that, from January 1, 2016, all hourly generation and consumption data began to be published on an official web page of Turkish Energy Exchange Company (EPİAŞ), which is called the Transparency Platform.

After energy marketing was established in Turkey, data on the day-ahead and intra-day matching amounts were published daily on the web page of the EPİAŞ. In the electricity market, there are three major parts, which are the bilateral contracts, the day-ahead market, and the intra-day market. Bilateral contracts cover more than half of the annual electricity generation. Since the amount of electricity generated and its price are certain in bilateral contracts, matching of the day-ahead market is a major concern for authorities. Table I shows the total consumption and the matching amount of day-ahead and intra-day as annually in TWh and percent of total consumption, from 2017 to 2020 [1]. Approximately half of the annual consumption was matched at the day-ahead market in the first years of energy marketing, and last year, this rate was more than 60%. Thus, it can be seen from the data in Table I that true forecasting of the consumption amount is very important.

Load estimation models can be divided into four groups: very short-term, short-term, medium-term, and long-term forecasts. While very short-term load estimates cover from a few seconds to a day, short-term load estimates are estimates extend up to 2 weeks. Similarly, medium-term forecasting estimates cover between a week and year, and the result of long-term forecasting gives estimates for more than a year [2]. In order to form the energy production plan, load estimates can be made short-term, such as an hour or a week later, or they can be made on a long-term, annual, or seasonal basis to direct investments.

Corresponding author: Nalan Özkurt, nalan.ozkurt@yasar.edu.tr

Received: April 7, 2021
Accepted: May 7, 2021
Published online: August 27, 2021

Fig. 1. Milestones of the development of energy markets.

This study is a review of the articles on research done on forecasting the electric energy consumption and its price in Turkey between the years 2003 and 2020. In section 2 of the paper, the profiles of all the articles are detailed with respect to information on the distribution of the university, organization, profession of the authors, year of publication, etc. The forecasting methods are given in section 3, while the data analyses are introduced in section 4. Finally, conclusions are drawn in the last section.

II. FORECASTING STUDY PROFILES

First, the number of articles published each year is obtained, shown in Fig. 2. There is a noticeable increase in the number of papers after the EPİAŞ obtained a market operation license and the data were made publicly available on the Transparency Platform in 2016.

Another classification is made with respect to the disciplines in which the authors hold bachelor's degrees. There are only three papers written by the researchers from the social departments, while the others belong to engineering. The distribution can be seen in Fig. 3. It is clear that the most of the researchers are electrical and electronics engineers.

There are 96 authors in all, and 85 of them have published only one paper on forecasting of energy consumption. Eight of them have published two papers, while only three authors have three research papers to their credit. The number of papers authored is shown in Fig. 4. This means that very few authors have continued their studies on this subject.

There are 201 universities in Turkey, and 131 of them are the state universities. The forecasting studies of electrical energy consumption covered in this review have been conducted in the 14 universities located in the three largest cities and in the 18 universities at Anatolia. The distribution of the papers with respect to the universities is given in Table II. There are three papers written by the government departments related to energy, such as the Energy Market Regulatory Authority (EMRA), the General Directorate of Energy Affairs, the Electricity Generation Company (EGC), and TÜBİTAK.

Main Points

- Electricity forecasting is crucial for plans and strategies in energy production.
- The competencies in electricity energy forecasting should be identified nationwide.
- This paper summarizes the author and institution profiles, forecasting methods, and data collection for Turkey after 2003.
- In addition, useful interpretations are made on trend, motivation, and continuity of the studies.

III. OVERVIEW OF FORECASTING METHODS

Forecasting is an important problem involving the prediction of events for certain time periods, such as hours, days, or years, by identifying and constructing a model examining the history of the data. The phases of forecasting are problem definition, data collection, data analysis, model selection and fitting, model validation, forecasting, and monitoring model performance [3].

The data are usually available as a time series in the form of $Y = \left[y_1 \; y_2 \cdots y_N \right]$ sampled at N time instants, where the measurements $y_i \in \mathbb{R}^d$ and *d* are the number of observed variables. The time series is considered as univariate if *d* = 1, otherwise it is called as multivariate. Assuming the univariate case, in one-step-ahead prediction, the *k*th value of the series is predicted using previous observations as in (1):

$$y_k = f\left(y_{k-1}, y_{k-2}, \ldots\right) \tag{1}$$

In *m*-step-ahead forecasting, the predicted value is *m*-step advance of the current value. One way of multi-step-ahead prediction is to use m one-step-ahead predictors, and another way is to create a model directly to estimate y_k as in (2):

TABLE I
ELECTRICITY-RELATED DATA AFTER THE ENERGY MARKET WAS ESTABLISHED

Year	Installed Capacity	Consumption	Day-Ahead Matching Quantity	%	Intra-day Matching Quantity	%
2017	85 200 MW	296.7 TWh	123.32 TWh	41.56	1.72 TWh	0.58
2018	88 526 MW	300.1 TWh	149.39 TWh	49.78	2.93 TWh	0.98
2019	91 267 MW	280.49 TWh	152.12 TWh	54.23	5.45 TWh	1.94
2020	95 891 MW	290.93 TWh	181.36 TWh	62.33	6.88 TWh	2.36

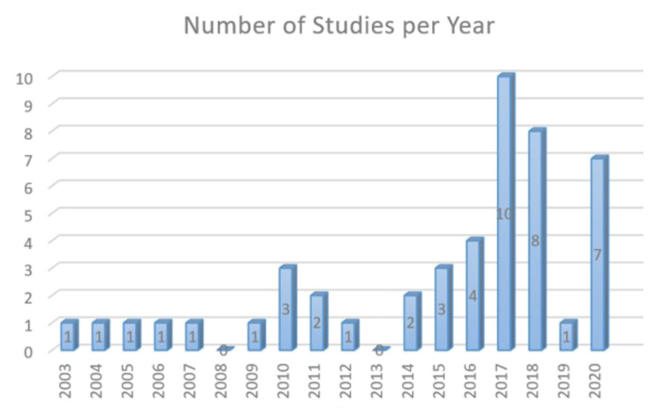

Fig. 2. The published year distributions of the papers.

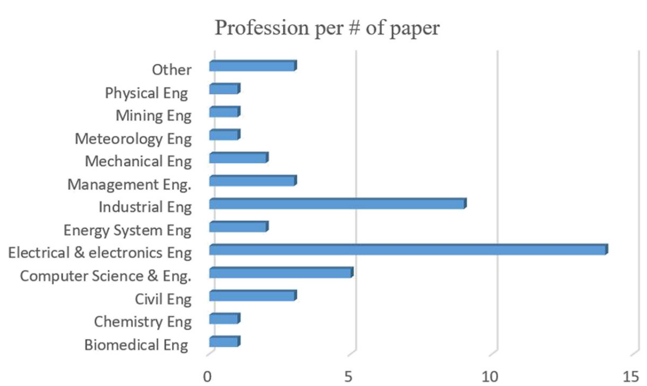

Fig. 3. The professions of the authors distributions of the articles.

$$y_k = f\left(y_{k-m}, y_{k-m-1}, \ldots\right) \tag{2}$$

To evaluate the performance of the forecast algorithm, several error criteria are used. The absolute error is defined as

$$AE_k = \left| y_k^{Target} - y_k^{Predicted} \right| \tag{3}$$

where y_k^{Target} is the actual measurement value and $y_k^{Predicted}$ is the output of the forecasting algorithm. Suppose that there are n observations for $k = 1, 2, \ldots, n$. Then the average error or mean absolute error can be calculated as

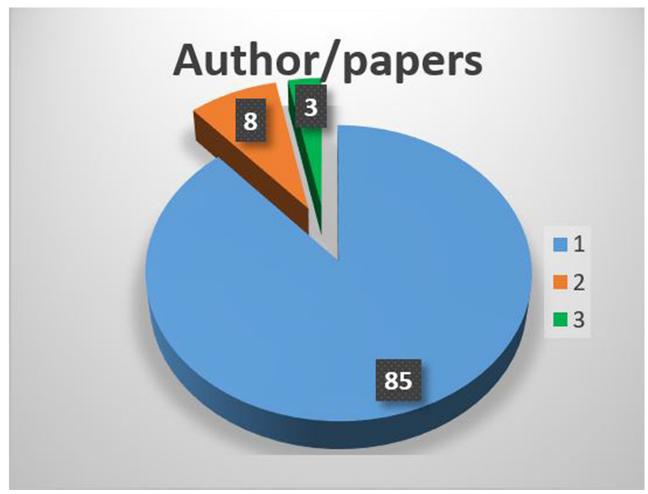

Fig. 4. The distributions of how many articles written by per authors.

$$MAE = \frac{1}{n} \sum_{k=1}^{n} AE_k. \tag{4}$$

MAE measures the variability of the forecast error. Since the range of the forecasting variable is varied, to compare the performance of the forecasting algorithms applied to different data, another type of measure is needed. To solve this issue, a relative error measure, the Mean Absolute Percentage Error (MAPE) is defined as

$$\%MAPE = \frac{100}{n} \sum_{i=1}^{n} \frac{\left| y_k^{Target} - y_k^{Predicted} \right|}{\left| y_k^{Target} \right|} = \frac{100}{n} \sum_{i=1}^{n} \frac{AE_k}{\left| y_k^{Target} \right|} \tag{5}$$

assuming that there are no zero values in the time series. Another criterion which measures the fitting performance of the model with the actual observations is *R*-squared statistics

$$R^2 = 1 - \frac{\sum_{k=1}^{n} \left(y_k^{Target} - y_k^{Predicted} \right)}{\sum_{k=1}^{n} \left(y_k^{Target} - \bar{y} \right)^2} \tag{6}$$

where $\bar{y}$ is the mean value of the target vector [3].

TABLE II
AUTHORING INSTITUTIONS OF THE RESEARCHES

University/Organization (Alphabetic Order)	Number of Papers	University/Organization (Alphabetic Order)	Number of Papers
Anadolu University	1	İstanbul Ticaret University	1
Ankara University	3	Karadeniz Teknik University	2
Aksaray University	1	Karaelmas University	1
Özyeğin University	1	Kırıkkale University	1
Bilecik Şeyh Edebali University	1	Kadir Has University	2
Bülent Ecevit University	1	Kocaeli University	1
Cumhuriyet University	1	Military Academy	1
Düzce University	1	Marmara University	1
Erzurum University	1	Muğla Sıtkı Koçman University	1
Erciyes University	2	Necmettin Erbakan University	1
EMRA	1	Niğde University	1
EGC	1	Orta Doğu Teknik University	3
Gazi University	4	Pamukkale University	2
Gebze Teknik University	1	Selçuk University	3
General Directorate of Energy Affairs	1	TÜBİTAK	1
Ege University	1	Ondokuz Mayıs University	1
İstanbul Bilgi University	1	Yaşar University	1
İstanbul Teknik University	4	Yıldız Teknik University	2

The load/demand forecasting methods can be mainly divided into two categories, statistical techniques and machine learning algorithms. However, the distinction between the two types is not clear since there are several studies which combine both to obtain hybrid models.

The main statistical techniques are regression methods such as linear regression (LR) [4] and multiple linear regression (MLR) [5], support vector regression (SVR) [6], auto-regressive and moving average (ARMA) models, and their variants such as seasonal autoregressive integrated moving average (SARIMA) [7-12], exponential smoothing models [13], and grey box models [14-17]. Autoregressive models estimate the parameters of the ARMA model including auto-regression and moving average polynomial coefficients. In nonstationary time series cases as in load forecasting, the auto-regressive integrated moving average (ARIMA) model provides a more appropriate solution since it removes the trend from the data. Moreover, electricity consumption data has seasonal dependencies. Thus, seasonal ARIMA, that is SARIMA, was proposed to represent data more accurately.

Machine learning methods include artificial neural networks [18-32], fuzzy logic algorithms [33, 34], swarm intelligence methods [35-38] and recursive methods such as recurrent neural networks (RNN) [39, 40], gated recurrent unit (GRU) [41], and long short-term memory (LSTM) [42, 43]. In traditional machine learning approaches such as multilayer perceptron (MLP) with backpropagation learning and SVM, the data set is analyzed and features describing the data in a lower dimensional space are extracted. Then the dependencies between features are discarded, and the best features are selected with methods such as principal component analysis or optimization algorithms like genetic algorithms. Finally, a prediction is made based on these features. Since machine learning approaches can learn the interrelationships of features and the output, successful forecast results were obtained for both short-term, medium-term, and long-term studies.

The challenge in traditional machine learning algorithms is that the performance of the forecast algorithm depends on the selection of suitable features. A solution is to use representation learning methods such as those employing deep learning models that learn, in some sense, the representative features in the first layers of their multilayer architecture. These algorithms learn from data when even the raw time series data is applied as the input. Recursive methods such as RNN, GRU, and LSTM are efficient forecasting tools since they extract the information from long time series.

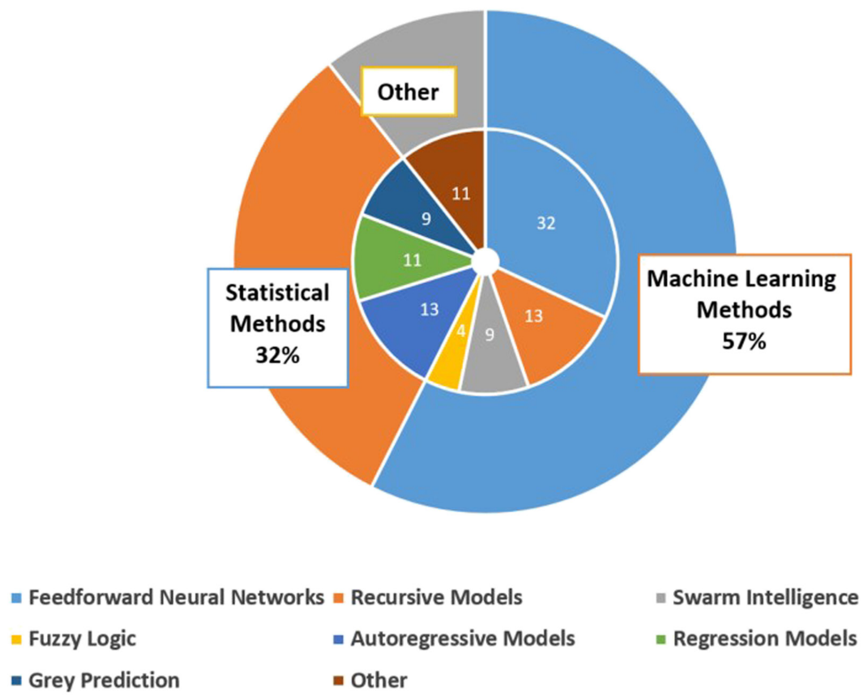

Fig. 5. Overview of the forecasting methods.

When the major electricity forecast studies for Turkey are examined from 2003 to 2020, it is observed that 57% of the studies use machine learning methods. The statistical methods are the second group, with 32%. The other studies mentioned in this paper use methods such as empirical models, Fourier methods, surface fitting, and Mittag-Leffler functions. The ratio of all methods is summarized in Fig. 5.

Let us consider the studies under consideration in detail. In Topalli and Erkmen [39], the models based on recursive MLP for forecasting were used in a hybrid learning scheme. The load values of year 2000 were used for offline training of the network, with random initial weights. Then, the trained network weights were updated during the online training phase with new data from 2001. Thus, the network adapts to the real-time changes and convergence time is reduced. In another study, an Elman's recurrent neural network model was employed [40]. Topallı et al. [40] a hybrid learning process combining offline training and online updating. They also analyzed the effect of seasons, day of the week and special days, and added a correction term to the forecast, which produces a reduced error rate compared to the ARMA structure.

A long-term forecast study uses total power consumption for Turkey starting from 1970, and predicts the yearly load by using artificial neural networks [18]. The performances of two models such as the backpropagation network and the radial basis network were compared with the regression networks. It is observed that the neural network techniques outperform regression methods for this study.

In another study, Yalçınöz and Eminoğlu predicted the peak load of the day, a total load of the day, and monthly electricity consumption using MLP, using temperature and load values for Niğde [19].

Kavaklıoğlu et al. [20] modeled electricity consumption with MLP as a function of economic indicators such as population, gross national product (GNP), imports and exports, and time.

In another study, forecasting performances of the Adaptive Network Based Fuzzy Inference (ANFIS) and the ARMA model [33] were analyzed. The data of GNP, population, energy produced and consumed, and installed capacity for the years 1970–2007 were used to predict energy demands from 2006 to 2010.

In Kaytez et al. [21], backpropagation networks were compared with Elman's recurrent neural network to forecast yearly electricity consumption. They showed that when social and economic factors such as GNP, gross domestic product (GDP), population, number of trade holds, Index of Industrial Production, and crude oil prices, along with electricity consumption with price as features, neural network techniques succeed in forecasting better than the model analysis of energy demand (MAED) of MENR. Moreover, the error rate of RNN was obtained as lower than that of MLP.

Kuçukali and Bariş [34] predicted annual demand by using only GNP. They showed that the fuzzy logic approach outperforms regression and MENR.

A swarm intelligence application of electricity demand forecast was made based on socio-economic indicators of GDP, population, import and export from 1979 to 2006 [35]. Artificial bee colony (ABC) and ant colony optimization (ACO) approaches were used for forecasting the annual demand.

In another study [32], the nonlinear autoregressive artificial neural network (NARANN) model and the seasonal autoregressive iterative moving average (SARIMA) method were employed to estimate future independent factors. Monthly data of gross production, imports, transmitted energy and export were determined as independent factors. Then, LASSO-based ADaptive Evolutionary Simulated annealing (LADES) and Ridge-based ADaptive Evolutionary Simulated annealing (RADES) models were applied to forecast the future electricity consumption.

The least squares-SVM (LS-SVM) method was compared with MLP for forecasting yearly consumption. Data on installed capacity, gross electricity generation, population, and total subscribership data were used for analysis in Kaytez et al. [22].

Kölmek and Navruz [23] predicted the day-ahead price for the Turkish market with MLP using historical load data, available capacity information (nuclear, thermal, hydro, etc.), forecast load/demand, temperature, the settlement period, day code, season code, and historical prices. They showed that MLP with the Levenberg–Marquardt learning algorithm generates better MAPE than the ARIMA model on average.

Another swarm intelligence study used a hybrid method of ACO and iterated local search (ILS) for estimating domestic electricity consumption [36].

The annual gross electricity demand of Turkey was modeled by using some socio-economic indicators such as population, GDP per capita, inflation percentage, unemployment percentage, average summer temperature, and average winter temperature [24]. MLP was used as the forecast method and it was shown that it outperforms the MLR model.

Table III summarizes the methods, data, and performances of the forecasting studies using artificial intelligence algorithms between the years 2003 and 2016.

When machine learning algorithms used for forecasting after the year 2017 are considered, it is seen that Bozkurt et al. [25] compared the forecasting performance of SARIMA and MLP models. To train models, the data on load, electricity price, and weather were collected at hourly intervals and the USD/TRY exchange rates at monthly intervals, for 2 years. They analyzed the performance of the systems when the model was trained with 1, 3, 6, and 12 months, with selected features from the whole set. The forecast was made for 1 week. They observed that MLP is more successful than SARIMA, and the success rate depends highly on whether the day is a national/religious holiday or not.

In Sonmez et al. [37], the ABC model was used to forecast annual transportation energy demand using data on GNP, population, and annual vehicle-kilometers. They showed that the linear model performs slightly better than quadratic and exponential models. Another swarm intelligence study was done by Gulcu and Kodaz [38] to predict annual electricity demand using data on GDP, population, and import and export from 1979 to 2013. They also made a forecast until 2030, using the model shown to be successful in the first part of their study.

Bulut and Başoğlu [26] proposed a hybrid system based on artificial neural networks and rule-based expert systems called EPSIM-NN to estimate 24-hour daily demand estimates. They used a neural network structure to estimate the daily average consumption and 24-hour electricity consumption waveform, and then combined them. The parameters they used include historical load data, calendar dates, and seasonal and economic indicators.

In Kocadayı et al. [27], demographic data such as population, building area, and import and export data were used as features for MLP, and they predicted annual electricity consumption of the TR81 region which includes Zonguldak, Karabük and, Bartın, from 2016 to 2020.

Toros and Aydın [28] analyzed how electricity consumptions of the 12 largest cities of Turkey were affected by social and economic variables such as population, cost, and GDP, as well as by climatic variables such as temperature and rainfall. They accomplished their experiments for the winter and summer seasons separately, since the seasonality changes the model parameters.

In another study, the energy consumption of an industrial zone was investigated. The historical temperature and consumption data were used as input to MLP to forecast energy demand [29]. They compared these estimates with time series predictions made by the NARANN model and concluded that temperature as an input to MLP carries important information about electricity consumption.

Arslan et al. [30] used hourly electricity consumption data of the Niğde province for 5 years between 2013 and 2018. Using MLP, they forecasted yearly, monthly, weekly and hourly consumption, considering the effect of different input sizes.

The LSTM method was used to forecast the electricity price 2 hours-ahead, using hourly data with 16 variables constructed from lagged average price values, calendar date, and some economic variables [42]. Authors from the same group used multilayer GRUs for electricity price estimation and compared it with MLP and LSTM [41]. They observed that deeper networks with three layers produce better results where the GRU-3 network has slightly better performance.

Özkurt et al. [43] forecasted 24-hour electricity consumption for the day-ahead market. Hourly electricity consumption for 336 hours (2 weeks) was applied as input LSTM. A 36 hours-ahead prediction was made for 24 hours, which is suitable with the day-ahead electricity market closing time. It was observed that the error rate

TABLE III
SUMMARY OF MACHINE LEARNING STUDIES IN 2003–2016

Authors	Method	Data Time Range	Features	Output	Forecast Error
Topalli and Erkmen [39]	Recursive MLP	2000 for offline training 2001 for online training and test	One-day advance hourly load	Hourly load	Average percent error 10.65% offline 12.96% online
Topallı et al. [40]	Elman's RNN ARMA	2001 for offline training 2002 for online training and test	Load and temperature	Hourly load	Average percent error 1.60% RNN 2.33% ARMA
Hamzaçebi and Kutay [18]	MLP RBF ARIMA	1970–1990 for training 1991–1998 for validation 1999–2002 for test	Load in GWh total in years	Annual consumption	MAPE 2.77% MLP 3.43% RBF 8.69% ARIMA(2,2,0)
Yalçınöz and Eminoğlu [19]	MLP	1991–2001 train 2002–2005 different intervals for test	Past and current load and temperature	Peak and total load of day, monthly consumption	Error 3.12% daily 0.47–4.7% peak 2.21% monthly
Kavaklıoğlu et al. [20]	MLP	1975–2000 train 2001–2006 test	Socio-economic indicators	Annual consumption	Relative RMS error 1.15%
Demirel et al. [33]	ANFIS ARMA	1970–2007 train 2006–2010 test	Socio-economic indicators	Annual demand	MAPE 0.47% ANFIS 5.32% ARMA
Çunkaş and Altun [21]	MLP RNN MAED	1981–2002 training 2003–2007 test	Consumption, price, socio-economic indicators	Annual demand	MAPE 0.77% RNN 1.53% BP 6.83% MAED
Kuçukali and Barış [34]	Fuzzy Logic Regression	1970–2014	GDP	Annual demand	MAPE 3.9% Fuzzy 7.3% Regression
Kıran et al. [35]	ACO ABC	1976–2006	Socio-economic indicators	Annual demand	R^2 0.995 ABC 0.98 ACO
Tutun et al. [32]	SARIMA and NARANN with LADES and RADES	1990–2005 for training 2006–2010 for test	Socio-economic indicators	Monthly electricity consumption	MAPE 1.60% LADES 1.96% RADES
Kaytez et al [22]	LS-SVM MLP	1970–2009 2/3 for train 1/3 for test	Generation and social indicators	Annual electricity consumption	MAPE 1.004% LS-SVM 1.19% MLP
Kölmek and Navruz [23]	MLP ARIMA	December 1, 2009–November 9, 2010 342 days 80 days for test	Historical load/demand, capacity, seasonal data	Day-ahead price	MAPE 14.15% MLP 15.60% MLP
Toksarı [36]	ACO	1990–2013	Socio-economic indicators	Annual domestic consumption	MAPE 3.7% Linear 5.0% Quadratic
Günay [24]	MLP	1975–2006 train 2007–2013 test	Socio-economic indicators	Annual gross demand	RMSE 5.7%

TABLE IV
SUMMARY OF MACHINE LEARNING STUDIES IN 2017–2020

Authors	Method	Data Time Range	Features	Output	Forecast Error
Bozkurt et al. [25]	SARIMA MLP	2013–2014 Specific date intervals for train and test	Load, price, weather	Hourly load	MAPE (lowest) 0.98% 1.36%
Sonmez et al. [37]	ABC	1970–2013	GDP, population and total annual vehicle-kms	Annual transportation energy demand	MAPE 11% Linear 12% Quadratic 16% Exponential
Gulcu and Kodaz [38]	PSO	1979–2013	Economic indicators	Annual energy demand	R^2 0.99
Başoğlu and Bulut [26]	EPSIM-NN	2005–2016 Two weeks test in 2016	Calendar day, holidays, historical load data, economic factors	Hourly consumption for 24 hours	MAPE 1.8% and 1.0%
Kocadayı et al. [27]	MLP	2002–2014 train 2016–2020 forecast	Demographic and economic indicators	Annual electricity consumption	R^2 0.91
Aydın and Toros [28]	MLP	2012–2016 intervals Train January 2016 winter test August 2016 summer test	Historical consumption, socio-economic factors, weather	Daily and hourly consumption	MAPE (daily-hourly) 1.04–1.62% Summer 1.34–1.94% Winter
Özden and Öztürk [29]	MLP NARANN	2014–2016 (763 days) 70% train, %15 validation 15% test	Historical temperature and consumption	Daily	R^2 0.99 MLP 0.94 NARANN
Arslan et al. [30]	MLP	September 2018–September 2019 train 2–14 Sep 2019 test	Lagged consumption values in chunks	24-step-ahead hourly consumption	MAE Min 1.91
Yorulmuş et al. [42]	LSTM	February 8, 2017–March 31, 2018 10000 observations 70% train, 10% validation 20% test	Lagged average price, date, economical factors	Two-hour-ahead price	MAPE 0.24%
Uğurlu et al. [41]	MLP LSTM GRU	2013–2015 train 356 days of 2016 test	Lagged price values, temperature, economical factors	24-step-ahead price	MAE 5.36 Euros/MWh (GRU-3)
Özkurt et al. [43]	LSTM	June 2016–July 2020 915 train-212 test	336-hours lagged hourly consumption	36-hours-ahead 24-hour consumption	MAPE 2.72% 2019 4.47% 2020
Gökgöz and Filiz [31]	MLP with GD, GDM, LM, BFGS	January 2012–March 2014 train March 2014–December 2014 test	Hourly load and temperature	Hourly load	MAPE 2.18% BFGS 2.2% LM >20% GD,GDM

of both the LSTM model and EPİAŞ predictions were increased because of the COVID-19 pandemic starting in 2020.

Gökgöz and Filiz used MLP for estimating hourly consumption by using different learning algorithms such as gradient descent (GD), gradient-descent momentum (GDM), the Broyden–Fletcher–Goldfarb–Shanno algorithm (BFGS), and the Levenberg–Marquardt algorithm (LM) [31]. They showed that the LM and BFGS algorithms have better forecasts considering MAPE values.

The machine learning studies published from 2017 to 2020 are given in Table IV.

Autoregressive models also have successful applications in electricity forecasting. In 2007, Erdogdu [12] developed an ARIMA model using quarterly time series data on real electricity prices, real GDP per capita, and net electricity consumption per capita for the period 1984–2004, a total of 84 observations. Then using annual data from 1923 to 2004, the demand forecast from 2005 to 2014 was implemented.

Boran [7] forecasted annual net electricity consumption with the ARIMA model by using annual time series starting from 1970 to 2008 with MAPE of 2.58%.

Akarsu [8] forecasted electricity demand of 21 regions between 1986 and 2013 using the data of electric distribution companies with different AR models.

Uğurlu et al. [11] showed that the SARIMA model represents the price data better than the other methods, when analysis of variance was used as a pre-whitening method for the Turkish day-ahead electricity market.

In another study, Kaytez proposed an hybrid LS-SVM and ARIMA model for an improved long-term prediction performance [9]. While the MAPE for single ARIMA (1, 1, 2) is 2.36%, the hybrid approach has 1.00% in the forecasting of annual electricity consumption.

Akdi et al. [10] compared the ARIMA model with harmonic regression for daily electric consumption. They concluded that the harmonic regression performs better when the variable to represent has periodicity behavior.

Grey prediction, inspired from grey box models, assumes that the information about the system is partially known and uses a decision-making process to generate unknowns from the partial information. Hamzaçebi and Es [14] used the grey model to forecast monthly electricity consumption by using past consumption from 1945 to 2010. It was shown that a direct optimized grey model performs better than an iterative model and the predictions of MENR. Hamzaçebi conducted a study on planning primary energy sources using a seasonal grey model [15]. By the addition of seasonality, the prediction error for the period from 2004 to 2020 in terms of MAPE was reduced from 8.39% to 5.18%. Another study used the Nonhomogeneous Discrete Grey Model by using data of 1970–2013 [16]. They showed that NGDM has lower errors than the previous grey models in prediction by providing a better fit to the curve. In Şahin [17], the grey prediction method was employed to model Turkey's electricity generation and consumption for 1996–2016, and MAPE of 3.12% and 3.08% were obtained for generation and consumption respectively.

Regression models were used to estimate the relationship between inputs and outputs by using statistical methods. In Yukseltan et al. [4], a linear regression model was used to forecast annual, week-ahead, and day-ahead demand by considering harmonics of the variations. Data were collected from 2012 to 2014 and predictions produced less than 3% MAPE. Especially when the relationship is not linear, nonlinear methods such as support vector machines can provide a better fit to the data. In Kavaklioğlu [6], SVR was used to model the annual electricity consumption as a function of socio-economic indicators such as population, GNP, imports, and exports, from 1975 to 2006. Relative RMS error for consumption is determined as 1.51% in this study. In another study, a genetic algorithm was employed to find the best parameters for support vector regressor to forecast annual electricity consumption [44]. Electricity consumption, population, import, export and GDP between 1975 and 2014 were used as input variables, and MAPE of 3.66% was obtained. In a recent study, Ülgen and Poyrazoğlu [5] used MLR to predict the electricity prices. Historical prices for 1 year, from September 2018 to September 2019, were used for forecasting and it was shown that 1-day, 1-week, and lagged moving average prices are important in the performance.

In Özkan et al. [13], Fourier analysis with least squares approach and the Holt–Winters exponential smoothing method were compared to predict electric consumption. They observed that the forecast models produced the lowest error with 12 months' data and that Winter's method outperformed the Fourier-based method.

Filik et al. [45] proposed a method based on quasi-periodic load characterization. Their model covers long-term to short-term characteristics by having coarse to fine models to achieve hourly accuracy. The multiresolution model was tested for the period from of 2002 to 2005 and 5.74% hourly, 1.87% weekly, 1.5% monthly, and 0.73% yearly MAPE were observed. Dönmez et al. [46] proposed a second-order curve fitting model to estimate the demand as a function of population and GNP with R^2 value of 0.994. In Çalık and Şirin [47], electricity consumption values were modeled with Mittag-Leffler functions and the annual consumption values showed that the model fit when it was compared to previous MLP and SVR predictions in literature. Melikoglu [48] forecasted annual electricity demand by 2023 after a detailed analysis of Turkey's capacity targets and energy potential. The model includes a simple nonlinear function of the current population, electricity demand per capita at the reference (base) year, average annual increase of electricity demand per capita, and difference between the current and reference year. Different scenarios were created according to demand growth. In a recent study, Yukseltan et al. [49] proposed an hourly electricity demand model based on Fourier analysis with an update structure. They used past demand data and forecasted hourly, daily, and yearly demands using data for the period 2012–2017. It was shown that the model works with MAPE of 0.87% in hour-ahead, 2.90% in day-ahead, and 3.54% in the year-ahead predictions, and that application of the AR model combined with Fourier series improves the system slightly.

IV. DATA ANALYSIS

When the data used in the forecasting studies are examined, the following observations are made. The data used include

- Historical electricity consumption, generation, and price;
- Electricity infrastructure such as installed capacity of different generation sources;
- Demographic data such as population;
- Economic indicators such as GNP, GDP, export and import rates, etc.;
- Weather;
- Time variables such as calendar date, seasons, weekday or weekend, official or religious holidays.

Most of the researchers have shown that there is a strong correlation between electricity demand/load/price and the factors listed above, and using data such as economic or social factors or seasonality will increase the performance of the forecast.

Before the electricity consumption/generation data were made publicly available on the Transparency Platform, the electricity-related data were provided by the MENR, local distribution companies, International Energy Agency, State Institute of Statistics (TÜIK), and SPO. Now, historical and current electricity generation/

consumption data, and installed capacity are available for all regions of Turkey. The economic and social indicators are collected from TÜIK and related ministries such as the Ministry of Treasury and Finance, and MENR.

Most of the studies concentrate on the forecast of load or demand while a few predict the price for the Turkish Energy Market. Where only a few studies focused on some specific region of Turkey such as industrial zones, a province, or a local distribution region, the others made their predictions for the whole of Turkey. More than half of the studies forecast annual amounts where the others made short- or medium-term predictions including monthly, weekly, or daily values.

V. CONCLUSIONS

The paper gives an overview of the electricity energy forecasting studies in Turkey for the period from 2003 to 2020. The paper analyzes the forecasting studies in terms of the forecasting methods used, the profiles of the researchers and their institutions, and the years and location information of the data. We apologize for not including some of the studies in the paper due to the space limitation, and also due to the inaccessibility of the works that are published in the scientific journals or conferences.

The paper reveals the following findings: ([1]) There is a tremendously growing need for electricity energy forecasting parallel to the development of smart grid systems; ([2]) The motives behind the studies on electricity forecasting for Turkey are diverse. Most of them can be said to be driven by the development of the data-driven forecasting methods such as neural network-based methods including deep neural network models for the time series. Some works are driven by the availability and accessibility of the sufficient number data of acceptable quality. The others are driven by the increasing need for smart energy management; ([3]) A large set of researchers and institutions aim to develop competencies in electricity energy forecasting, which are focused on Turkey's electricity energy problems from different perspectives; and ([4]) A part of the studies does not show long-term continuity. They feature a somewhat intermittent and temporary nature.

This paper would be useful to identify the already developed competencies on electricity energy forecasting by the individual researchers and the institutions of Turkey, in order to establish new competency centers to meet Turkey's need for forecasting of electricity production and consumption.

Peer-review: Externally peer-reviewed.

Conflict of Interest: The authors have no conflicts of interest to declare.

Financial Disclosure: The authors declared that this study has received no financial support.

REFERENCES

1. EPİAŞ Turkish energy Exchange. "EPİAŞ Turkish energy Exchange Annual report 2019," 2020. Available: https://www.epias.com.tr/wp-content/uploads/2020/08/EXIST-Annual-Report-2019.pdf. [accessed: Mar. 01, 2021].
2. T. Hong and S. Fan, "Probabilistic electric load forecasting: A tutorial review," *International Journal of Forecasting*, vol. 32, no. 3, pp. 914–938, 2016. [CrossRef]
3. D. C. Montgomery, C. L. Jennings and M. Külahçı, *Introduction to Time Series Analysis and Forecasting*. Chichester, UK: Wiley, 2008.
4. E. Yukseltan, A. Yucekaya and A. H. Bilge, "Forecasting electricity demand for Turkey: Modeling periodic variations and demand segregation," *Applied Energy*, vol. 193, pp. 287–296, 2017. [CrossRef]
5. T. Ülgen and G. Poyrazoğlu, "Predictor Analysis for Electricity Price Forecasting by Multiple Linear Regression," *2020 International Symposium on Power Electronics, Electrical Drives, Automation and Motion (SPEEDAM)* 2020, pp. 618–622, 2020. [CrossRef]
6. K. Kavaklioglu, "Modeling and prediction of Turkey's electricity consumption using Support Vector Regression," *Applied Energy*, vol. 88, no. 1, pp. 368–375, 2011. [CrossRef]
7. K. Boran, "The box Jenkins approach to forecast net electricity consumption in Turkey," *Energy Sources, Part A: Recovery, Utilization, and Environmental Effects*, vol. 36, no. 5, 515–524, 2014. [CrossRef]
8. G. Akarsu, "Forecasting regional electricity demand for Turkey," *International Journal of Energy Economics and Policy*, vol. 7, no. 4, 2017.
9. F. Kaytez, "A hybrid approach based on autoregressive integrated moving average and least-square support vector machine for long-term forecasting of net electricity consumption," *Energy*, vol. 197, no. Apr., 2020. [CrossRef]
10. Y. Akdi, E. Gölveren and Y. Okkaoğlu, "Daily electrical energy consumption: Periodicity, harmonic regression method and forecasting," *Energy*, vol. 191, 2020. [CrossRef]
11. U. Ugurlu, O. Tas and U. Gunduz, "Performance of electricity price forecasting models: Evidence from turkey," *Emerging Markets Finance and Trade*, vol. 54, no. 8, 1720–1739, 2018. [CrossRef]
12. E. Erdogdu, "Electricity demand analysis using cointegration and Arima modelling: A case study of turkey," *Energy Policy*, vol. 35, no. 2, pp. 1129–1146, 2007. [CrossRef]
13. E. Özkan, E. Güler and Z. Aladağ, "Elektrik enerjisi tüketim verileri için uygun tahmin yöntemi seçimi," *Endüstri Mühendisliği*, vol. 31, no. 2, pp. 198–214, 2020. [CrossRef]
14. C. Hamzacebi and H. A. Es, "Forecasting the annual electricity consumption of turkey using an optimized grey model," *Energy*, vol. 70, pp. 165–171, 2014. [CrossRef]
15. C. Hamzaçebi, "Primary energy sources planning based on demand forecasting: The case of turkey," *Journal of Energy in Southern Africa*, vol. 27, no. 1, 2016. [CrossRef]
16. B. Ayvaz and A. O. Kusakci, "Electricity consumption forecasting for Turkey with nonhomogeneous discrete grey model," *Energy Sources, Part B: Economics, Planning, and Policy*, vol. 12, no. 3, pp. 260–267, 2017. [CrossRef]
17. U. Şahin, "Forecasting of turkey's electricity generation and consumption with grey prediction method," *Mugla Journal of Science and Technology*, vol. 4, no. 2, pp. 205–209, Dec. 2018. [CrossRef]
18. C. Hamzaçebi and F. Kutay, "Yapay sinir ağlari ile Türkiye elektrik enerjisi tüketiminin 2010 yilina kadar tahmini," 2004. [Online]. Available: https://dergipark.org.tr/tr/pub/gazimmfd/88940. [Accessed: Dec. 27, 2020].
19. T. Yalcinoz and U. Eminoglu, "Short term and medium term power distribution load forecasting by neural networks," *Energy Conversion and Management*, vol. 46, no. 9–10, pp. 1393–1405, 2005. [CrossRef]
20. K. Kavaklıoğlu, H. Ceylan, H. K. Öztürk and O. E. Canyurt, "Modeling and prediction of Turkey's electricity consumption using Artificial Neural Networks," *Energy Conversion and Management*, vol. 50, no. 11, pp. 2719–2727, Nov. 2009. [CrossRef]
21. M. Çunkaş and A. A. Altun, "Long term electricity demand forecasting in Turkey using artificial neural networks," *Energy Sources, Part B:*

Economics, Planning, and Policy, vol. 5, no. 3, 279–289, 2010. [CrossRef]
22. F. Kaytez, M. C. Taplamacioglu, E. Cam and F. Hardalac, "Forecasting electricity consumption: A comparison of regression analysis, neural networks and least squares support vector machines," *International Journal of Electrical Power and Energy Systems*, vol. 67, pp. 431–438, 2015. [CrossRef]
23. M. A. Kölmek and İ Navruz, "Forecasting the day-ahead price in electricity balancing and settlement market of Turkey by using artificial neural networks," *Turkish Journal of Electrical Engineering and Computer Sciences*, vol. 23, no. 3, pp. 841–852, 2015. [CrossRef]
24. M. E. Günay, "Forecasting annual gross electricity demand by artificial neural networks using predicted values of socio-economic indicators and climatic conditions: Case of Turkey," *Energy Policy*, vol. 90, 92–101, 2016. [CrossRef]
25. Ö. Ö. Bozkurt, G. Biricik and Z. C. Taysi, "Artificial neural network and SARIMA based models for power load forecasting in Turkish electricity market," *PLOS ONE*, vol. 12, no. 4, e0175915, 2017. [CrossRef]
26. M. Bulut and B. Başoğlu, "Kısa Dönem Elektrik Talep Tahminleri İçin Yapay Sinir Ağları ve Uzman Sistemler Tabanlı Hibrid Tahmin Sistemi Geliştirilmesi," *Gazi Üniversitesi Mühendislik-Mimarlık Fakültesi Dergisi*, vol. 32, no. 2, pp. 575–583, Jun. 2017. [CrossRef]
27. Y. Kocadayı, O. Erkaymaz and R. Uzun, "Yapay Sinir Ağları ile Tr81 Bölgesi Yıllık Elektrik Enerjisi Tüketiminin Tahmini,", *2017, Bilge International Journal of Science and Technology Research*, 2017 .[Accessed: Dec. 26, 2020]. [Online]. Available: https://dergipark.org.tr/tr/pub/bilgesci/350353, Vol. 1, no. 1, pp. 59–64.
28. H. Toros and D. Aydın, "Kısa Vadeli Elektrik Tüketiminin Sıcaklığa Bağlı Yapay Sinir Ağları ile Tahmini," *European Journal of Science and Technology*, vol. 14, pp. 393–398, Dec. 2018. [CrossRef]
29. S. Özden and A. Öztürk, "Yapay Sinir Ağları ve Zaman Serileri Yöntemi ile Bir Endüstri Alanının (İvedik OSB) Elektrik Enerjisi İhtiyaç Tahmini," *Bilişim Teknolojileri Dergisi*, vol. 3, no. 11, pp. 255–261, 2018. [CrossRef]
30. Y. Arslan, *et al.*, "Short-term electricity consumption forecast using datasets of various granularities," *Lecture Notes in Computer Science (including subseries Lecture Notes in Artificial Intelligence and Lecture Notes in Bioinformatics)*, vol. 11325, pp. 116–126, 2018. [CrossRef]
31. F. Gökgöz and F. Filiz, "Electricity load forecasting via ANN approach in Turkish electricity markets," *Bilgi Yönetimi*, vol. 3, no. 2, pp. 170–184, Dec. 2020. [CrossRef]
32. S. Tutun, C. A. Chou and E. Caniyilmaz, "A new forecasting framework for volatile behavior in net electricity consumption: A case study in Turkey," *Energy*, vol. 93, pp. 2406–2422, 2015. [CrossRef]
33. Ö. Demirel, A. Kakilli and M. Tektaş, "ANFIS VE ARMA MODELLERİ İLE ELEKTRİK ENERJİSİ YÜK TAHMİNİ Özkan DEMİREL, Adnan KAKİLLİ ve Mehmet TEKTAŞ,", Feb. 2010. [Online]. Available: https://dergipark.org.tr/tr/pub/gazimmfd/88585. [Accessed: Dec. 27, 2020].
34. S. Kucukali and K. Baris, "Turkey's short-term gross annual electricity demand forecast by fuzzy logic approach," *Energy Policy*, vol. 38, no. 5, pp. 2438–2445, May 2010. [CrossRef]
35. M. S. Kiran, E. Özceylan, M. Gündüz and T. Paksoy, "Swarm intelligence approaches to estimate electricity energy demand in Turkey," *Knowledge-Based Systems*, vol. 36, pp. 93–103, 2012. [CrossRef]
36. M. D. Toksari, "A hybrid algorithm of Ant Colony Optimization (ACO) and Iterated Local Search (ILS) for estimating electricity domestic consumption: Case of Turkey," *International Journal of Electrical Power and Energy Systems*, vol. 78, 776–782, 2016. [CrossRef]
37. M. Sonmez, A. P. Akgüngör and S. Bektaş, "Estimating transportation energy demand in Turkey using the artificial bee colony algorithm," *Energy*, vol. 122, pp. 301–310, 2017. [CrossRef]
38. S. Gulcu and H. Kodaz, "The estimation of the electricity energy demand using particle swarm optimization algorithm: A case study of Turkey,", in *Procedia Computer Science*, vol. 111, pp. 64–70, 2017. [CrossRef]
39. A. K. Topalli and I. Erkmen, "A hybrid learning for neural networks applied to short term load forecasting," *Neurocomputing*, vol. 51, pp. 495–500, 2003. [CrossRef].
40. A. K. Topalli, I. Erkmen and I. Topalli, "Intelligent short-term load forecasting in Turkey," *International Journal of Electrical Power and Energy Systems*, vol. 28, no. 7, pp. 437–447, Sep. 2006. [CrossRef]
41. U. Ugurlu, I. Oksuz and O. Tas, "Electricity price forecasting using recurrent neural networks," *Energies*, vol. 11, no. 5, 2018. [CrossRef]
42. U. Ugurlu, O. Tas and H. Yorulmus, "A long short term memory application on the Turkish intraday electricity price forecasting,", *Pressacademia* vol. 7, no. 1, 126–130, 2018
43. N. Özkurt, H. Ş. Öztura and C. Güzeliş, "24-hour electricity consumption forecasting for day ahead market with long short term memory deep learning model," 12th International Conference on Electrical and Electronics Engineering, ELECO 2020, 2020, pp. 173–177. [CrossRef]
44. O. Kaynar, A. G. Yüksek and F. Demirkoparan, "Forecasting of Turkey's electricity consumption using support vector regression trained with genetic algorithm," *İktisat Fakültesi Mecmuası / Journal of the Faculty of Economics*, vol. 66, pp. 45–60, Dec. 2016. [CrossRef]
45. Ü. B. Filik, Ö. N. Gerek and M. Kurban, "A novel modeling approach for hourly forecasting of long-term electric energy demand,", in *Energy Conversion and Management*, vol. 52, no. 1, pp. 199–211, 2011. [CrossRef]
46. A. H. Dönmez, Y. Karakoyun and Z. Yumurtaci, "Electricity demand forecast of Turkey based on hydropower and windpower potential," *Energy Sources, Part B: Economics, Planning, and Policy*, vol. 12, no. 1, 85–90, 2017. [CrossRef]
47. A. E. Çalık and H. Şirin, "Türkiye'deki elektrik enerji ihtiyacının matematiksel bir modellemesi," *SAÜ Fen Bilimleri Enstitüsü Dergisi*, vol. 21, no. 6, pp. 1–1, Dec. 2017. [CrossRef]
48. M. Melikoglu, "Vision 2023: Scrutinizing achievability of Turkey's electricity capacity targets and generating scenario based nationwide electricity demand forecasts," *Energy Strategy Reviews*, vol. 22, 188–195, 2018. [CrossRef]
49. E. Yukseltan, A. Yucekaya and A. H. Bilge, "Hourly electricity demand forecasting using Fourier analysis with feedback," *Energy Strategy Reviews*, vol. 31, no. Sep., 2020. [CrossRef]